Electronic Supplementary Information

for

Binuclear ruthenium η^6-arene complexes with tetradentate *N*,*S*-ligands containing the *ortho*-aminothiophenol motif

Alberto Acosta-Ramirez[a], Edward D. Cross[a], Robert McDonald[b] and Matthias Bierenstiel*[a]

[a] *Cape Breton University, Department of Chemistry, 1250 Grand Lake Road, Sydney, Nova Scotia, B1P 6L2, Canada. Tel: +1 902 5631391; E-mail: Matthias_Bierenstiel@cbu.ca*

[b] *X-Ray Crystallography Laboratory, Department of Chemistry, University of Alberta, Edmonton, Alberta, T6G 2G2, Canada.*

*Corresponding Author:

Phone: 1 (902) 563-1391

Fax: 1 (902) 563-1899

Email: Matthias_Bierenstiel@cbu.ca

Contents

Figure S1. ^{1}H NMR spectrum (CD_2Cl_2) of **2a** (X = BF_4).

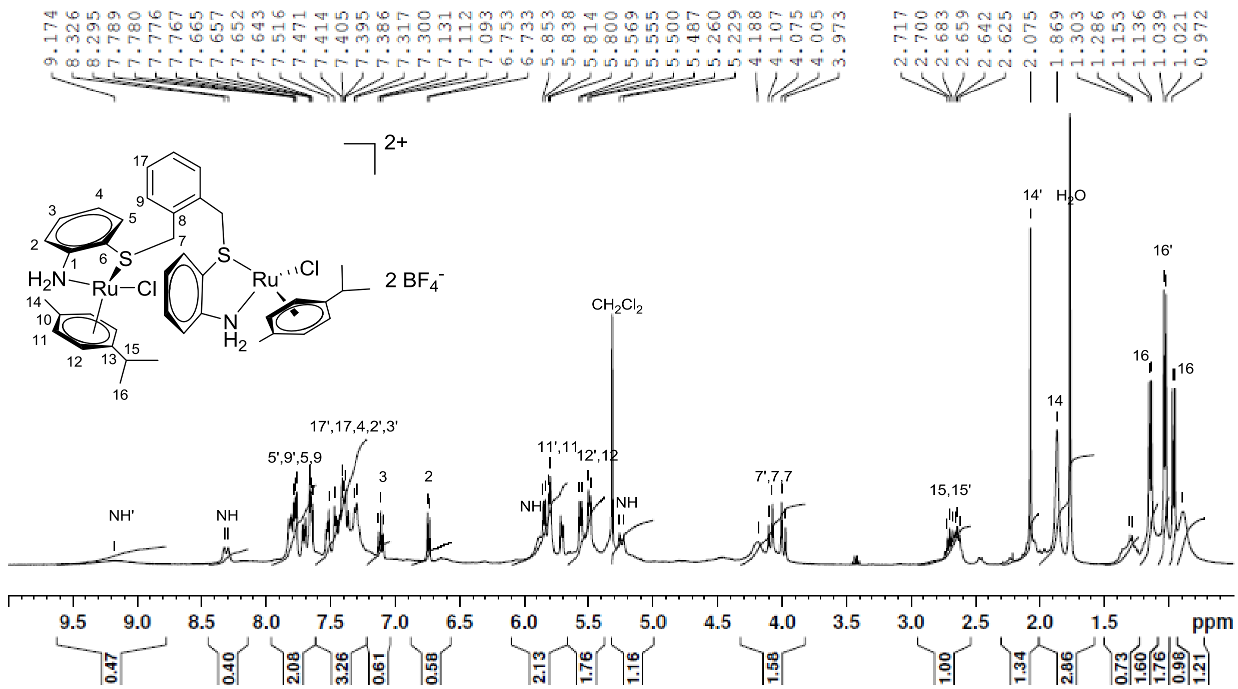

Figure S2. ^{13}C jmod NMR spectrum (CD_2Cl_2) of **2a** (X = BF_4).

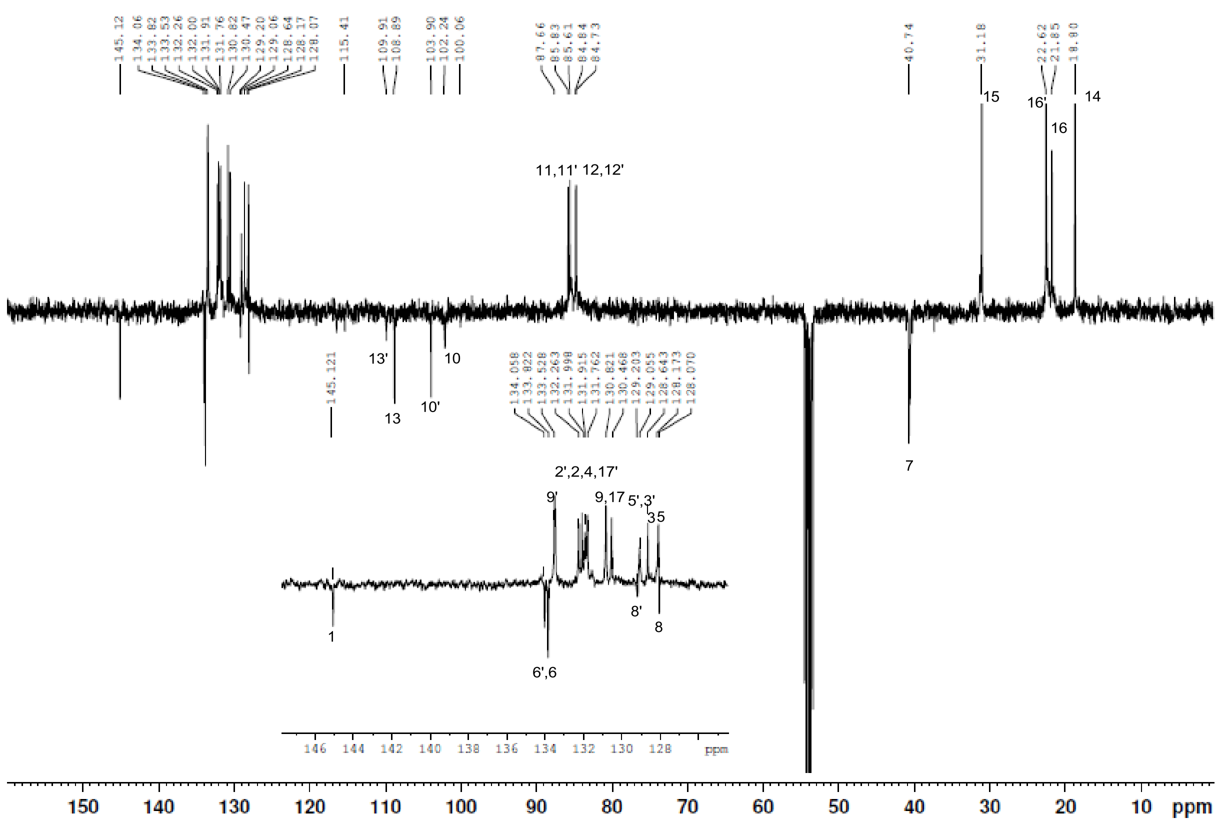

Figure S3. COSY NMR spectrum (CD_2Cl_2) of **2a** (X = BF_4).

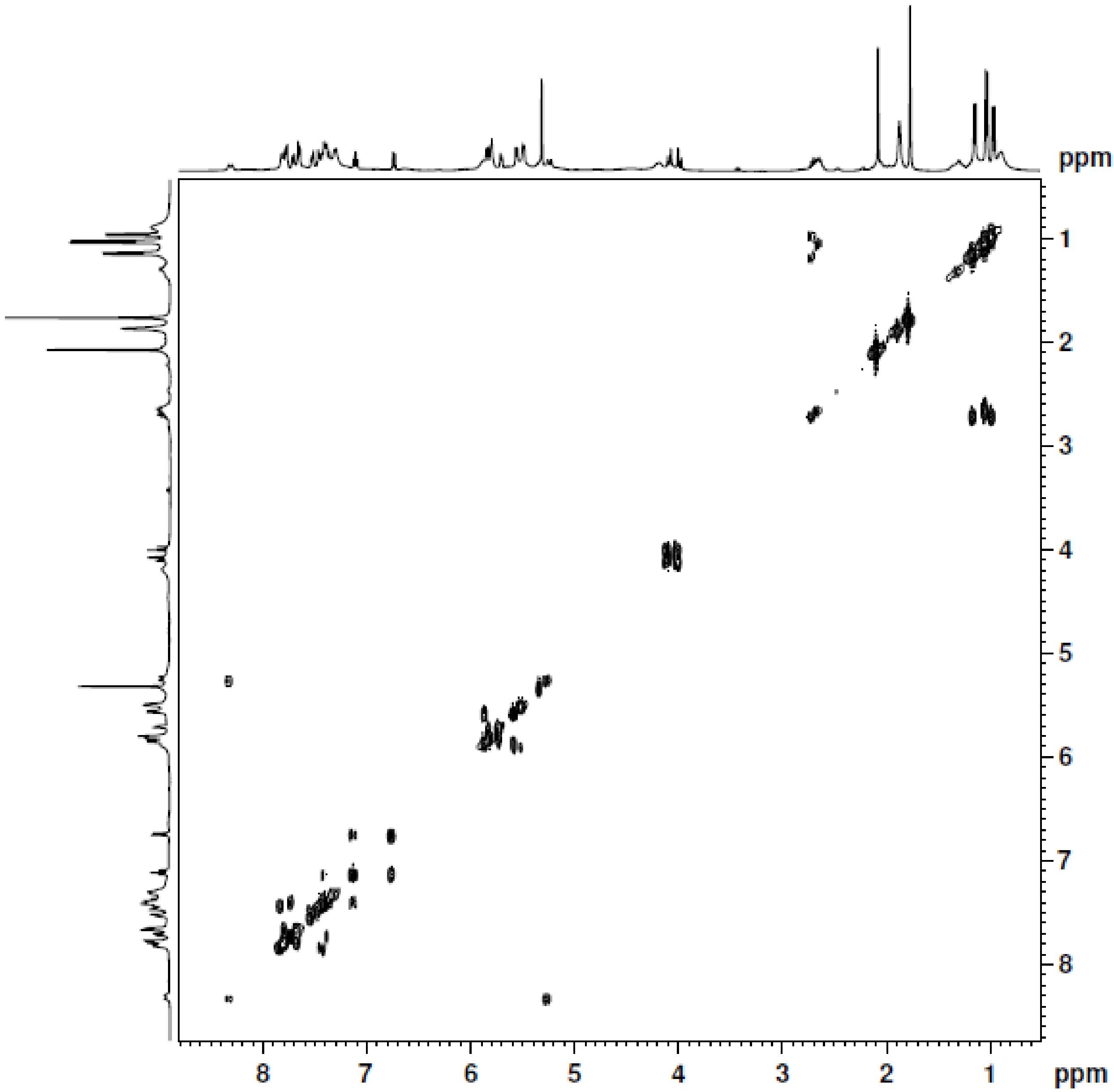

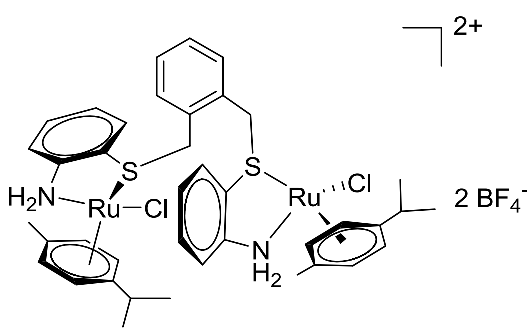

Electronic Supplementary Material (ESI) for Dalton Transactions

Figure S4. COSY NMR spectrum (zoom) (CD_2Cl_2) of **2a** (X = BF_4).

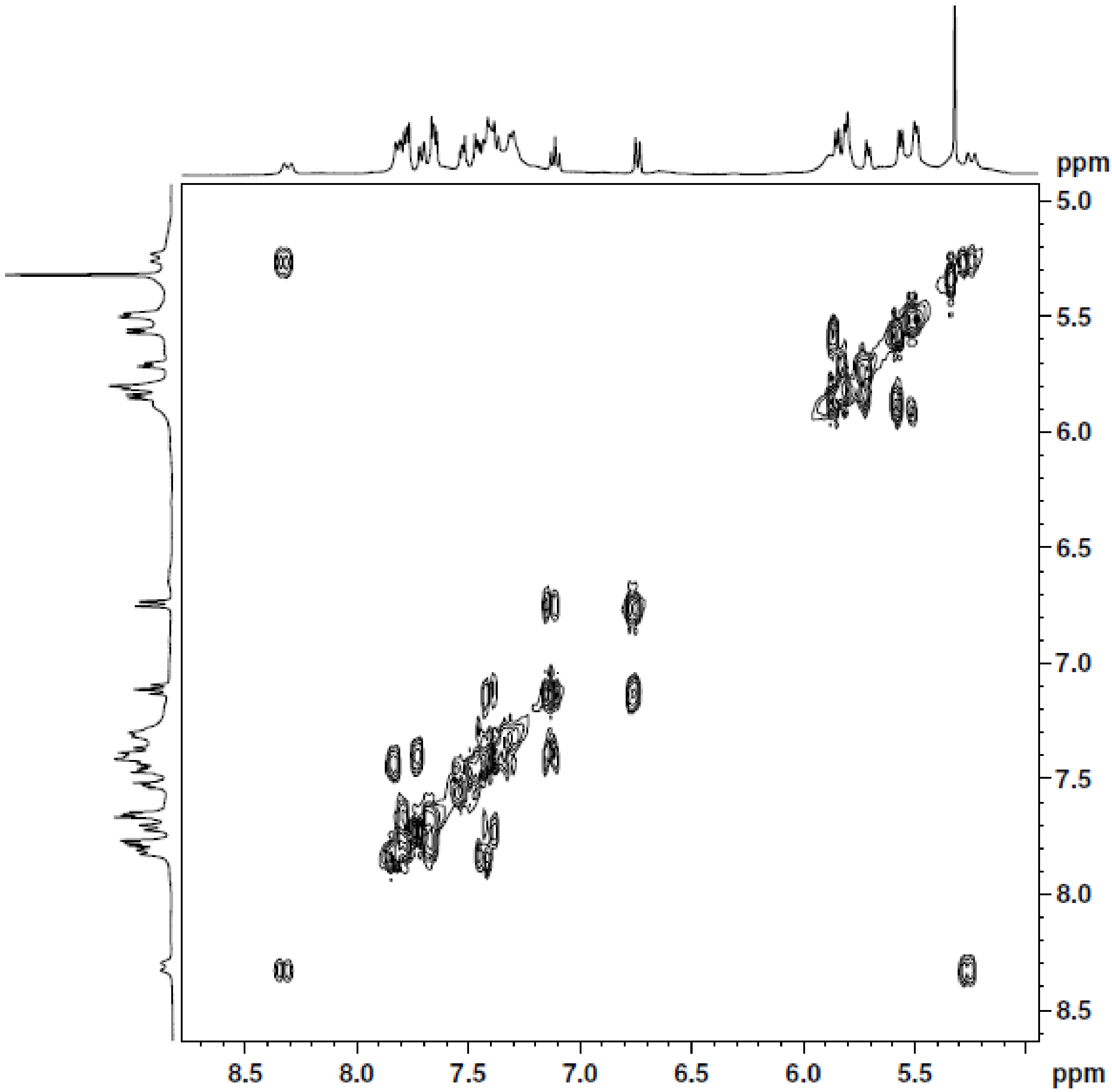

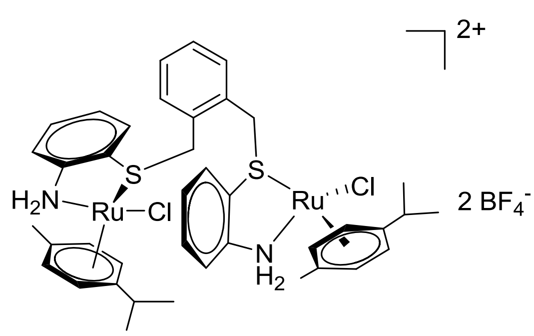

Figure S5. HSQC NMR spectrum (CD_2Cl_2) of **2a** (X = BF_4).

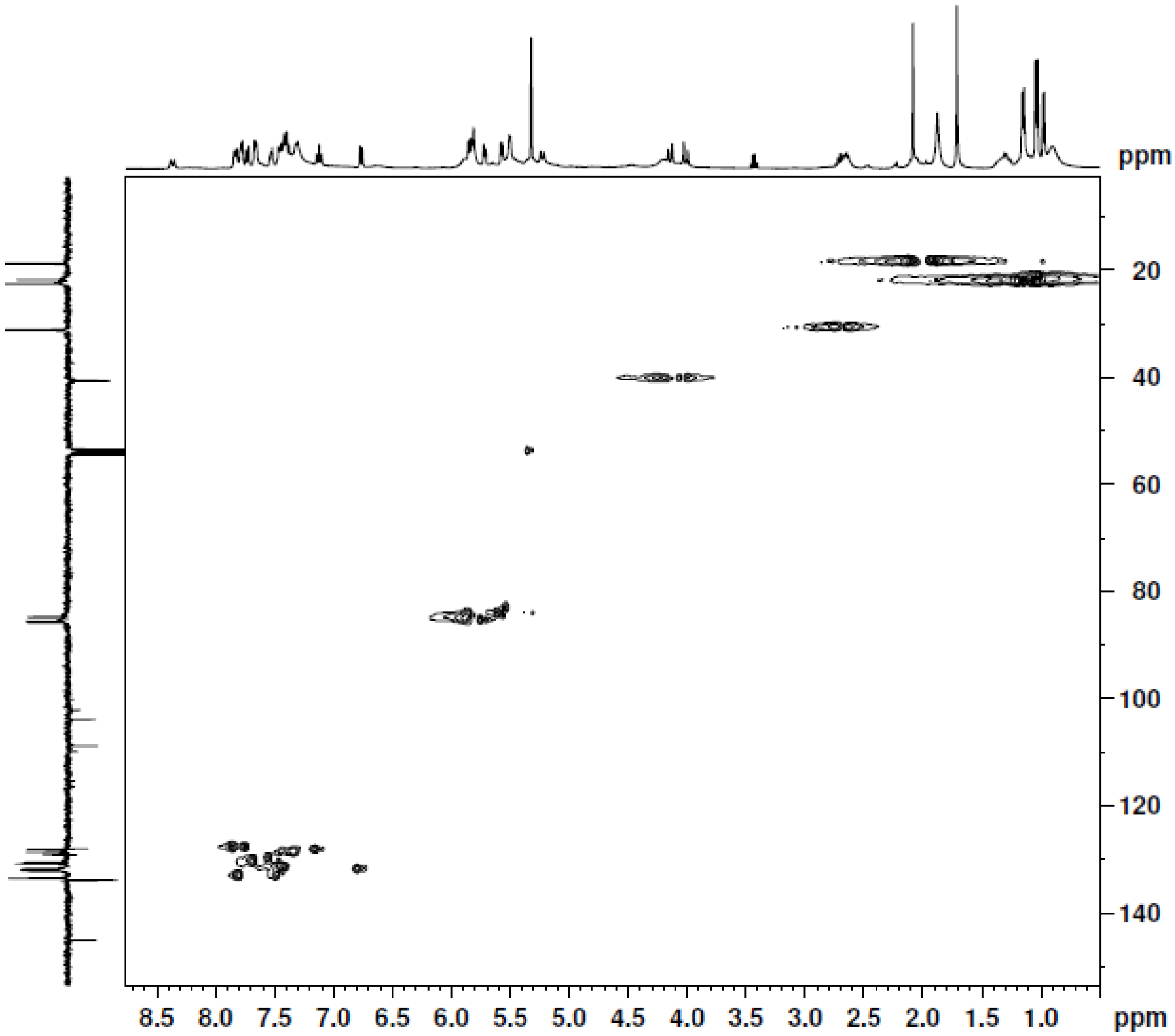

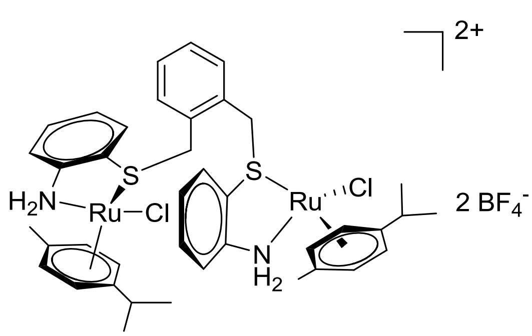

Figure S6. HSQC NMR spectrum (zoom) (CD_2Cl_2) of **2a** (X = BF_4).

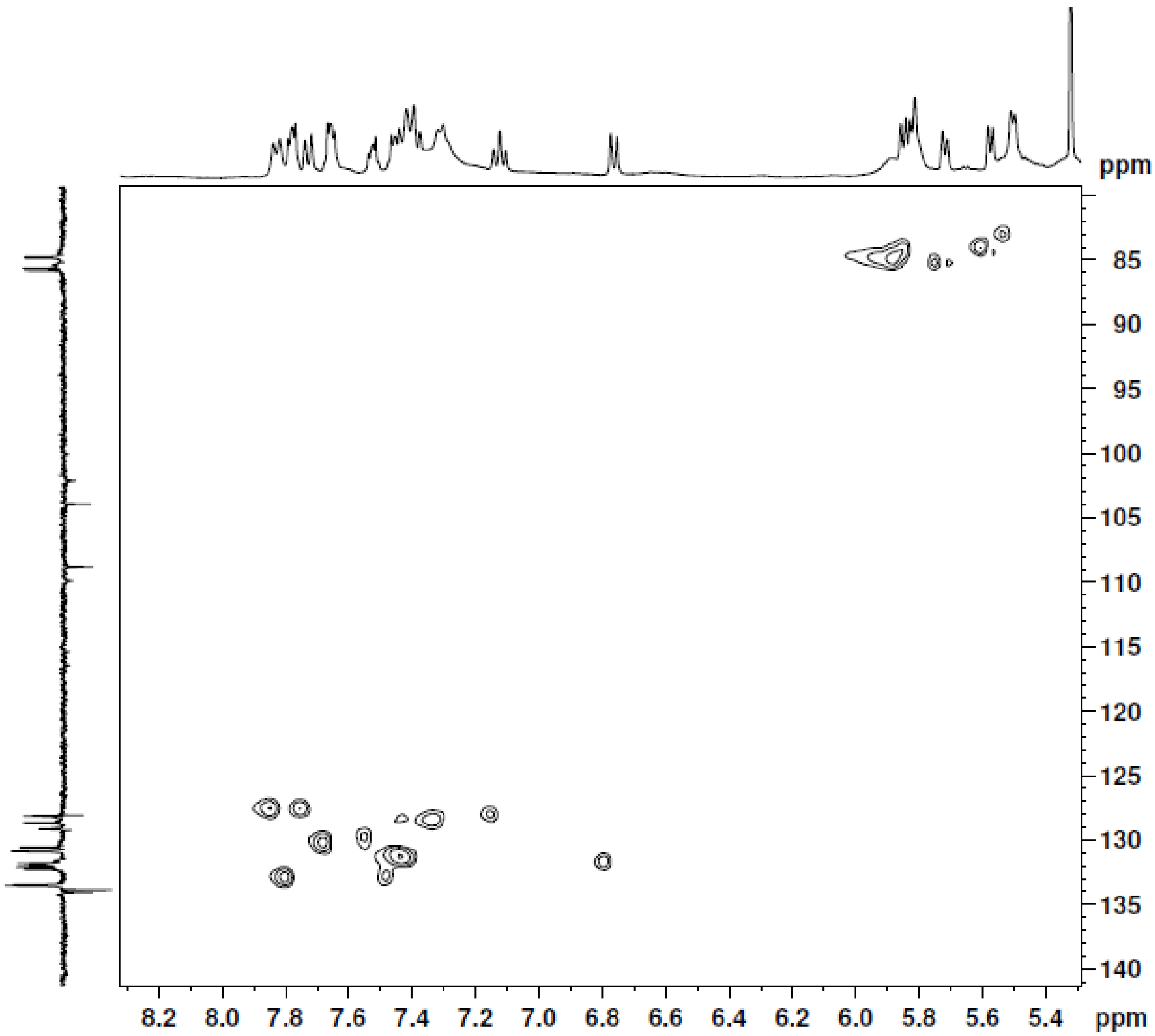

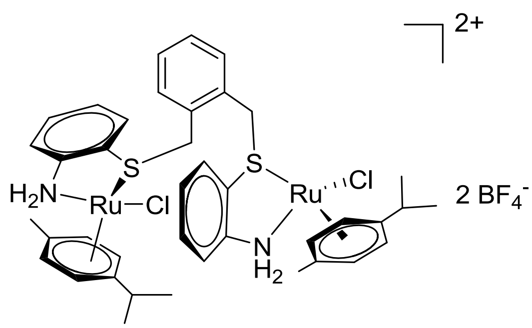

Figure S7. HMBC NMR spectrum (CD_2Cl_2) of **2a** (X = BF_4).

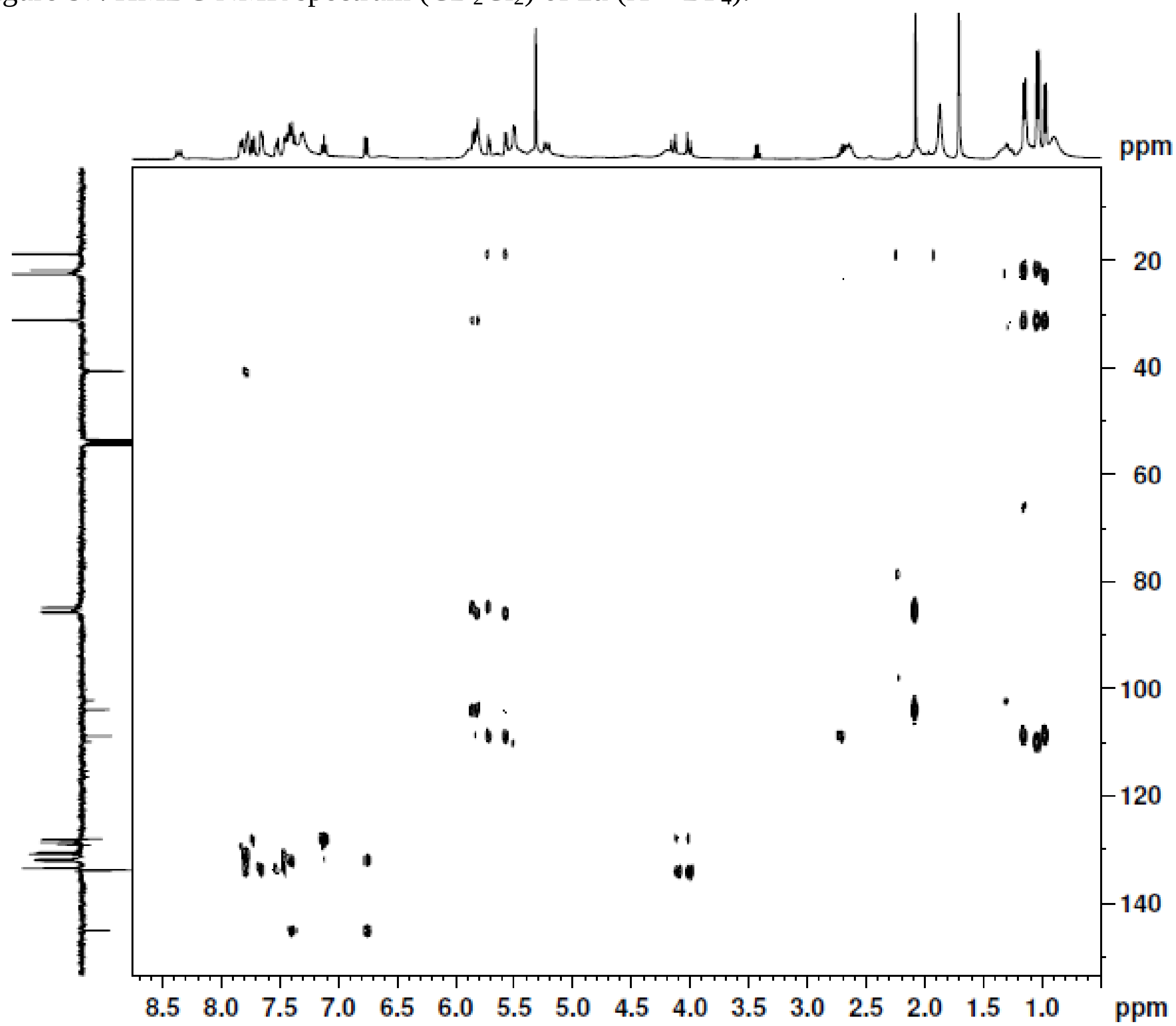

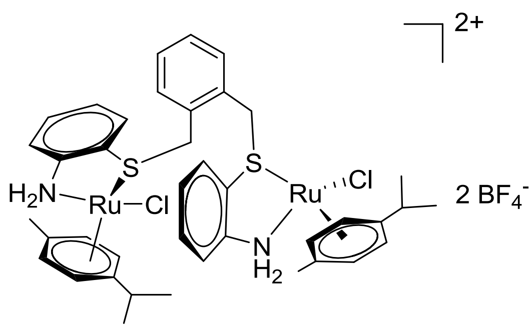

Electronic Supplementary Material (ESI) for Dalton Transactions
This journal is © The Royal Society of Chemistry 2013

Figure S8. HMBC NMR spectrum (CD_2Cl_2) of **2a** (X = BF_4).

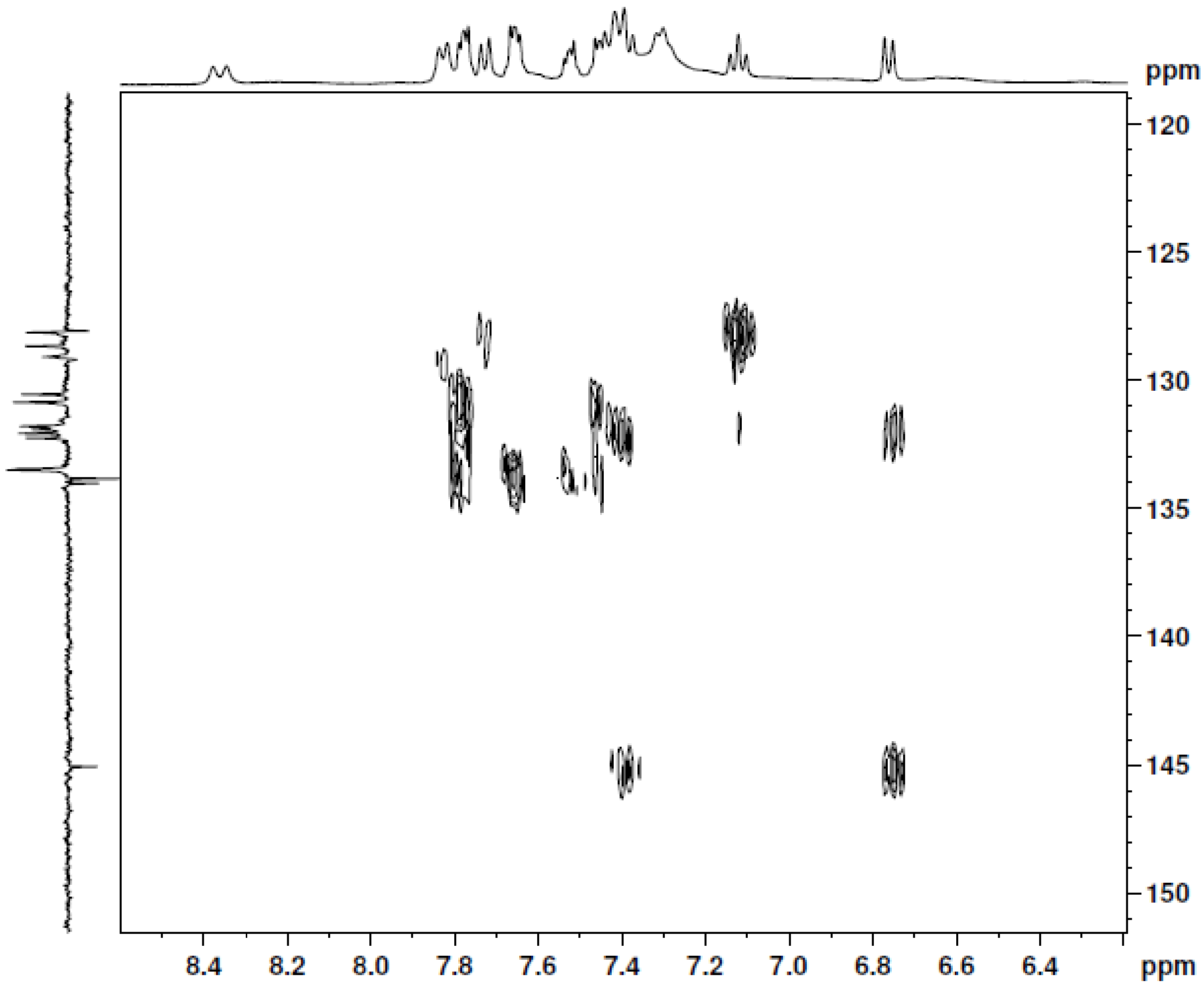

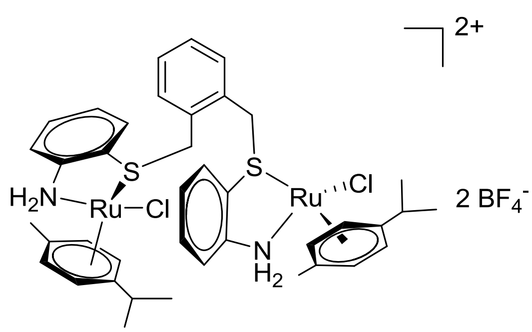

Figure S9. ^{1}H NMR spectrum (CD_2Cl_2) of **2a** (X = PF_6).

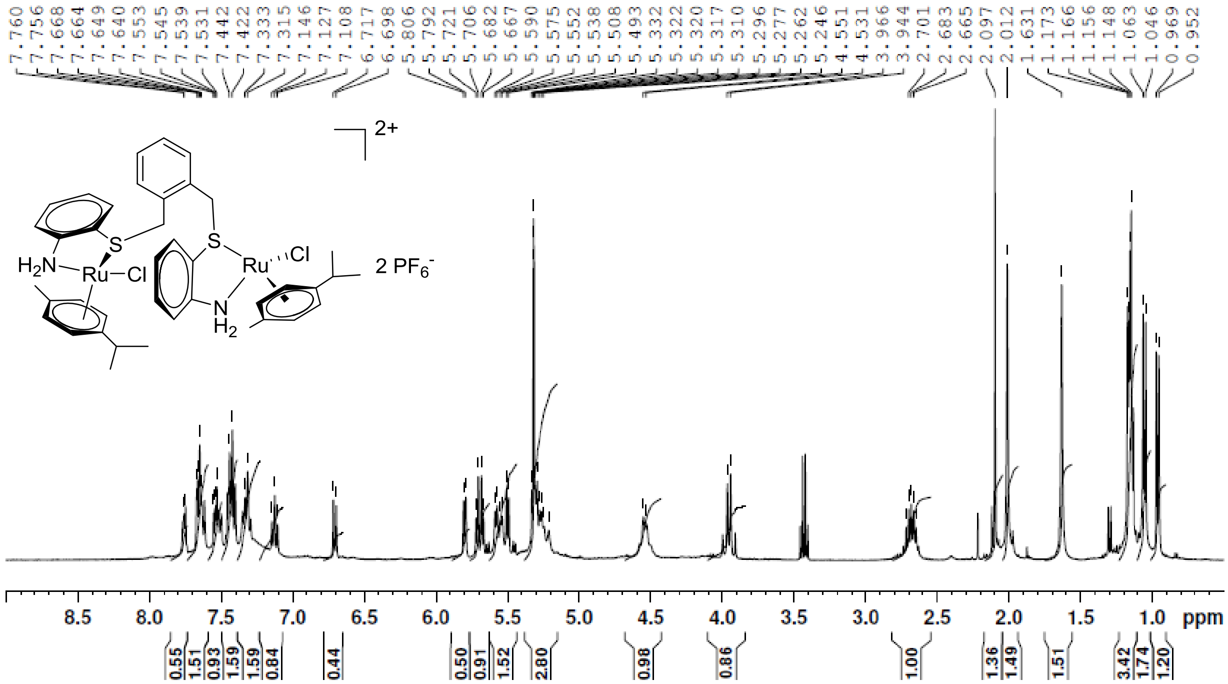

Figure S10. ^{1}H NMR spectrum (CD_2Cl_2) of **2b** (X = BF_4).

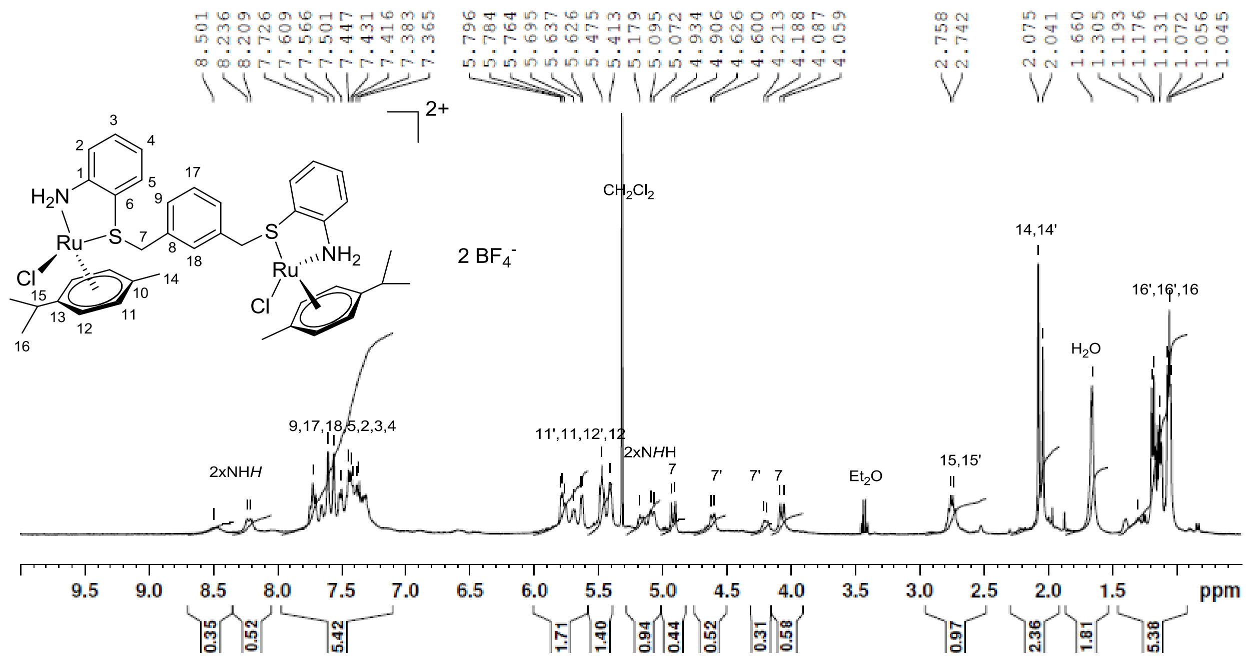

Figure S11. ^{13}C jmod NMR spectrum (CD_2Cl_2) of **2b** (X = BF_4).

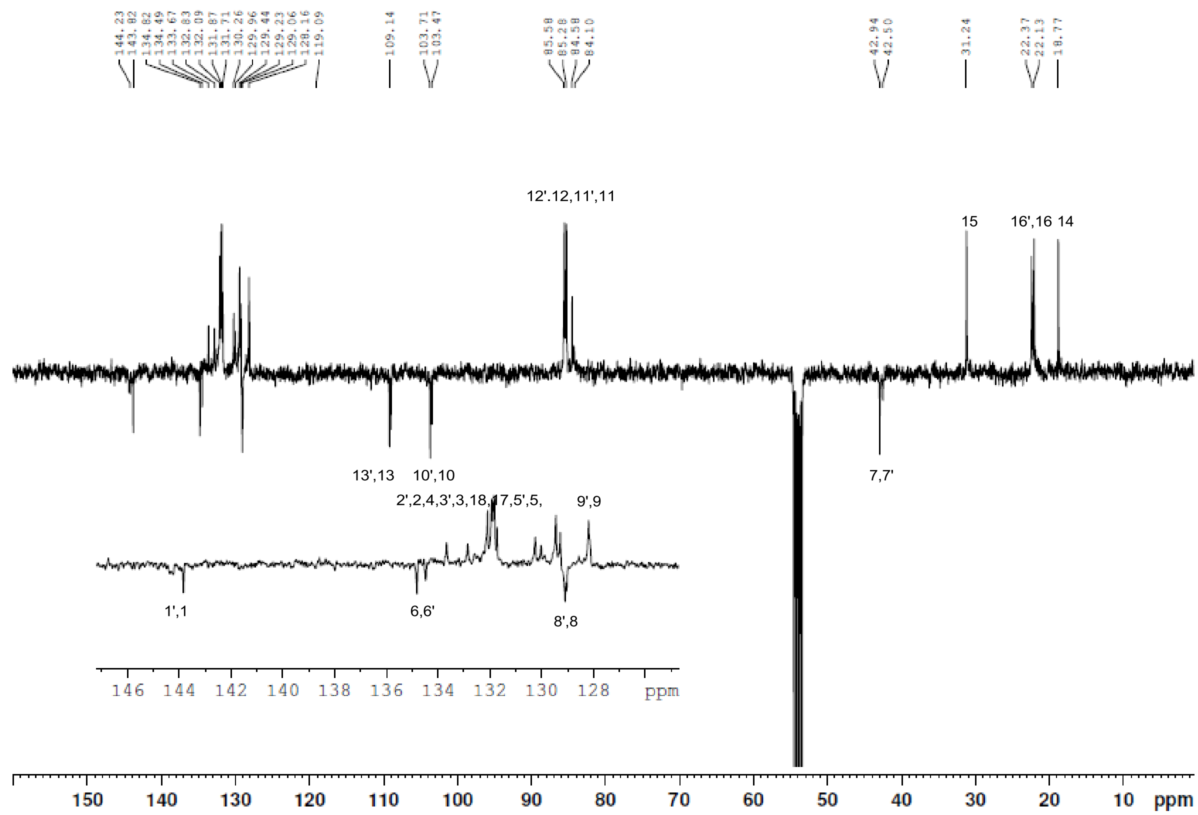

Figure S12. COSY NMR spectrum (CD_2Cl_2) of **2b** (X = BF_4).

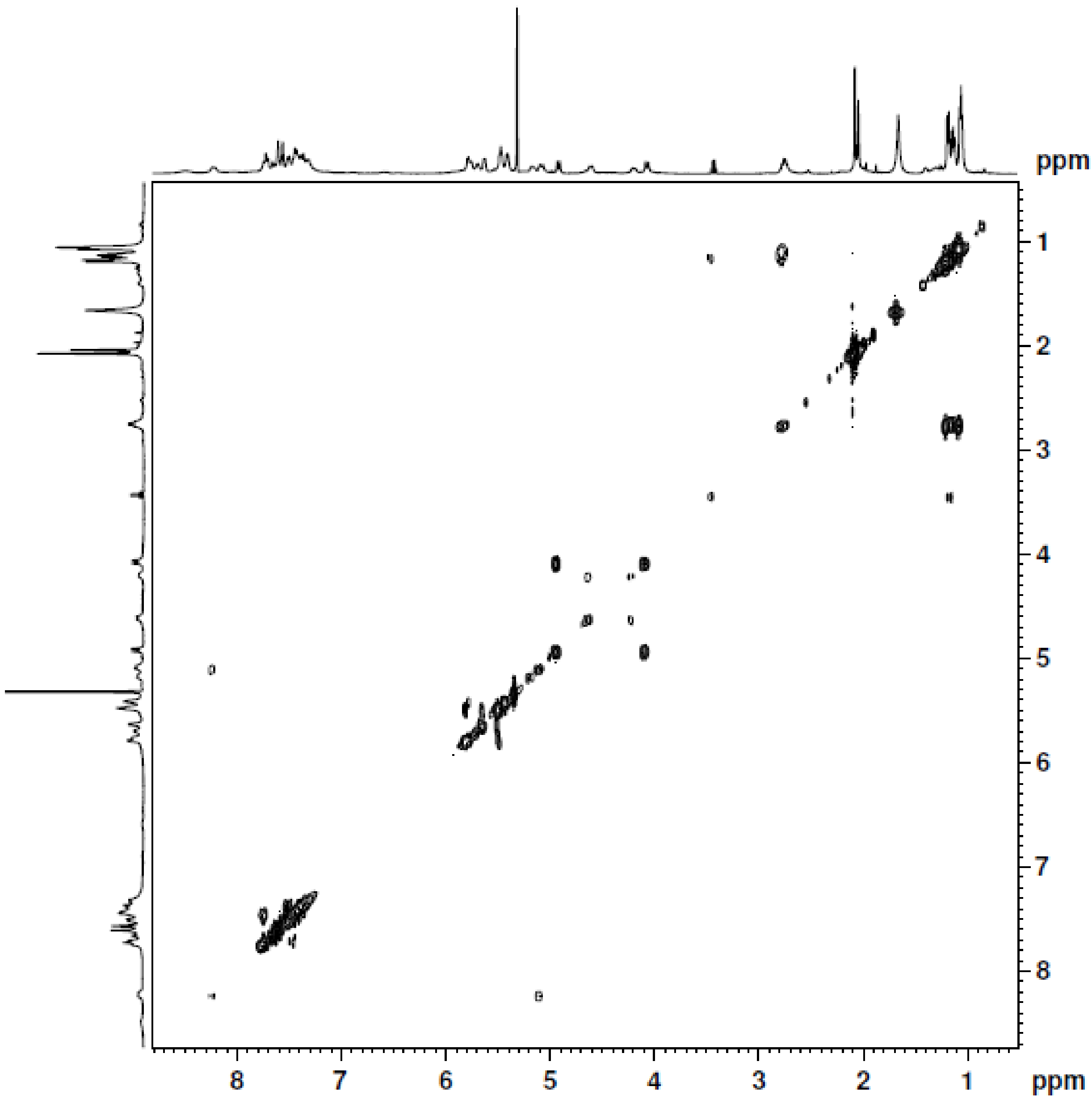

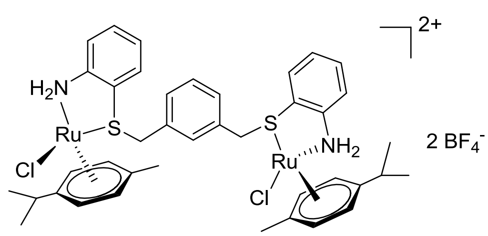

Figure S13. HSQC NMR spectrum (CD_2Cl_2) of **2b** (X = BF_4).

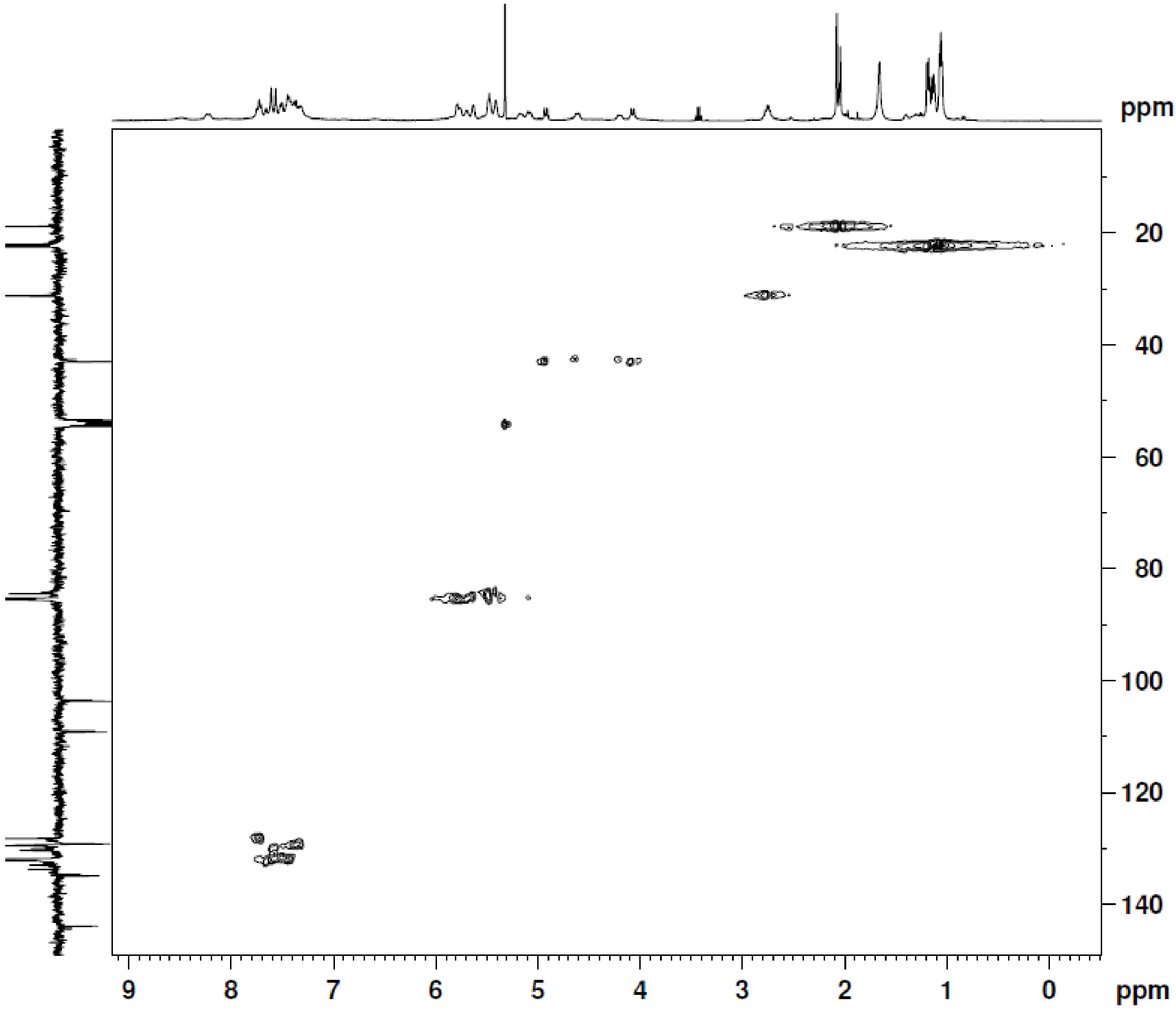

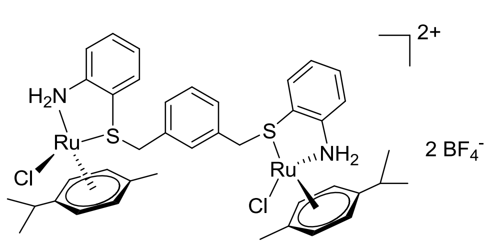

Figure S14. [1]H NMR spectrum (CD_2Cl_2) of **2b** (X = PF_6).

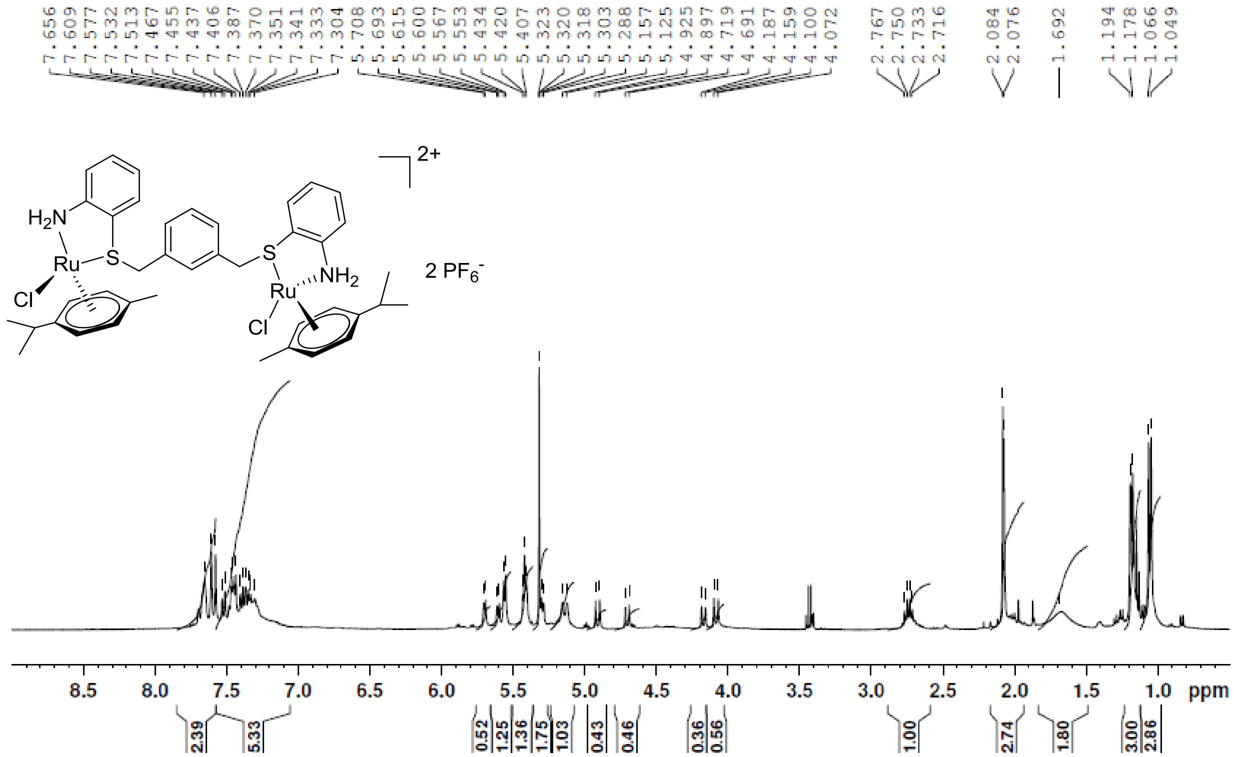

Figure S15. [13]C jmod NMR spectrum (CD_2Cl_2) of **2b** (X = PF_6).

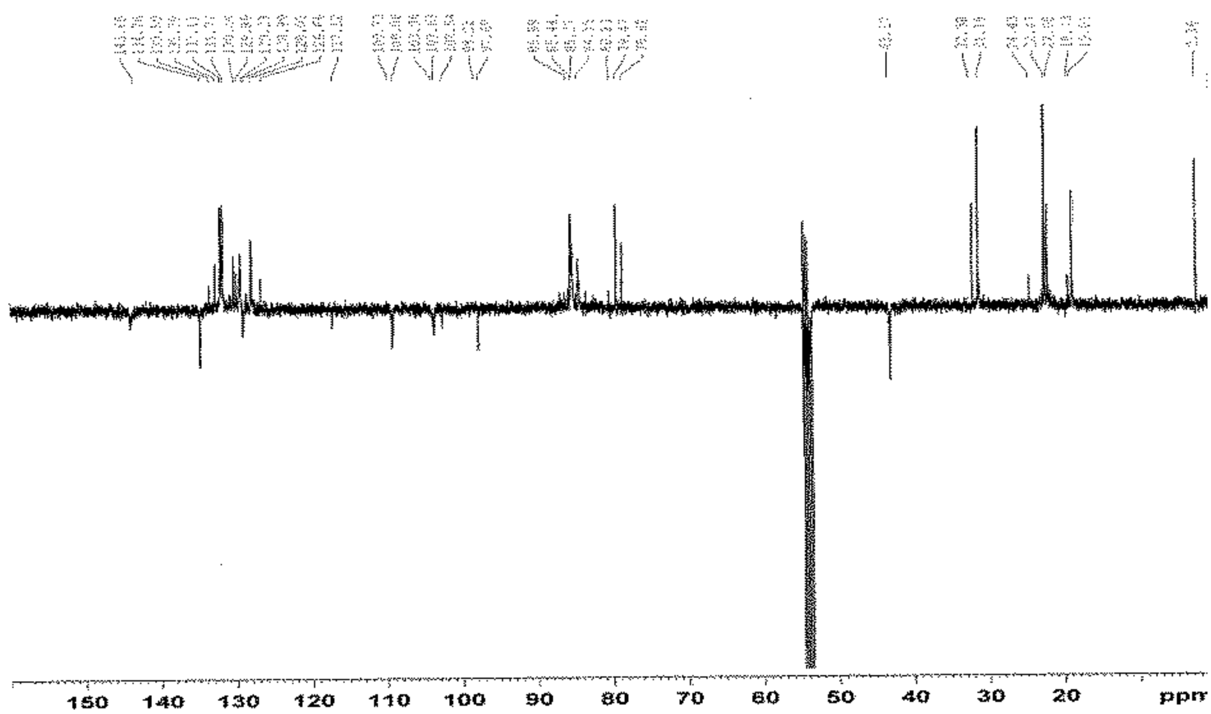

Figure S16. [1]H NMR spectrum (CD_2Cl_2) of **2c** (X = BF_4).

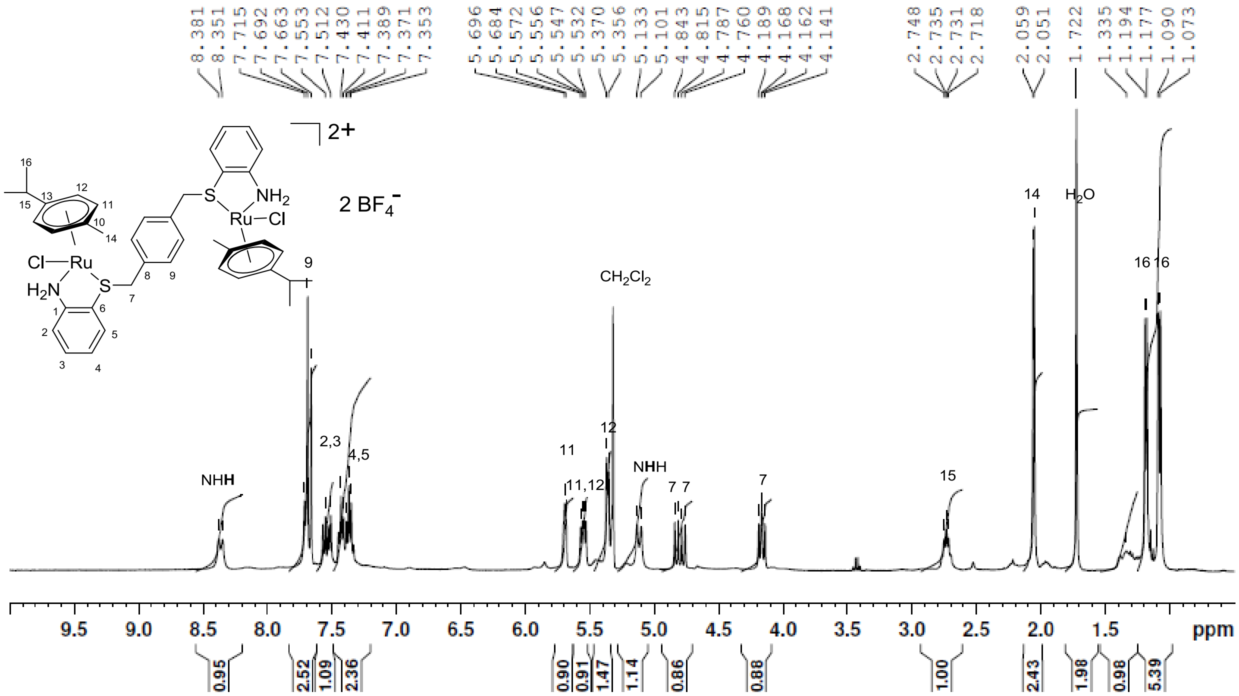

Figure S17. [13]C jmod NMR spectrum (CD_2Cl_2) of **2c** (X = BF_4).

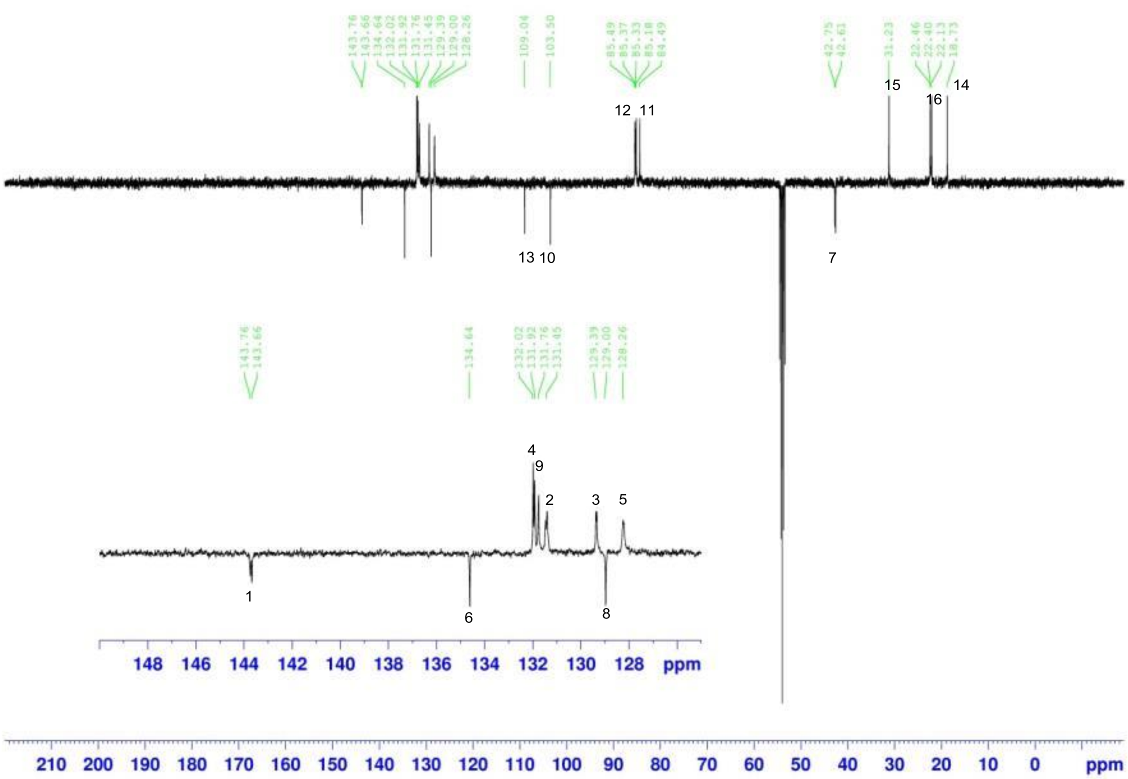

Figure S18. COSY NMR spectrum (CD_2Cl_2) of **2c** (X = BF_4).

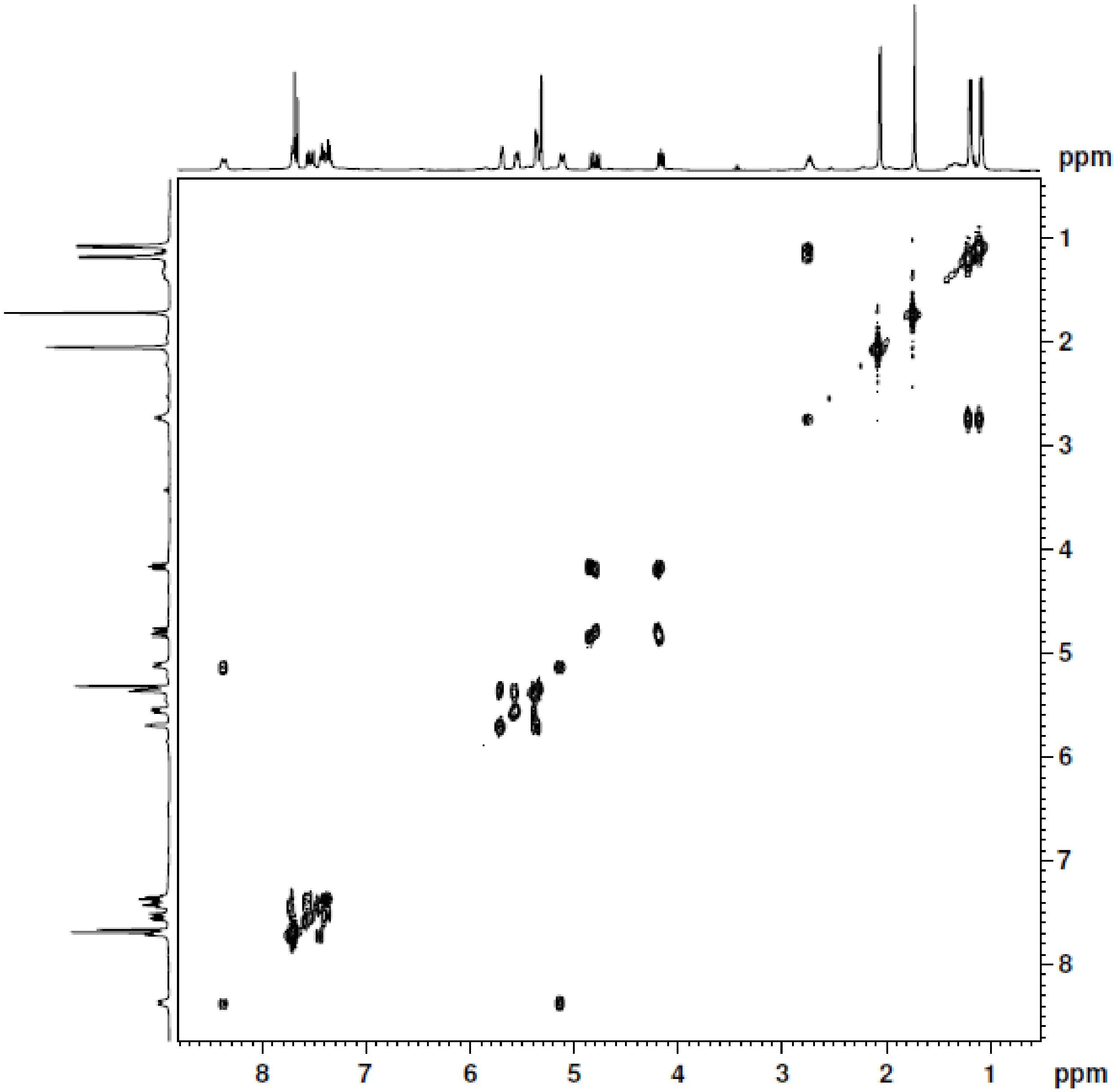

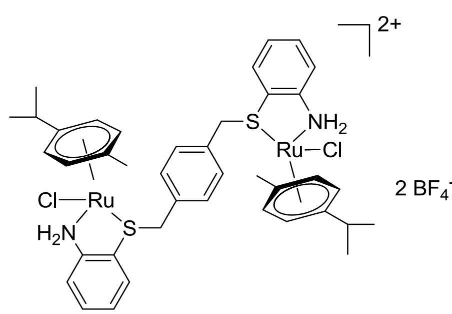

Figure S19. HSQC NMR spectrum (CD_2Cl_2) of **2c** (X = BF_4).

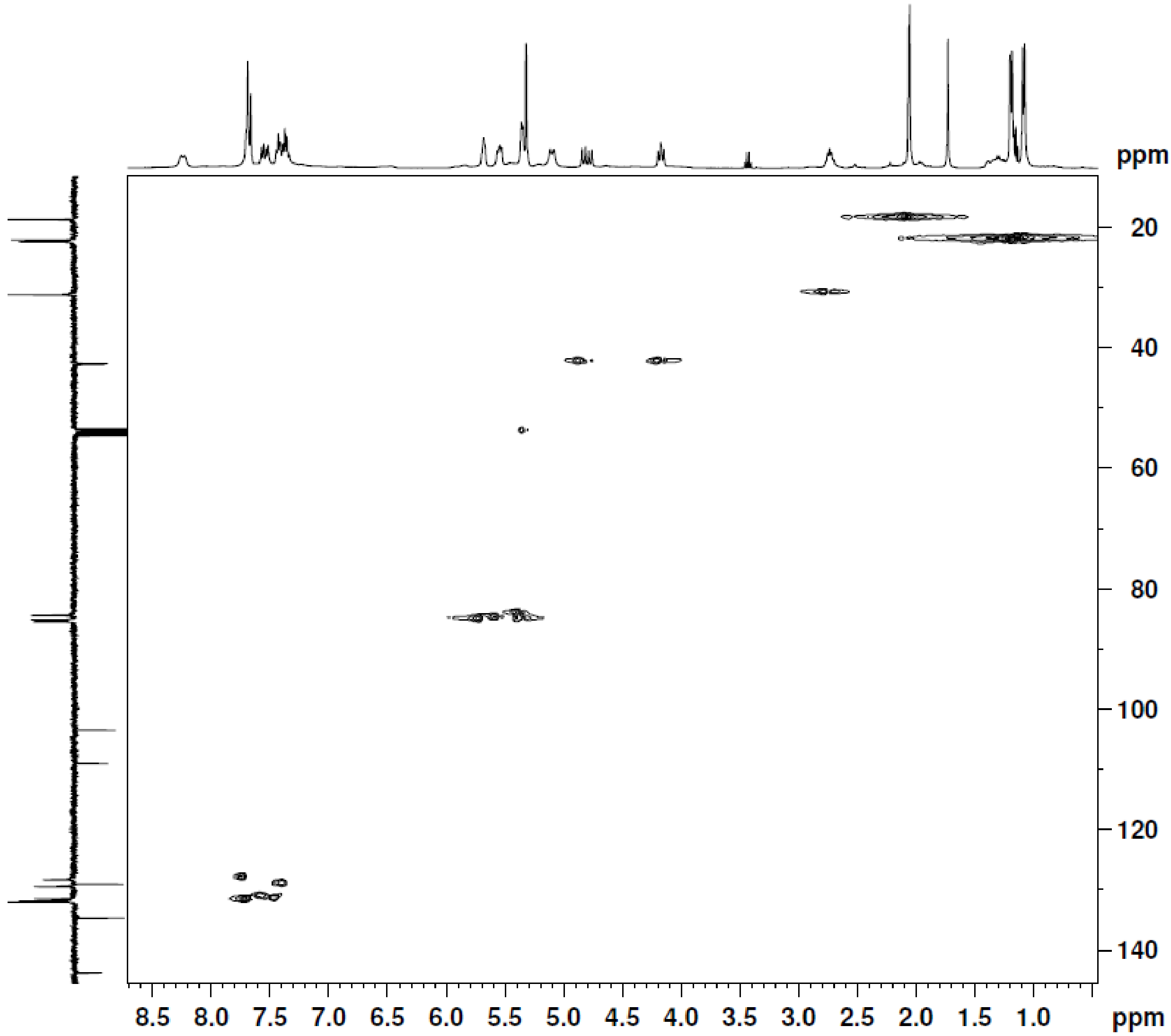

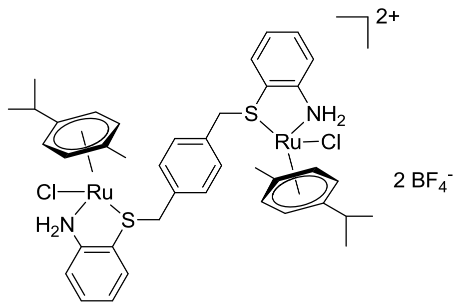

Figure S20. HMBC NMR spectrum (CD_2Cl_2) of **2c** (X = BF_4).

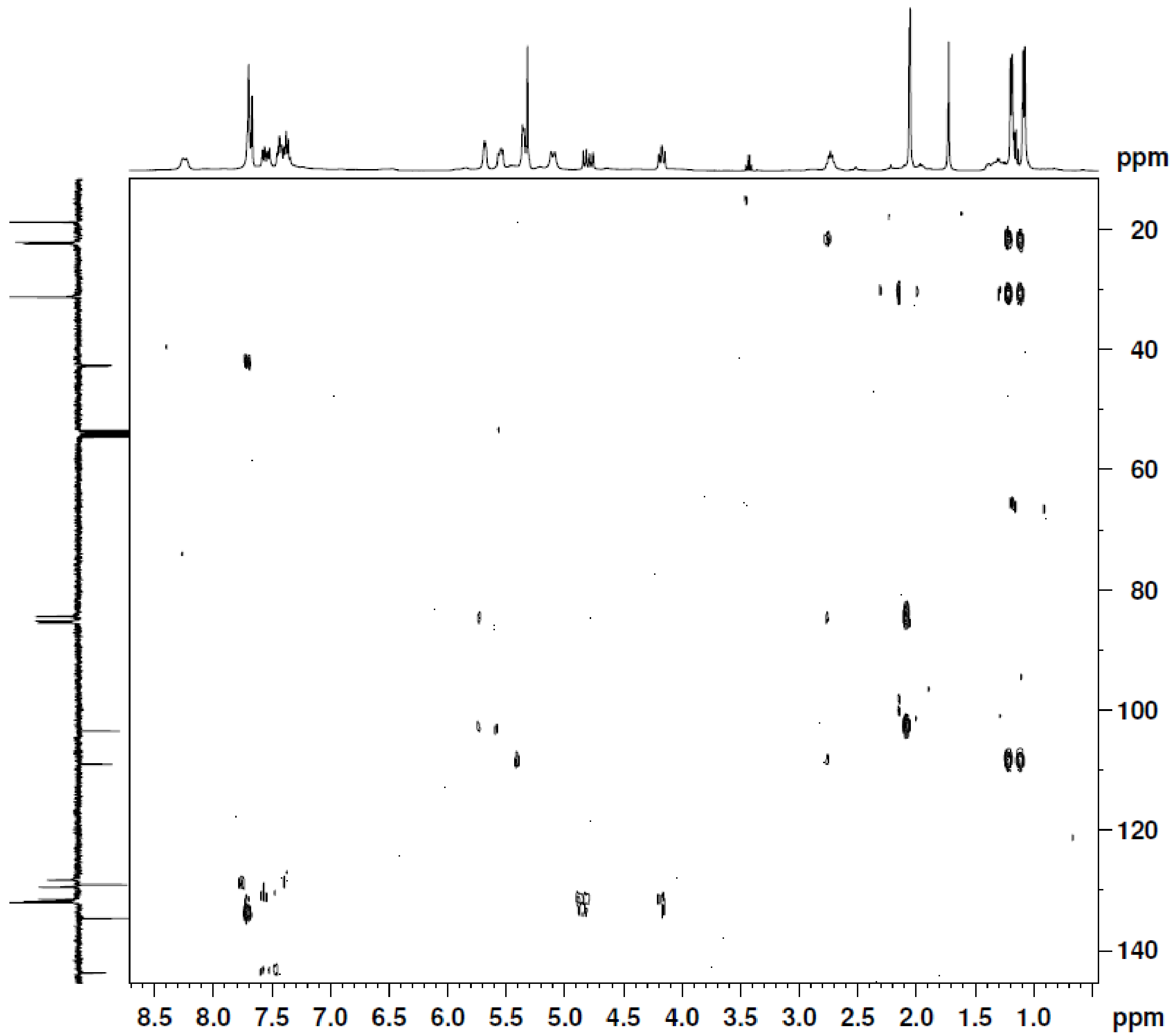

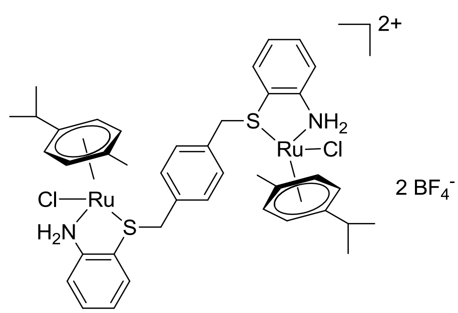

Figure S21. [1]H NMR spectrum (CD_2Cl_2) of **2c** (X = PF_6).

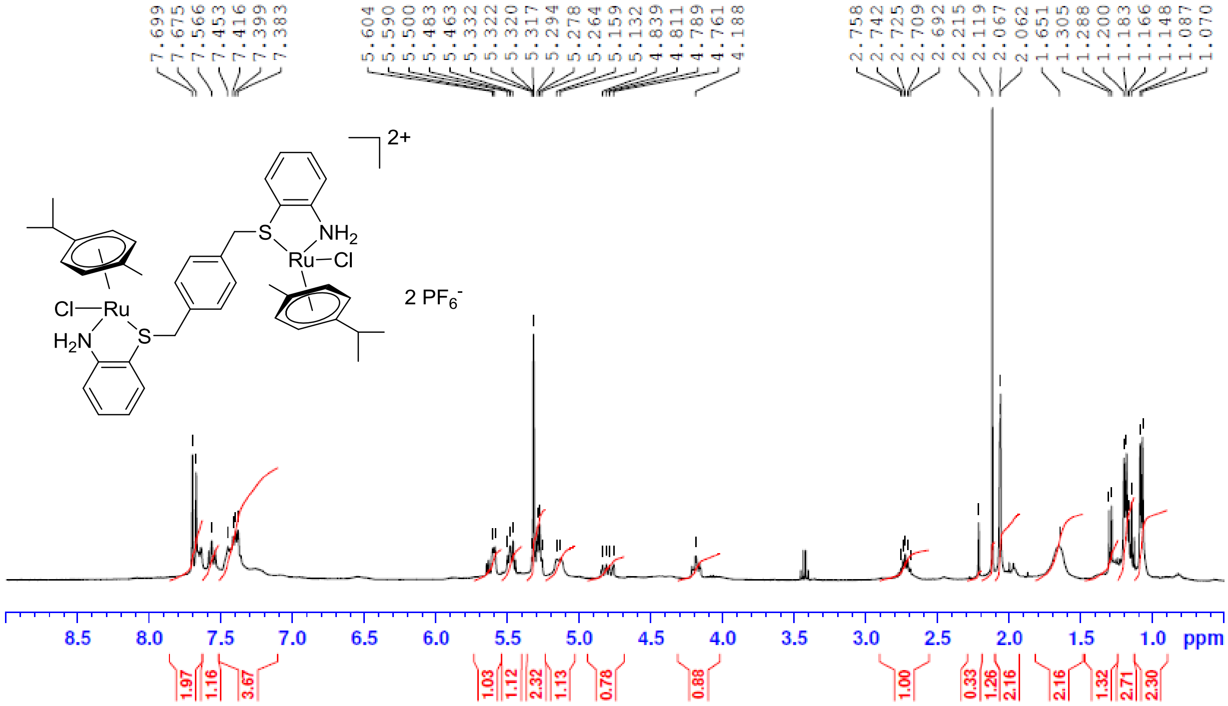

Figure S22. [1]H NMR spectrum (DMSO-d$_6$) of **3** (X = BF_4).

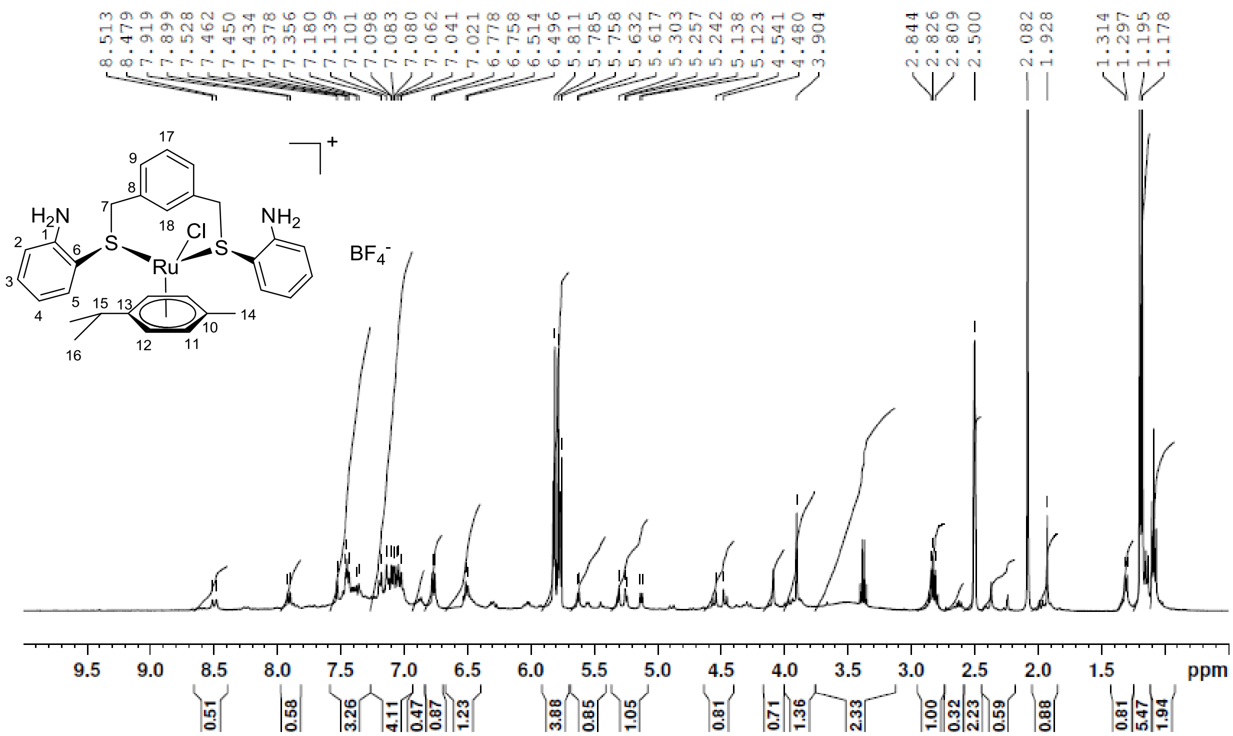

Figure S23. [13]C jmod NMR spectrum (DMSO-d$_6$) of **3** (X = BF_4).

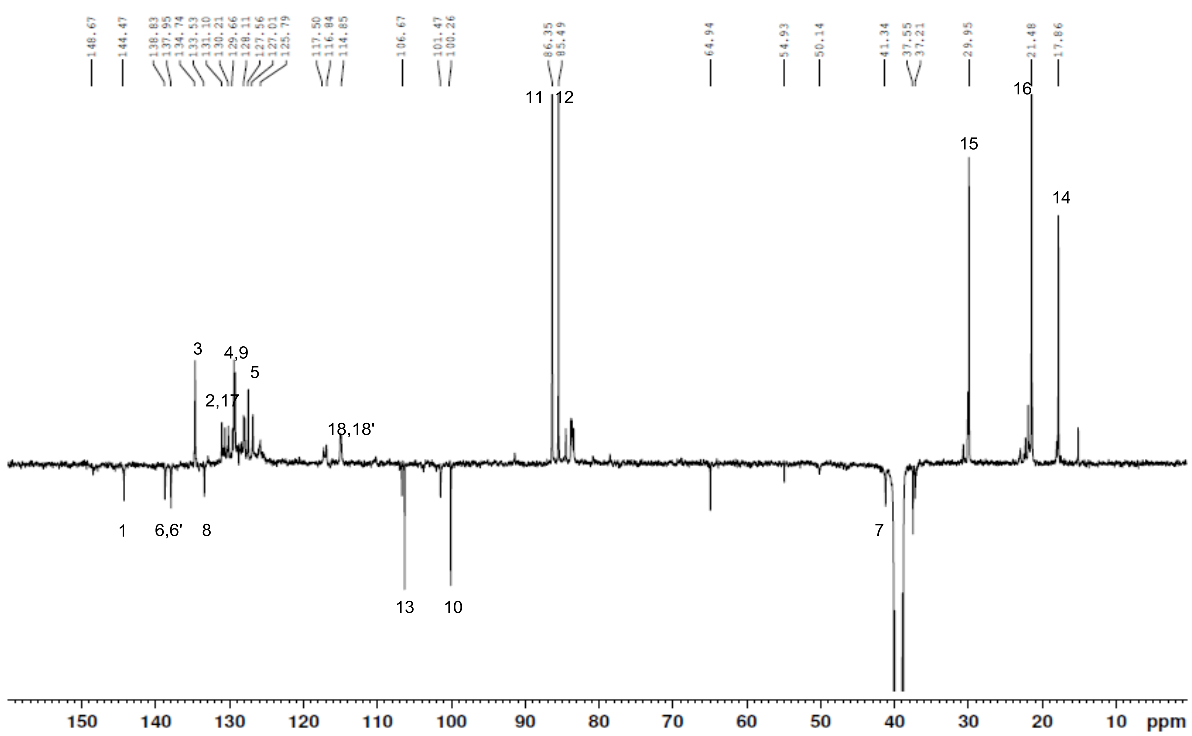

Contains the minor compound **3-*anti*** (not labelled).

Figure S24. COSY NMR spectrum (DMSO-d_6) of **3** (X = BF_4).

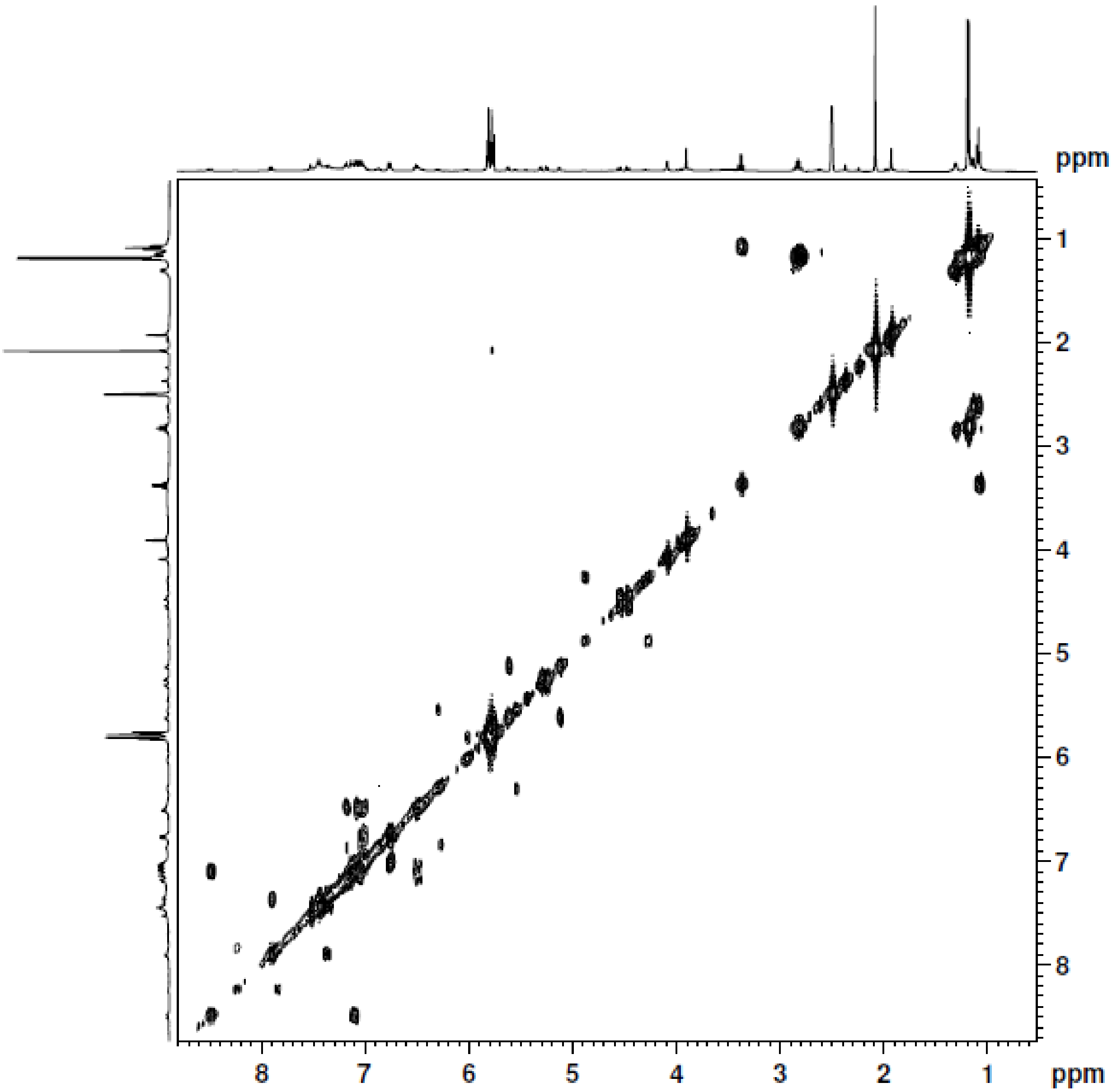

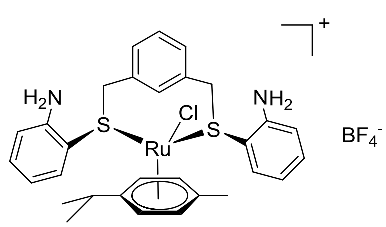

Figure S25. COSY NMR spectrum (zoom) (DMSO-d$_6$) of **3** (X = BF_4).

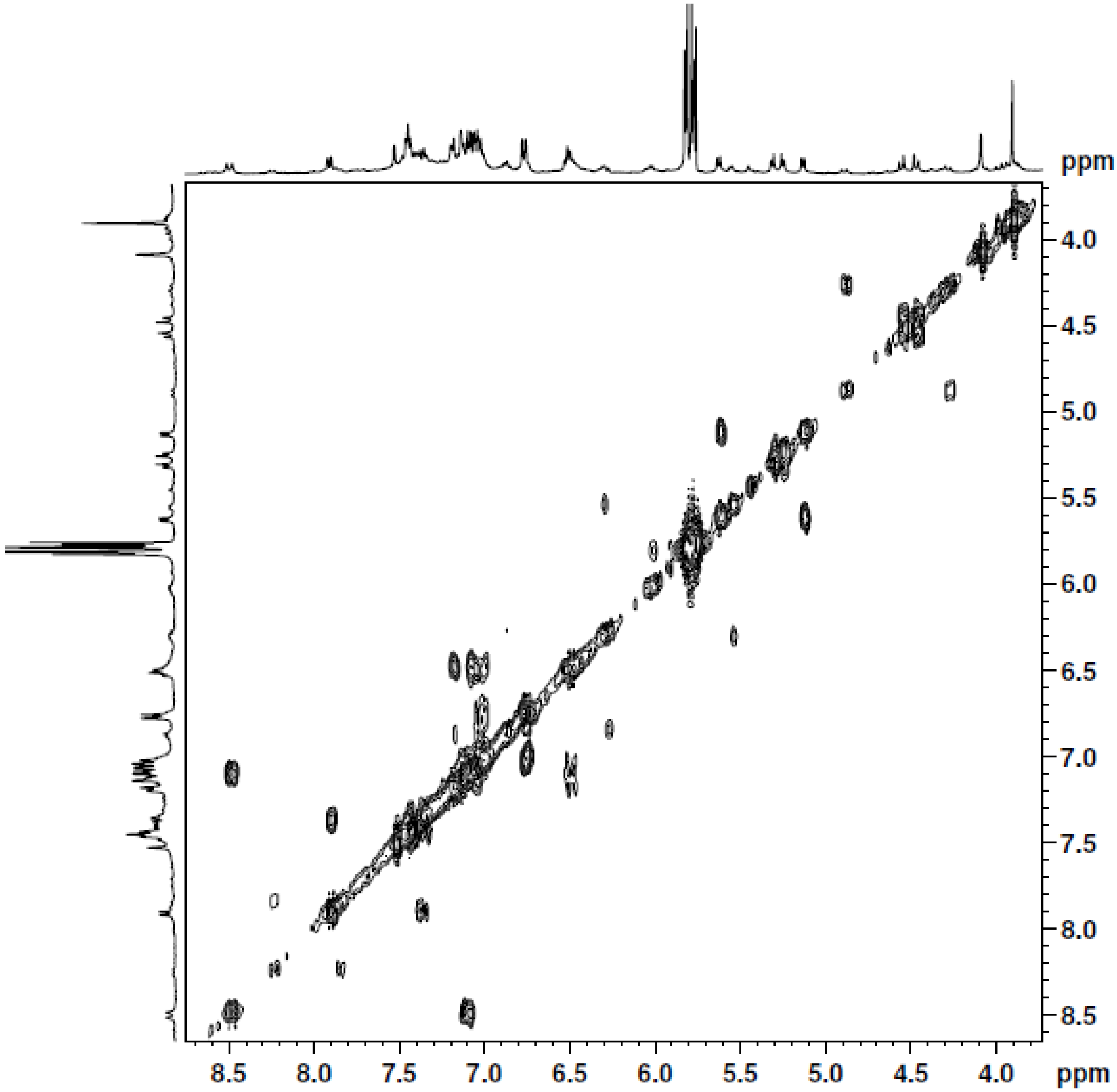

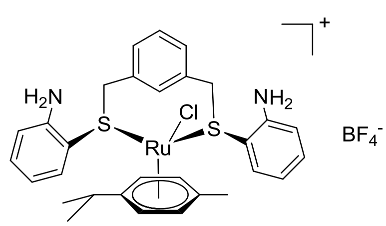

Electronic Supplementary Material (ESI) for Dalton Transactions

Figure S26. HSQC NMR spectrum (DMSO-d$_6$) of **3** (X = BF_4).

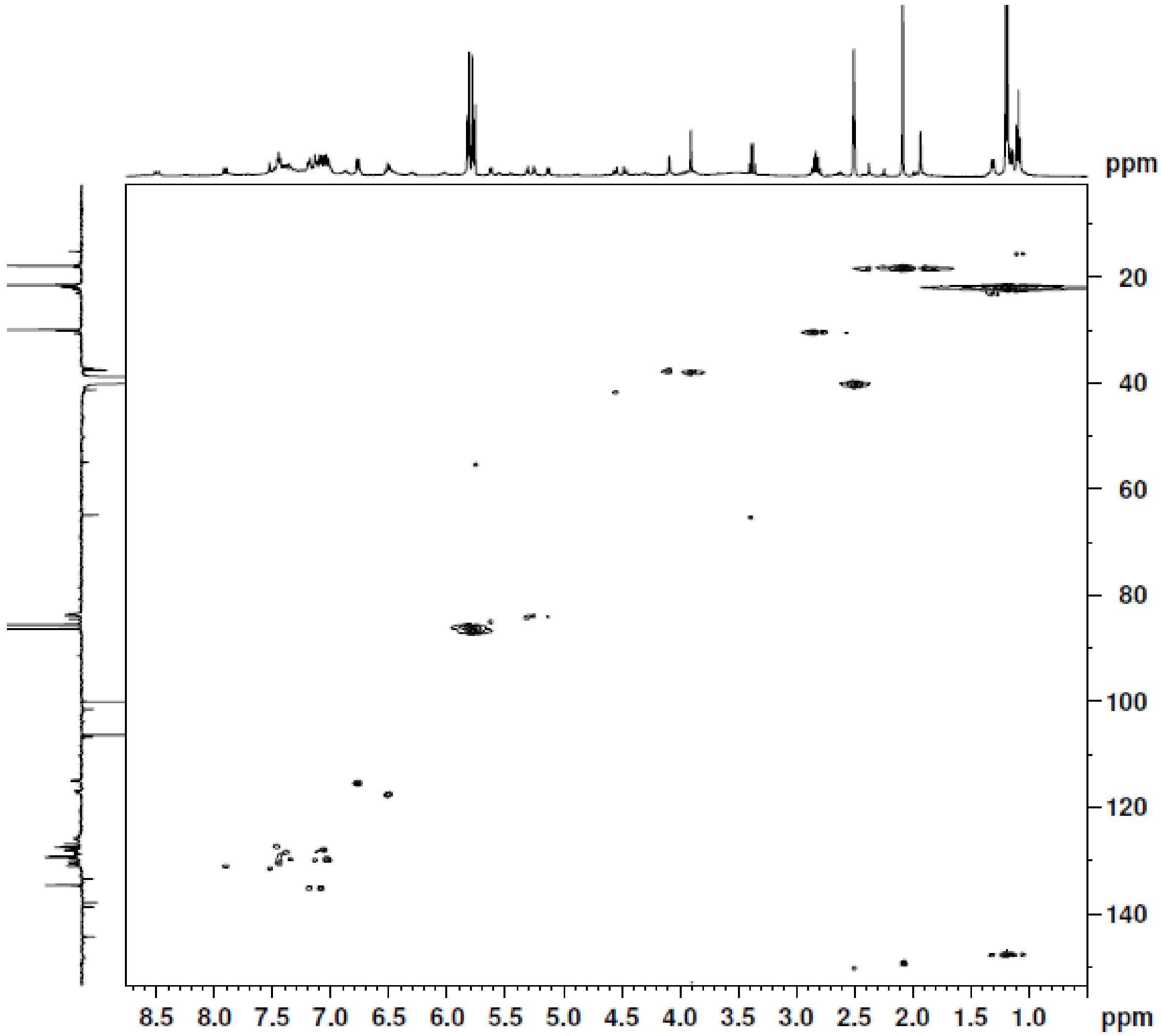

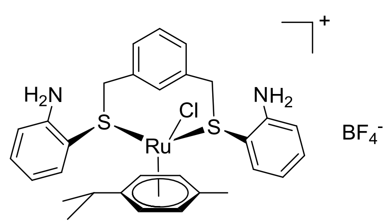

Figure S27. HSQC NMR spectrum (zoom) (DMSO-d_6) of **3** (X = BF_4).

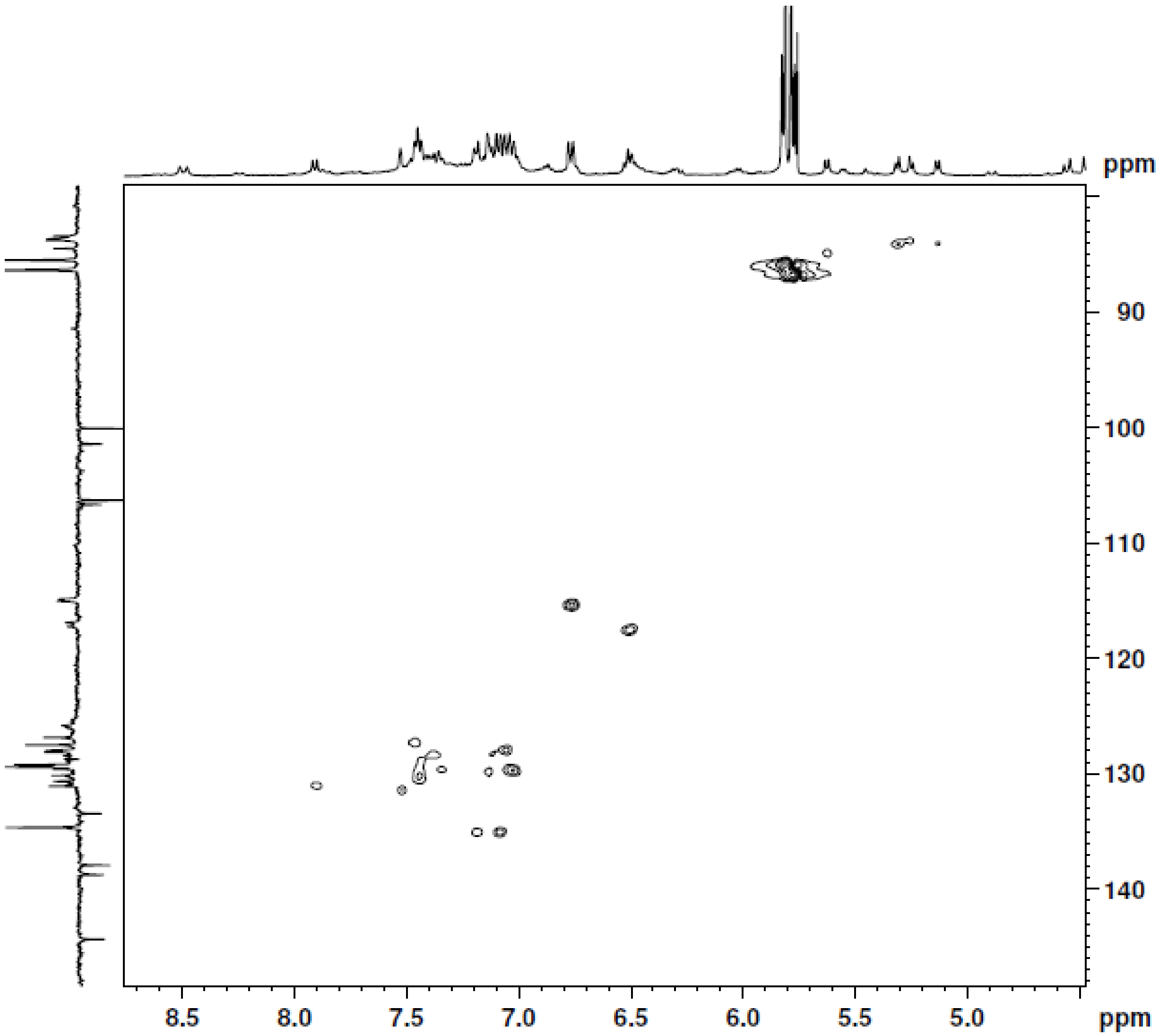

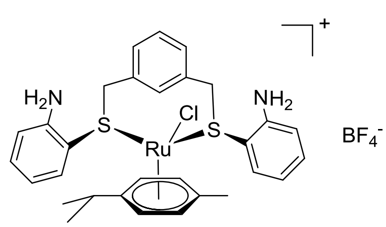

Electronic Supplementary Material (ESI) for Dalton Transactions

Figure S28. HMBC NMR spectrum (DMSO-d_6) of **3** (X = BF_4).

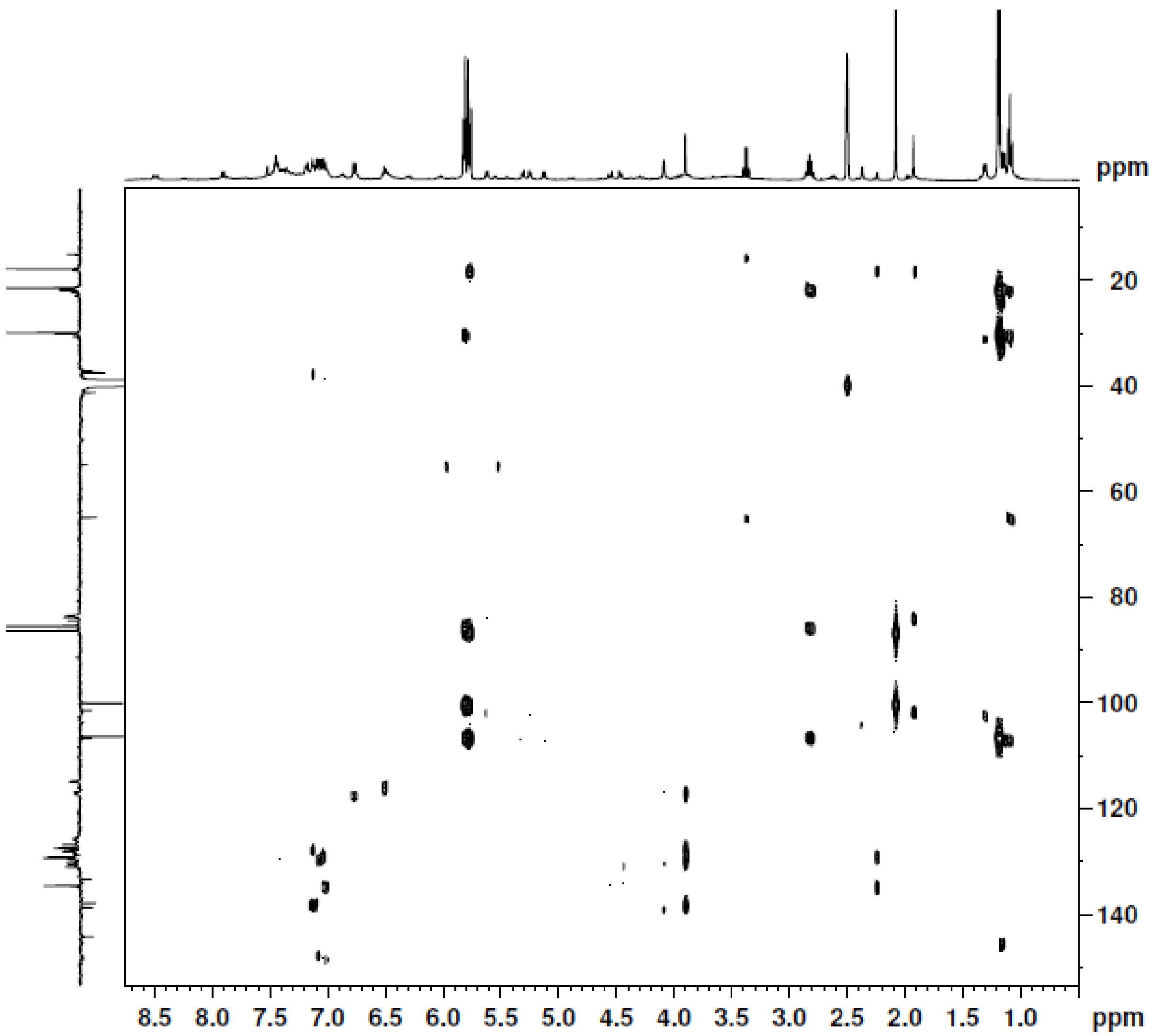

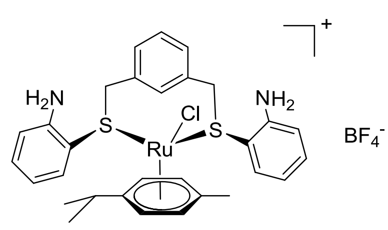

General Information on UPLC-MSMS

Instrument: Waters XevoG2 UPLC-MSMS

Column: Acquity UPLC BEH C18 1.7µm, 2.1 x 50 mm

ESI Naformate_positive mode

Enhance accurate mass range 50 to 1,200 m/z

Capillary 0.8 kV

Sampling cone 5 to 35.0 V

Source T: 100°C

Desolvation T: 550°C

Cone gas flow: 50 L/h

Desolvation gas flow: 1,000 L/h

Solvent: 90 Vol% CAN : 10Vol% water plus 0.1wt% formic acid

HRMS results were calibrated for leucine enkephalin lock masses 278.1141 *m/z* and 556.2771 *m/z* for **2a** (X = BF_4), **2b** (X = PF_6) and **2c** (X = PF_6).

Theoretical isotope pattern based on MassLynx software package using the following masses:

H Hydrogen

Rel. Abundance	Mass (amu)
99.9885	1.00782503
0.0115	2.01410178

N Nitrogen

Rel. Abundance	Mass (amu)
99.6360	14.00307401
0.3640	15.00010897

C Carbon

Rel. Abundance	Mass (amu)
98.9300	12.00000000

1.0700	13.00335484

O Oxygen

Rel. Abundance	Mass (amu)
99.7570	15.99491462
0.0380	16.99913150
0.2050	17.99916040

S Sulfur

Rel. Abundance	Mass (amu)
94.9900	31.97207073
0.7500	32.97145854
4.2500	33.96786687
0.0100	35.96708088

Cl Chlorine

Rel. Abundance	Mass (amu)
75.7600	34.96885271
24.2400	36.96590260

Ru Ruthenium

Rel. Abundance	Mass (amu)
5.5400	95.90760400
1.8700	97.90528700
12.7600	98.90593850
12.6000	99.90421890
17.0600	100.90558150
31.5500	101.90434880
18.6200	103.90543000

Figure S29. UPLC-MS chromatogram of **2a** ($X = PF_6$) – low energy ionization

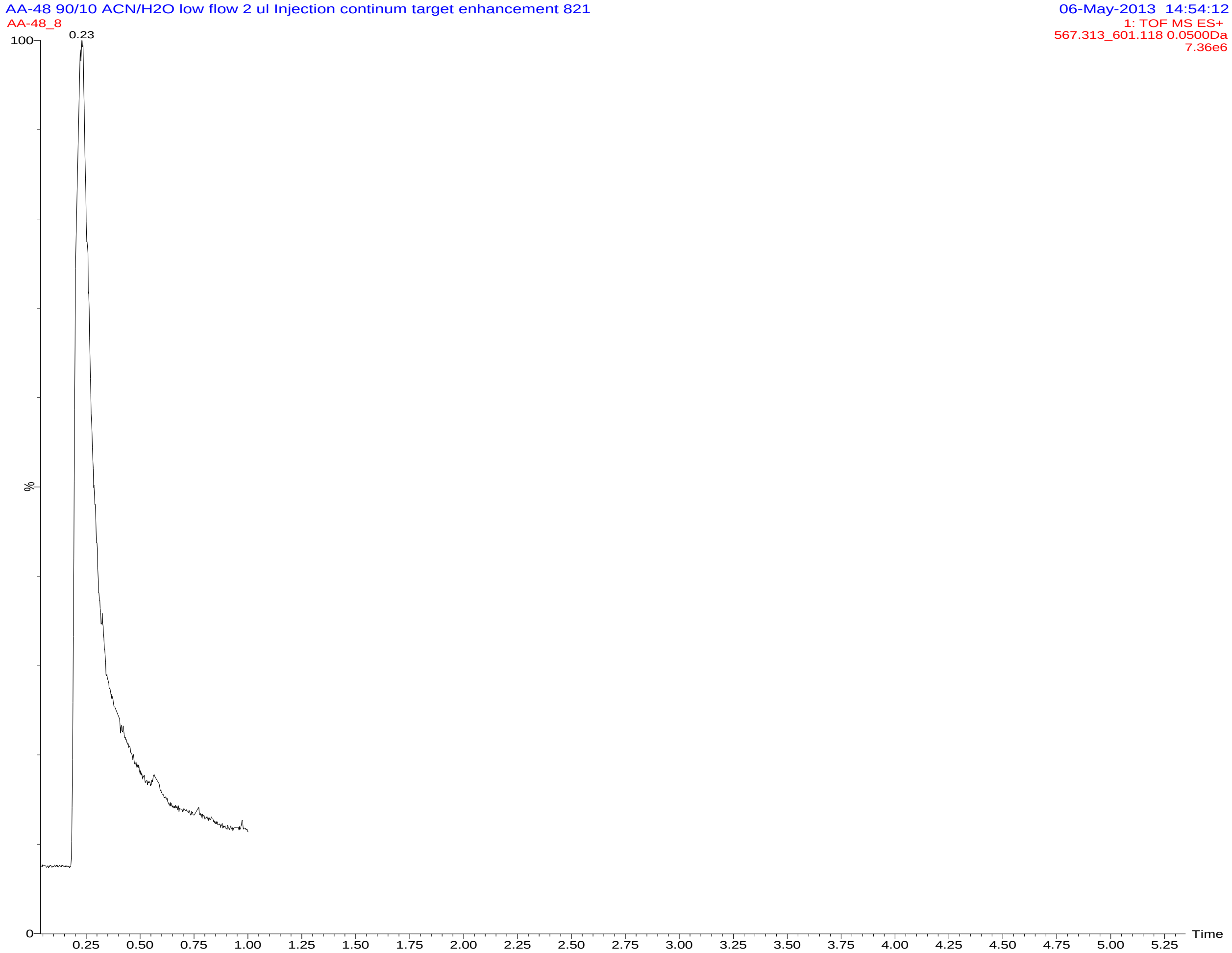

Figure S 30. HRMS of **2a** ($X = PF_6$) – low energy ionization

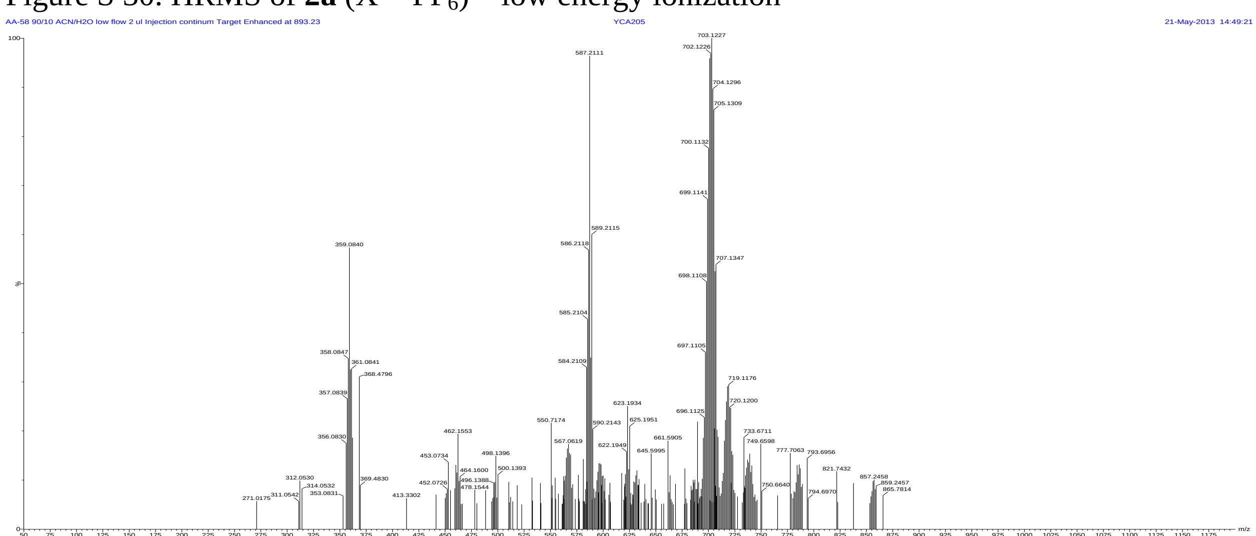

Figure S31. HRMS of **2a** (X = PF_6) signal 893 *m/z* (full); theoretical results above, experiment below – low energy ionization

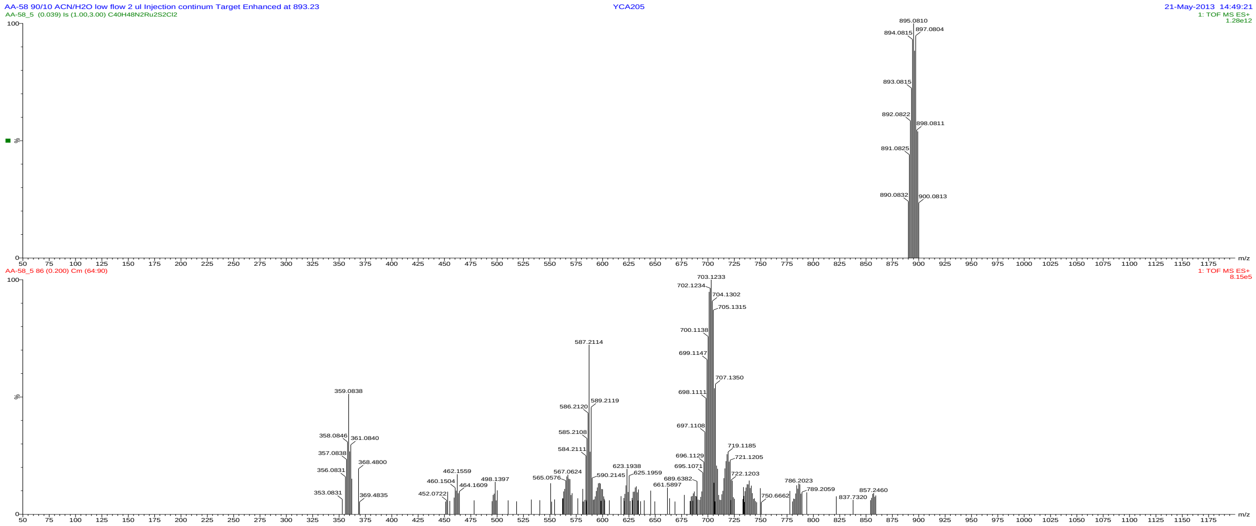

Figure S32. HRMS of **2a** (X = PF_6) signal 893 *m/z* (zoom); theoretical results above, experiment below – low energy ionization

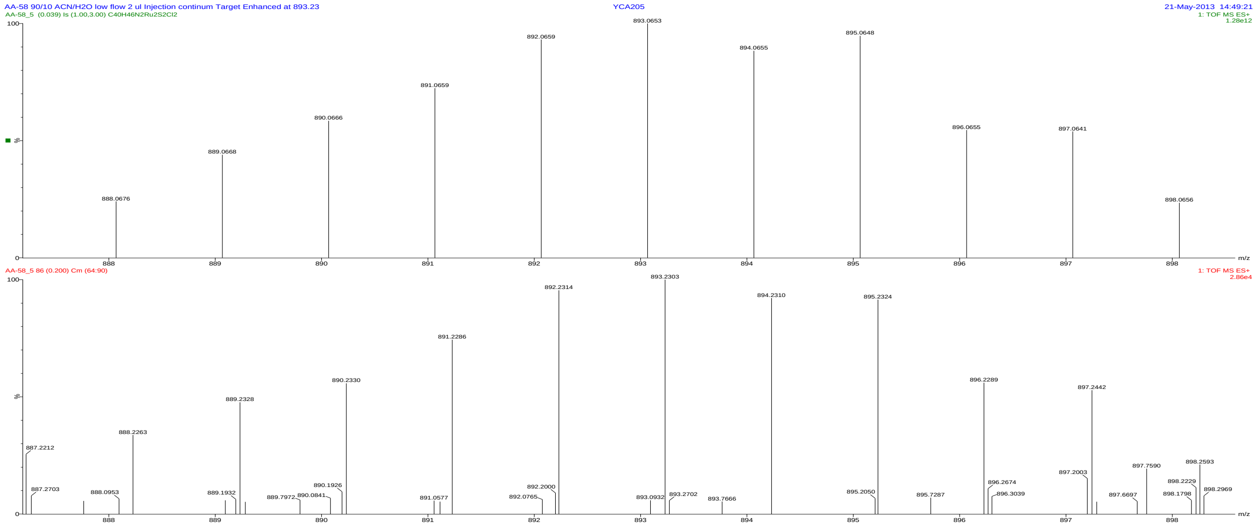

Figure S33. HRMS of **2a** (X = PF_6) signal 857 *m/z* (full); theoretical results above, experiment below – low energy ionization

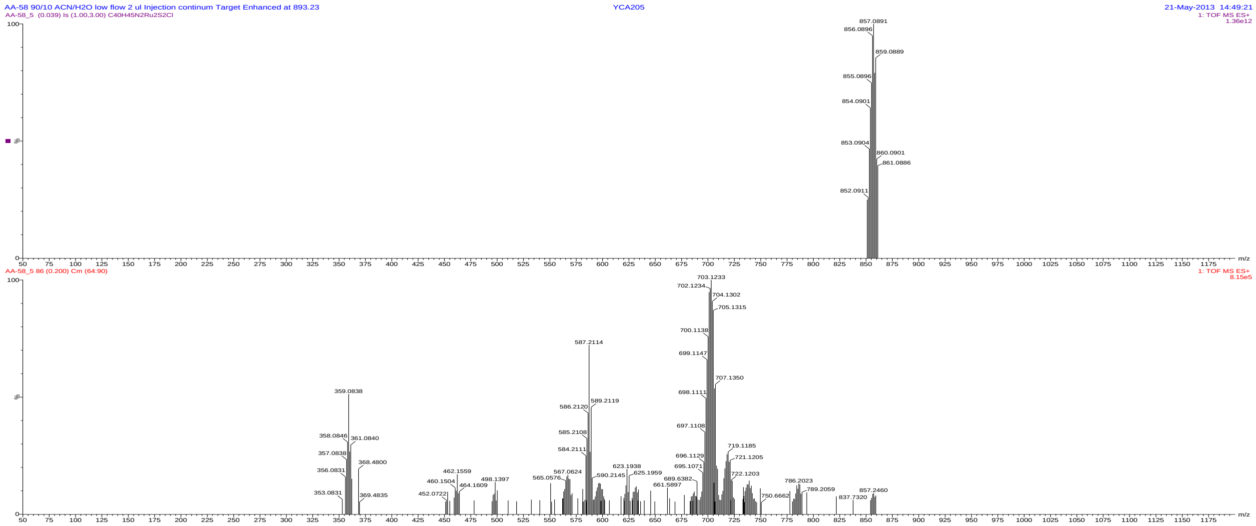

Figure S34. HRMS of **2a** (X = PF_6) signal 857 *m/z* (zoom); theoretical results above, experiment below – low energy ionization

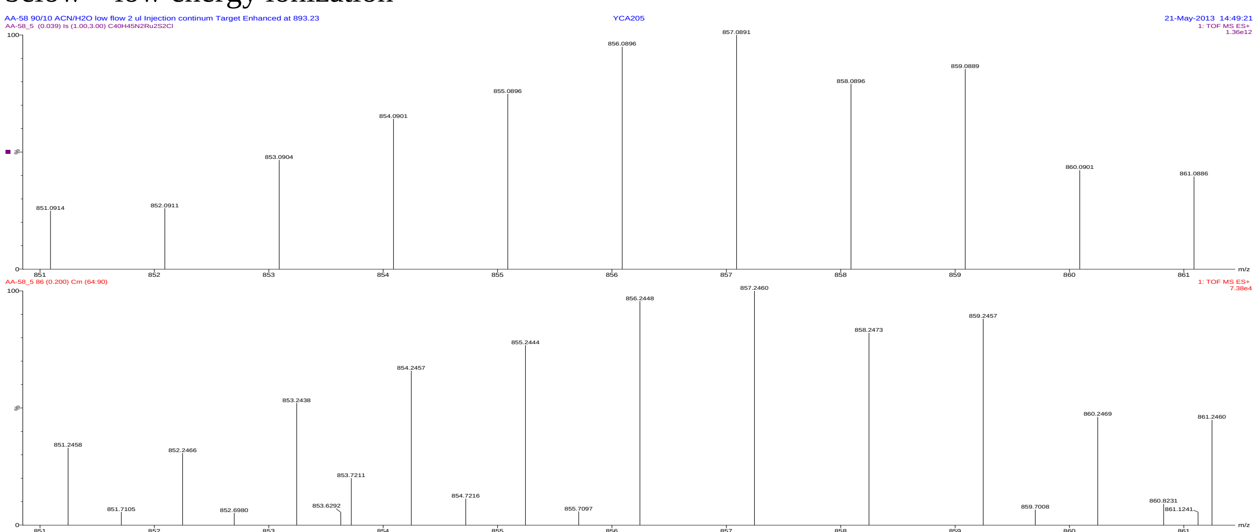

Figure S35. HRMS of **2a** (X = PF_6) signal 719 *m/z* (full); theoretical results above, experiment below – low energy ionization

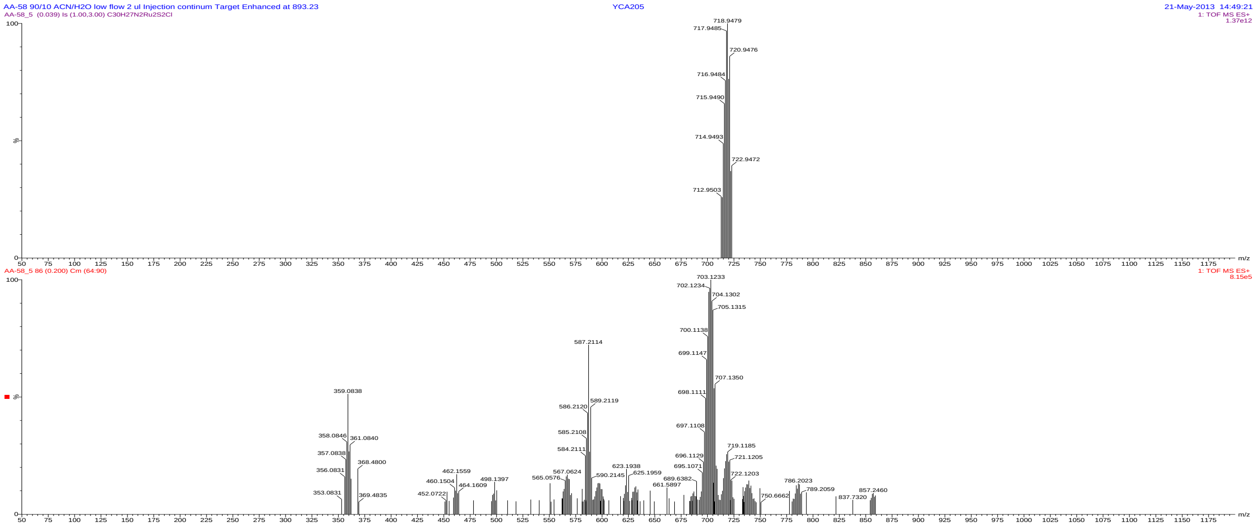

Figure S36. HRMS of **2a** (X = PF_6) signal 719 *m/z* (zoom); theoretical results above, experiment below – low energy ionization

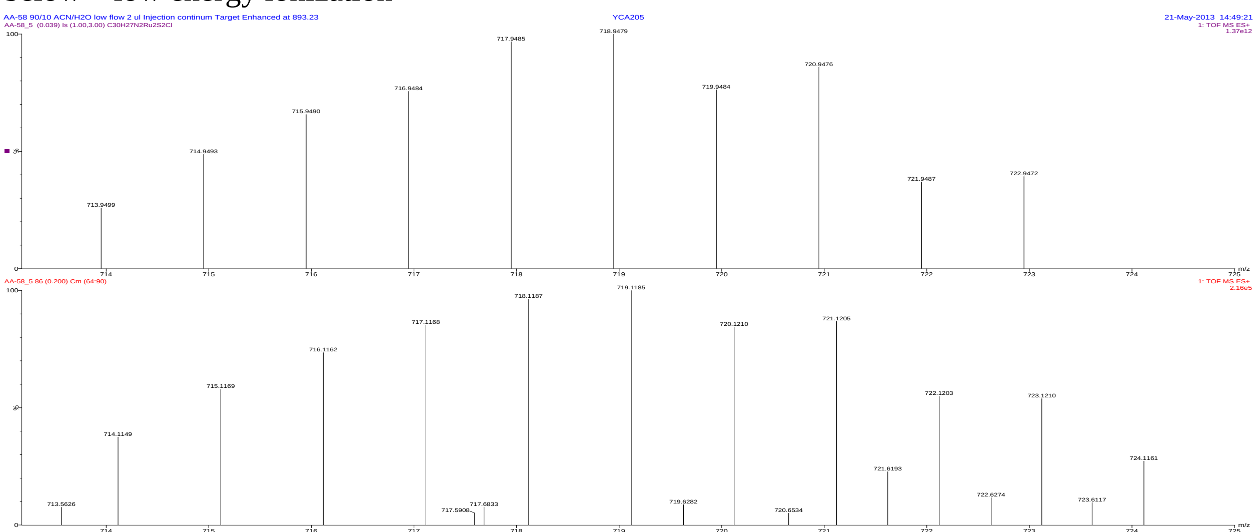

Figure S37. HRMS of **2a** (X = PF_6) signal 703 *m/z* (full); theoretical results above, experiment below – low energy ionization

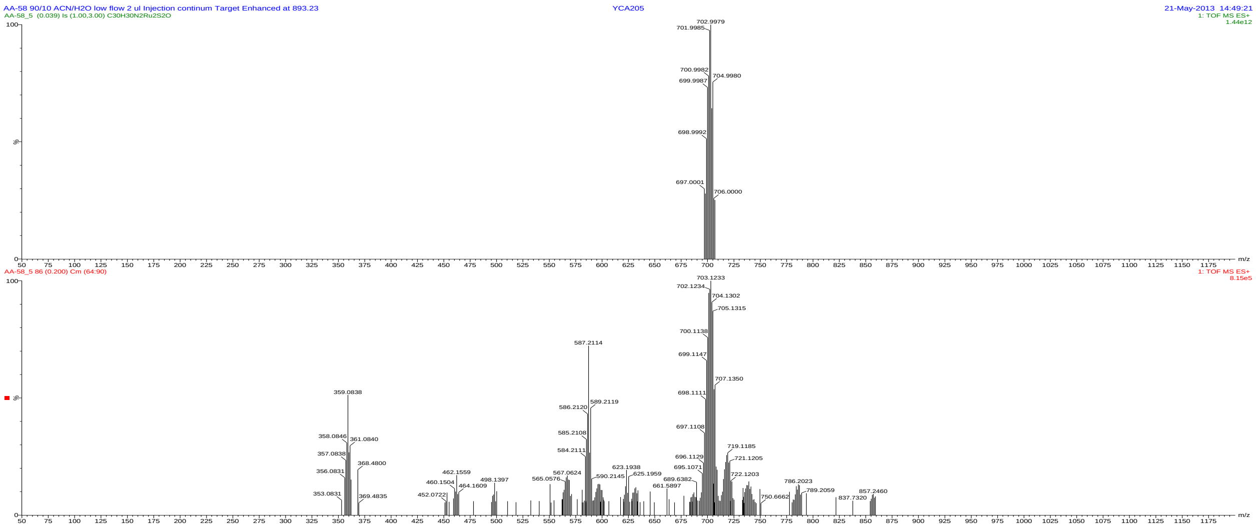

Figure S38. HRMS of **2a** (X = PF_6) signal 703 *m/z* (zoom); theoretical results above, experiment below – low energy ionization

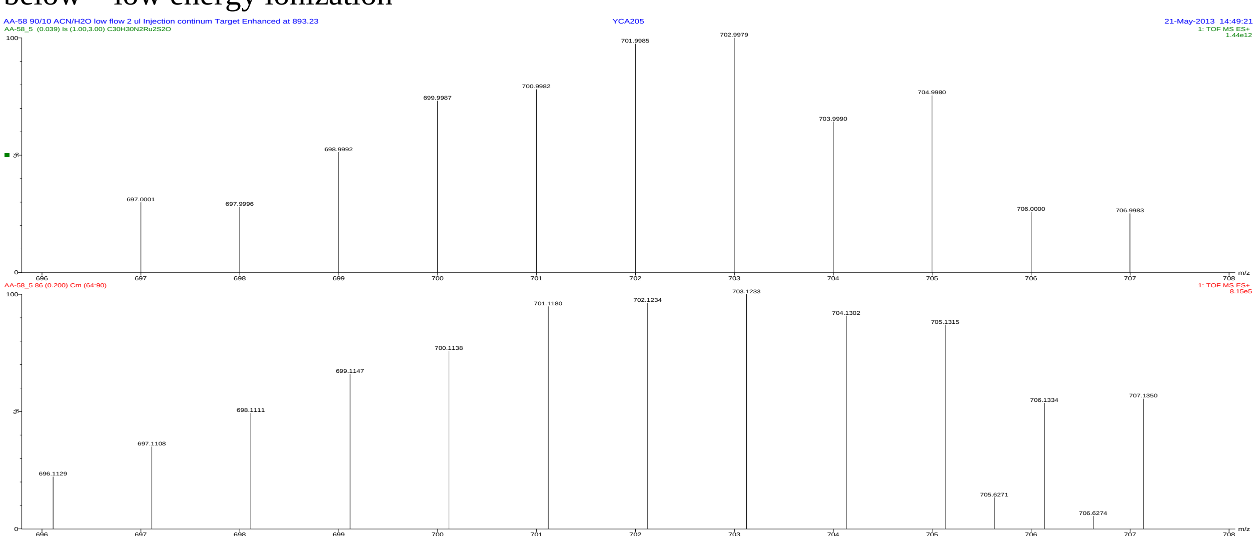

Figure S39. HRMS of **2a** (X = PF_6) signal 587 *m/z* (full); theoretical results above, experiment below – low energy ionization

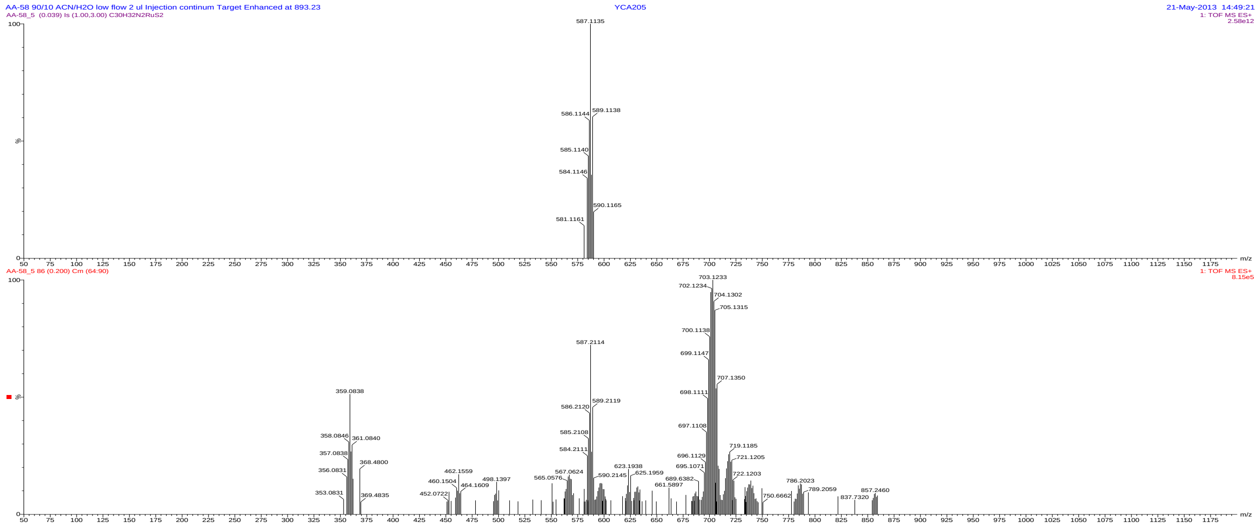

Figure S40. HRMS of **2a** (X = PF_6) signal 587 *m/z* (zoom); theoretical results above, experiment below – low energy ionization

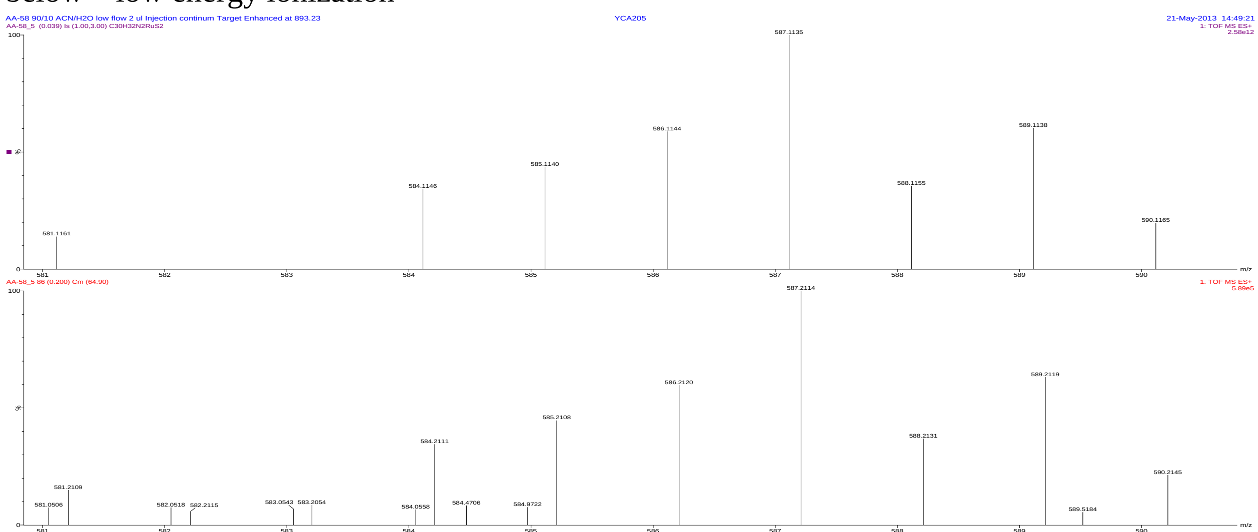

Figure S41. HRMS of **2a** (X = PF_6) signal 453 *m/z* (full); theoretical results above, experiment below – low energy ionization

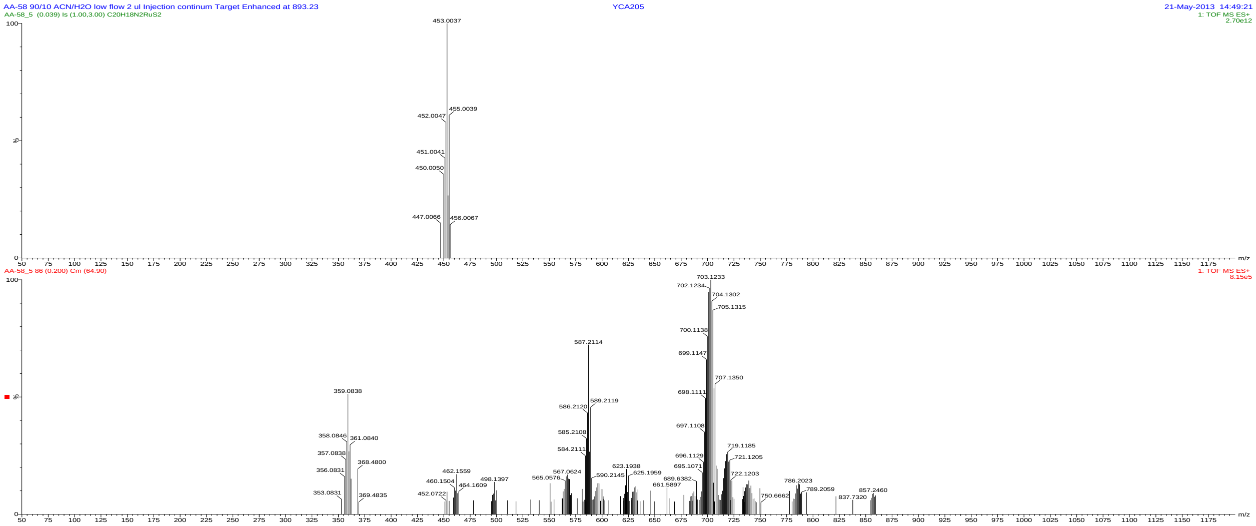

Figure S42. HRMS of **2a** (X = PF_6) signal 453 *m/z* (zoom); theoretical results above, experiment below – low energy ionization

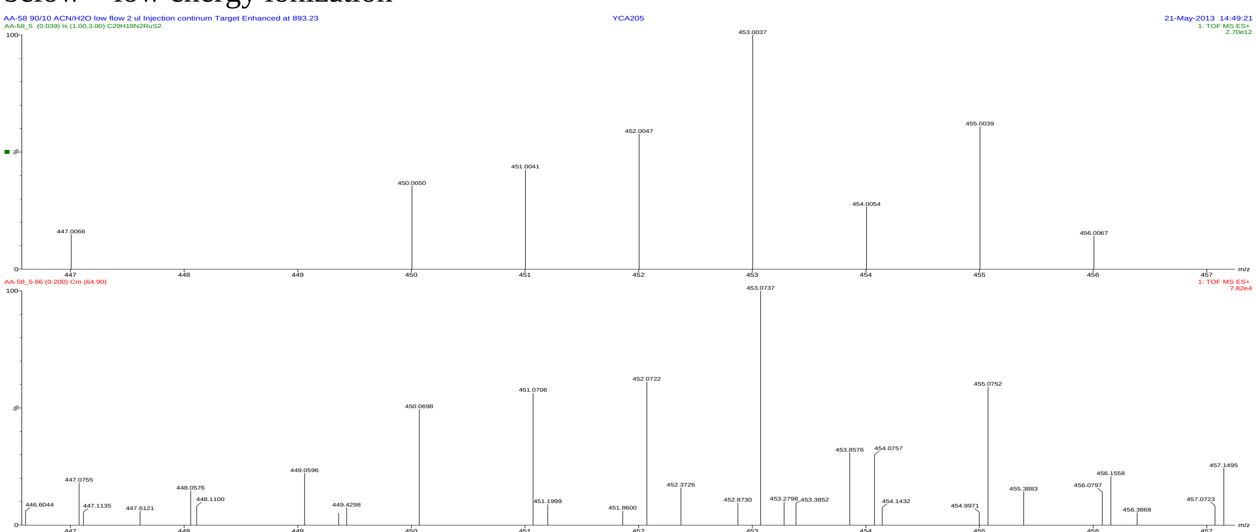

Figure S43. HRMS of **2a** (X = PF_6) signal 359 *m/z* (full); theoretical results above, experiment below – low energy ionization

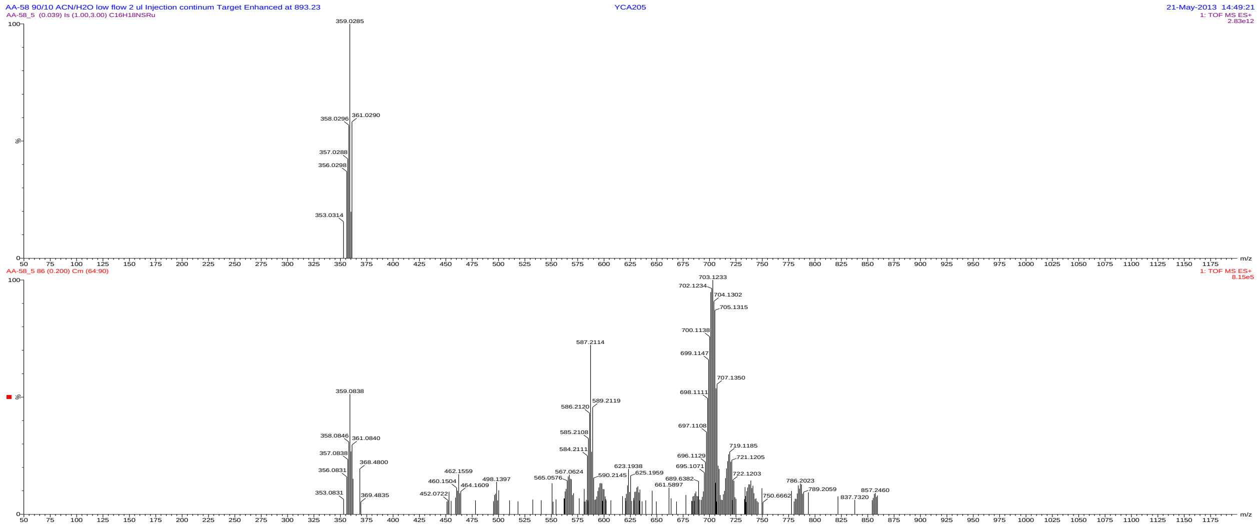

Figure S44. HRMS of **2a** (X = PF_6) signal 359 *m/z* (zoom); theoretical results above, experiment below – low energy ionization

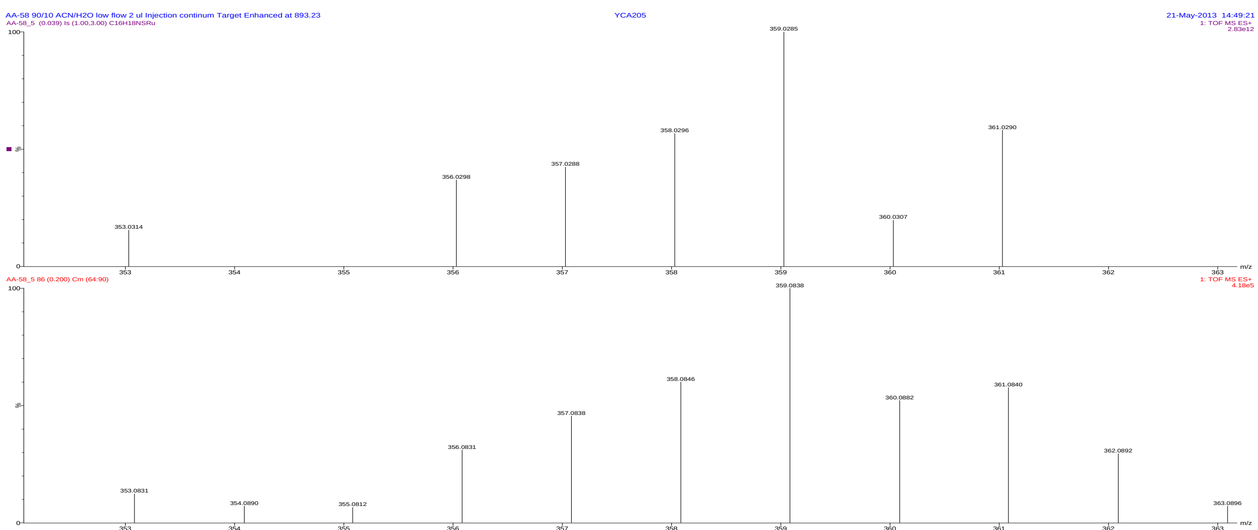

Figure S45. UPLC-MS chromatogram of **2a** ($X = PF_6$) – medium energy ionization

Figure S46. HRMS of **2a** ($X = PF_6$) – medium energy ionization

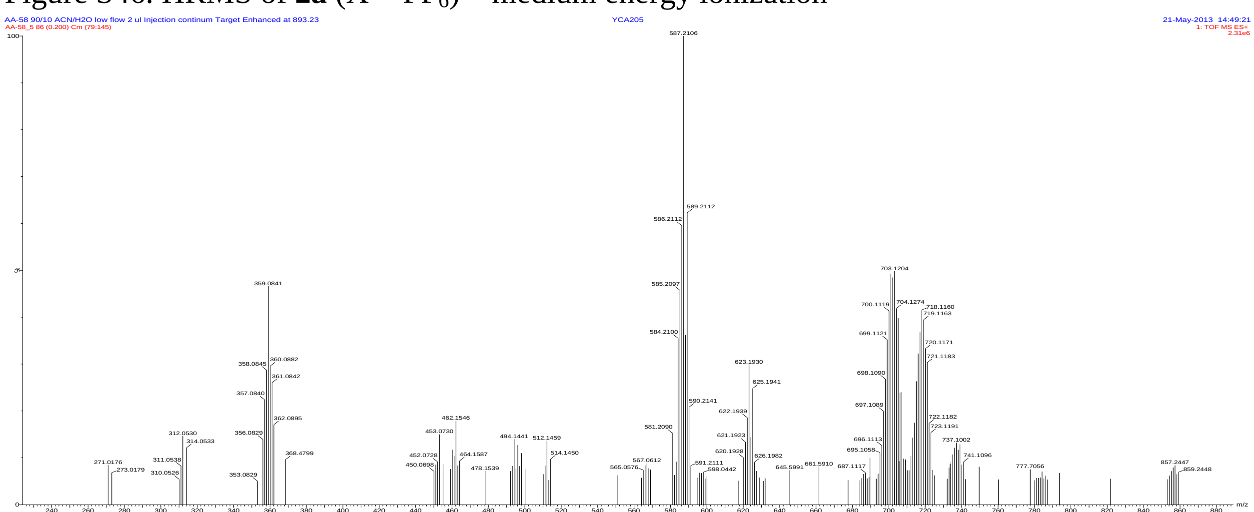

Figure S47. UPLC-MS chromatogram of **2a** (X = PF_6) – high energy ionization

Figure S48. HRMS of **2a** (X = PF_6) – high energy ionization

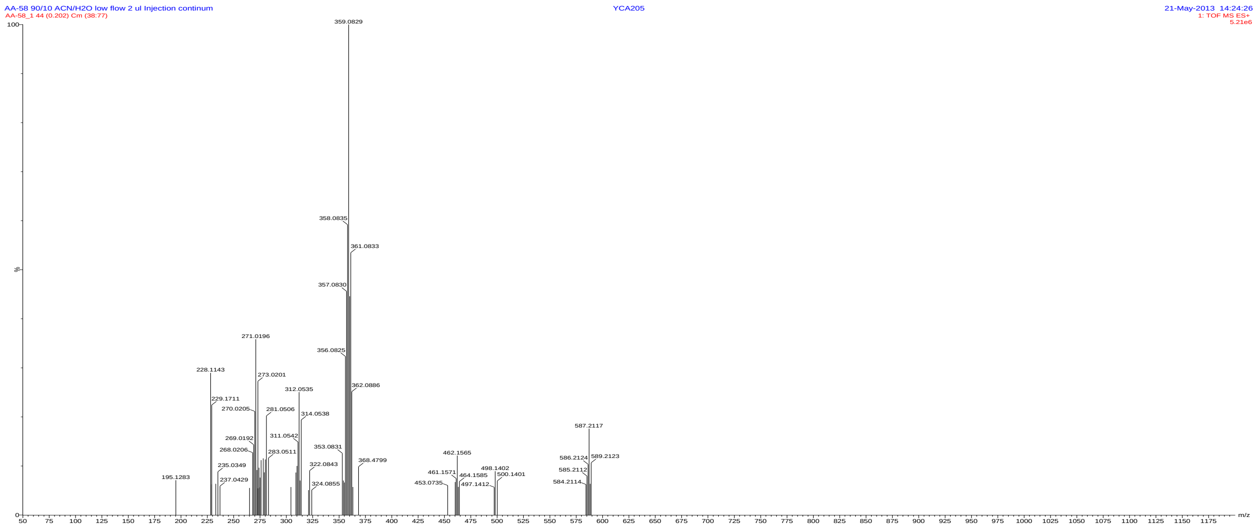

Figure S49. HRMS of **2a** (X = PF_6) signal 587 *m/z* (full); theoretical results above, experiment below – high energy ionization

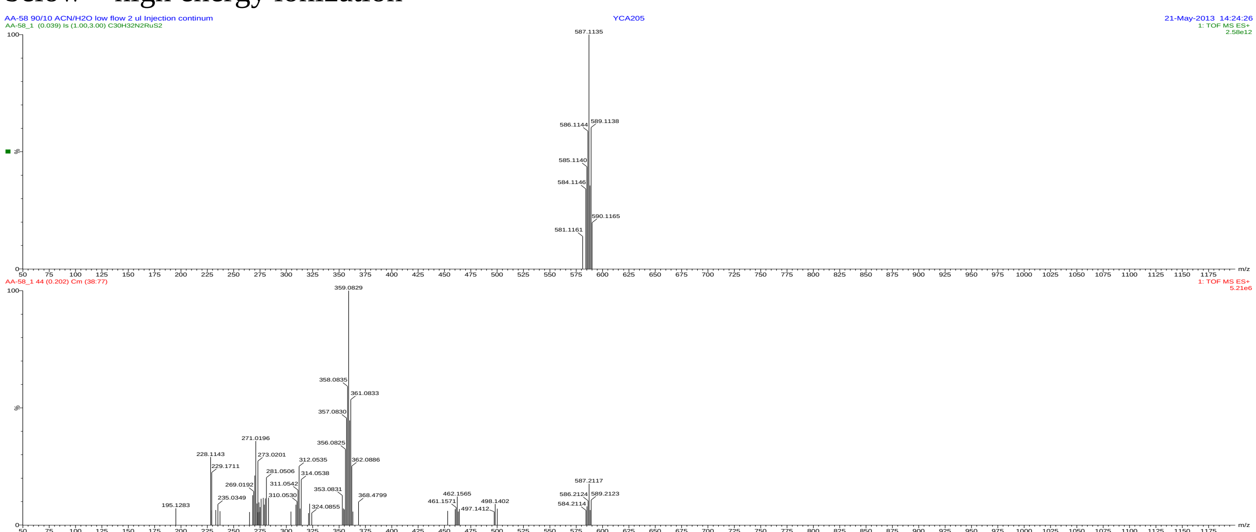

Figure S50. HRMS of **2a** (X = PF_6) signal 587 *m/z* (zoom); theoretical results above, experiment below – high energy ionization

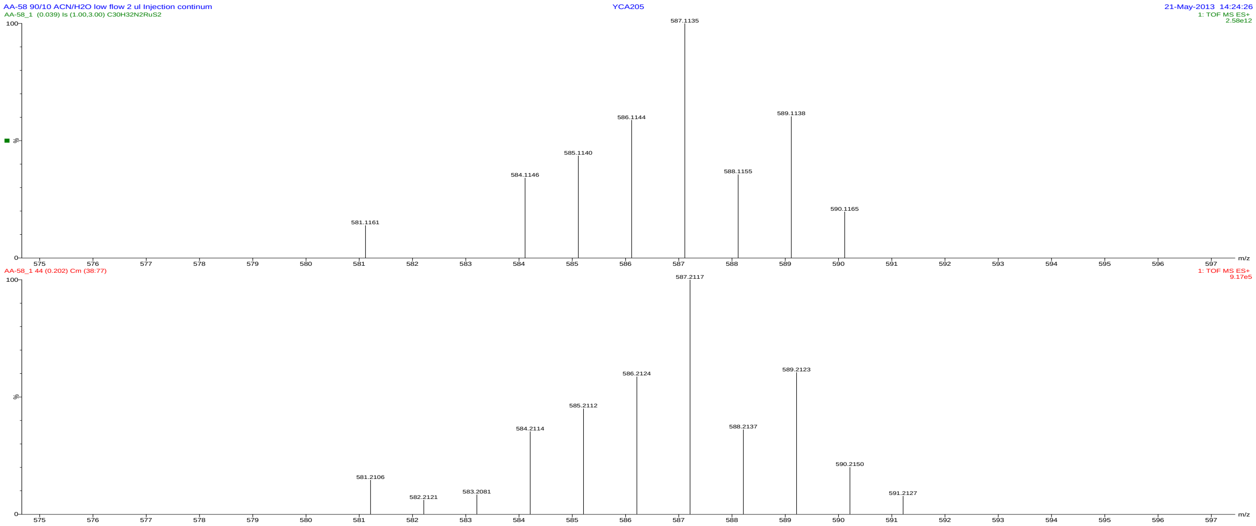

Figure S51. HRMS of **2a** (X = PF_6) signal 359 *m/z* (full); theoretical results above, experiment below – high energy ionization

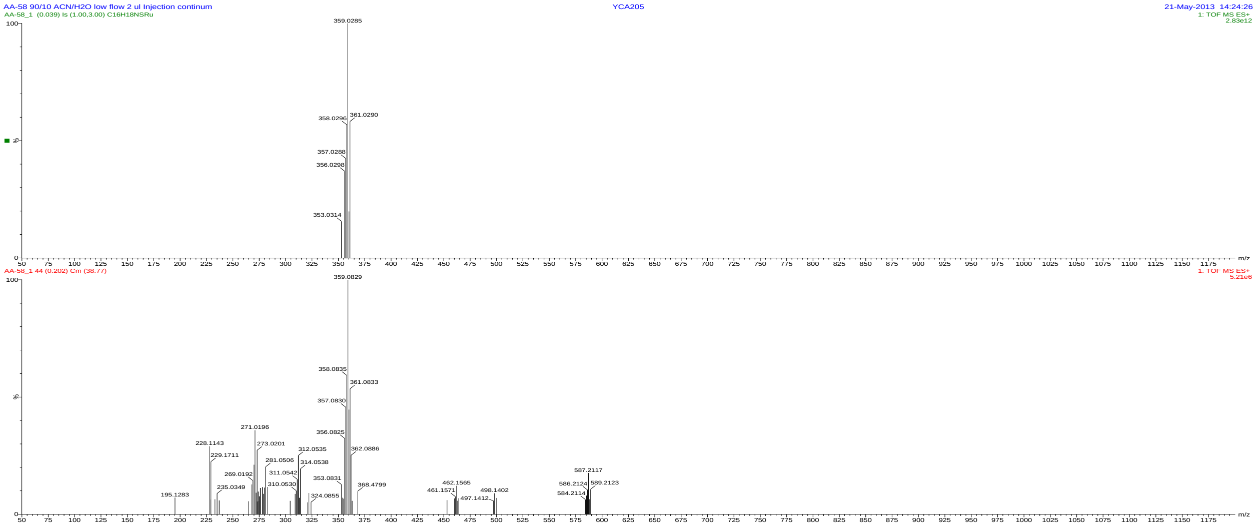

Figure S52. HRMS of **2a** (X = PF_6) signal 359 *m/z* (zoom); theoretical results above, experiment below – high energy ionization

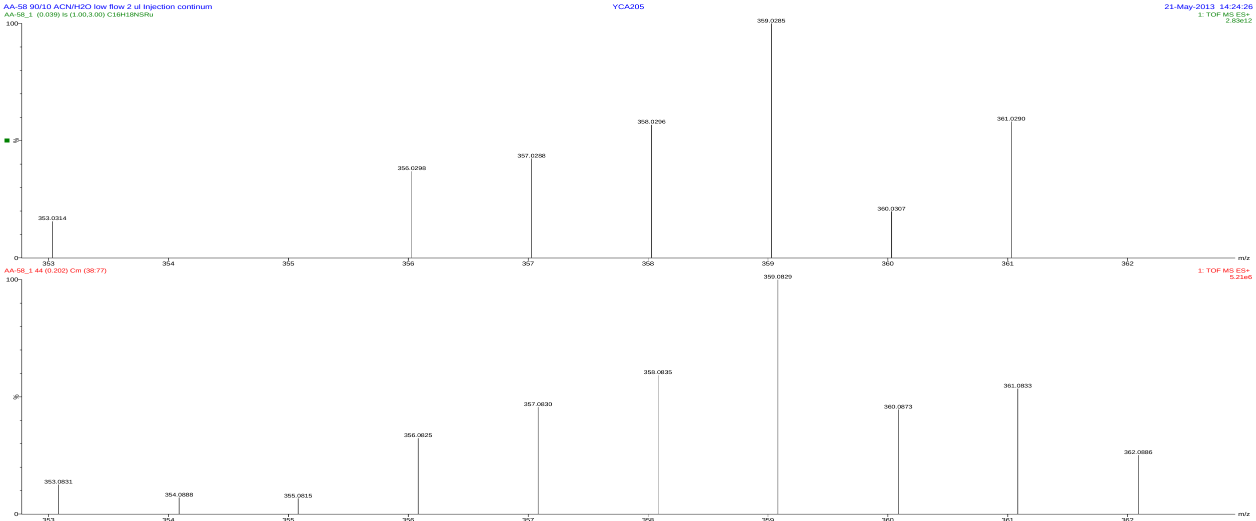

Figure S53. HRMS of **2a** (X = PF_6) signal 312 *m/z* (full); theoretical results above, experiment below – high energy ionization

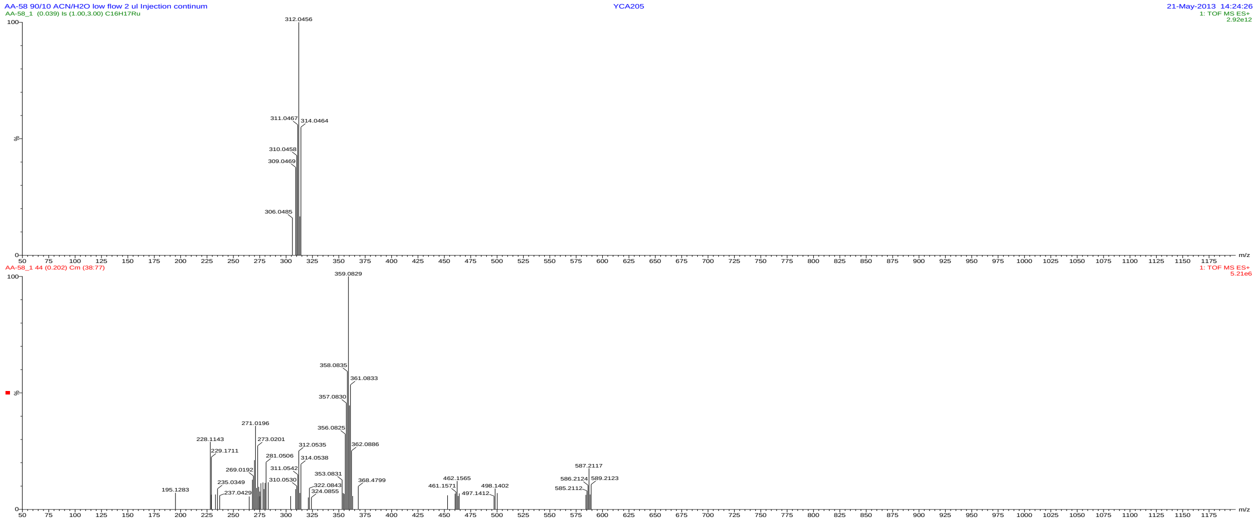

Figure S54. HRMS of **2a** (X = PF_6) signal 312 *m/z* (zoom); theoretical results above, experiment below – high energy ionization

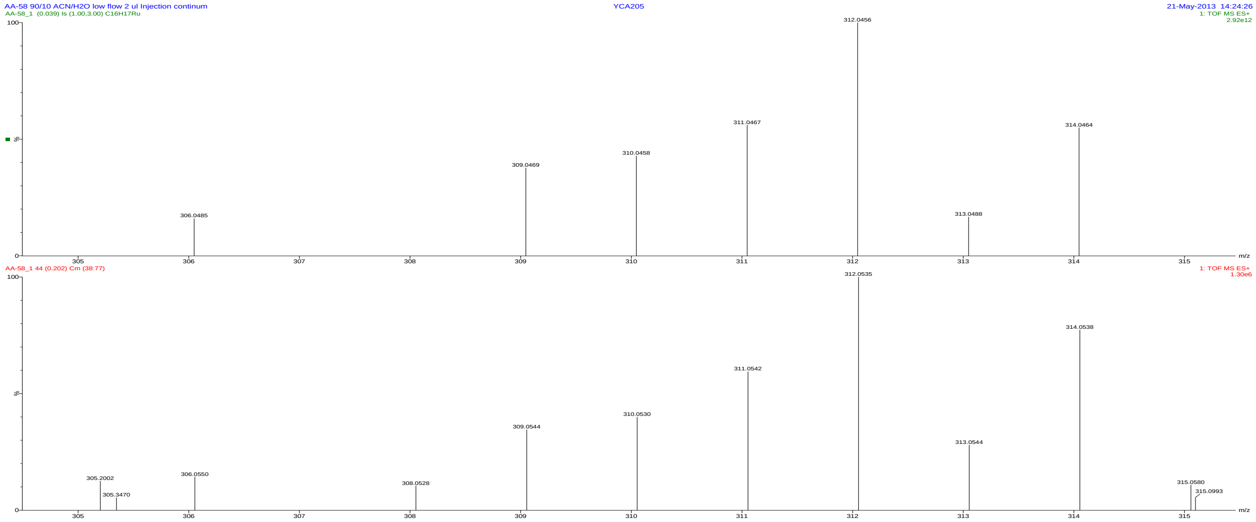

Figure S55. UPLC-MS chromatogram of **2a** (X = BF4) – high energy ionization

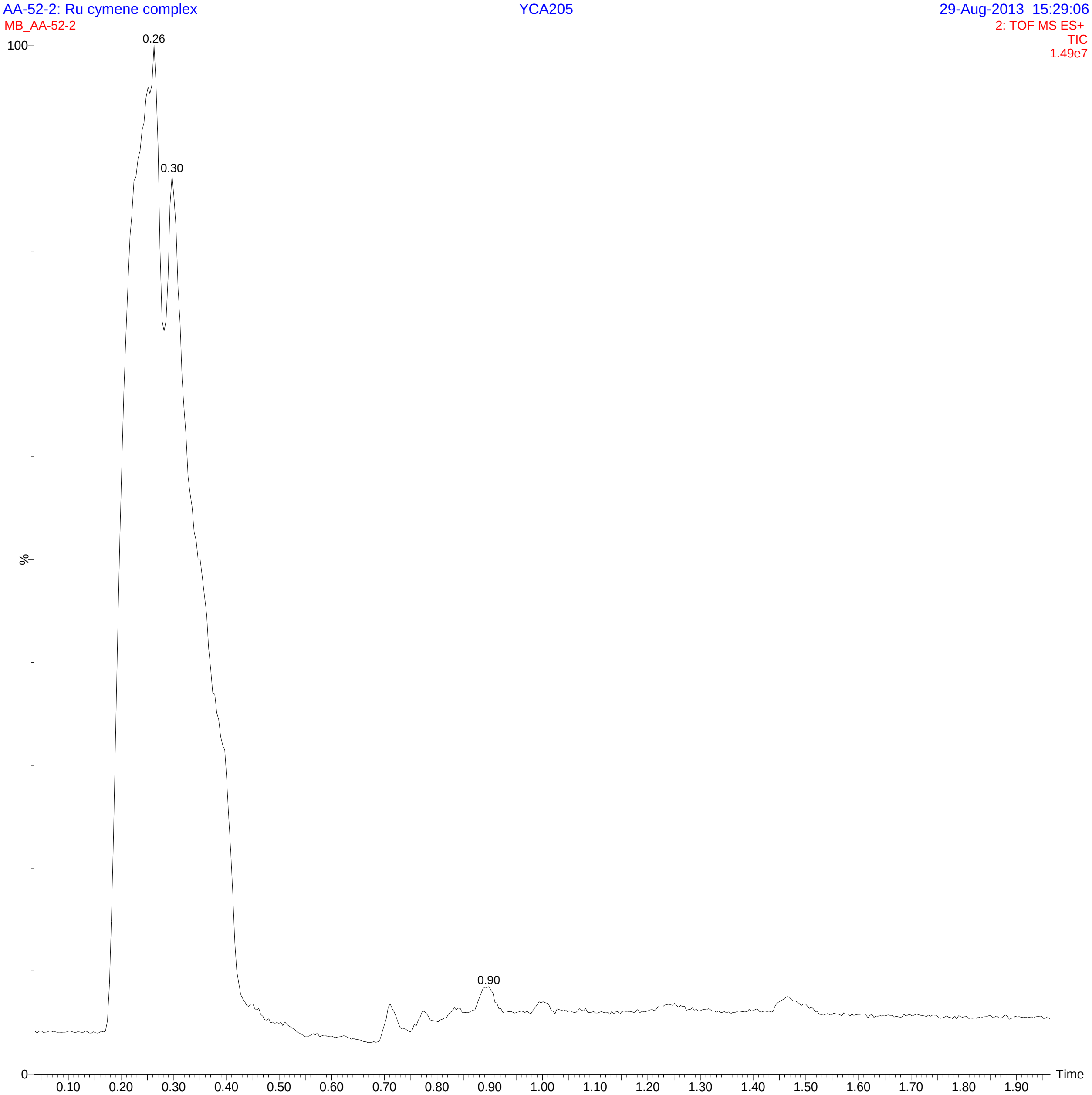

Electronic Supplementary Material (ESI) for Dalton Transactions
This journal is © The Royal Society of Chemistry 2013

Figure S56. HRMS of **2a** (X = BF4) – high energy ionization

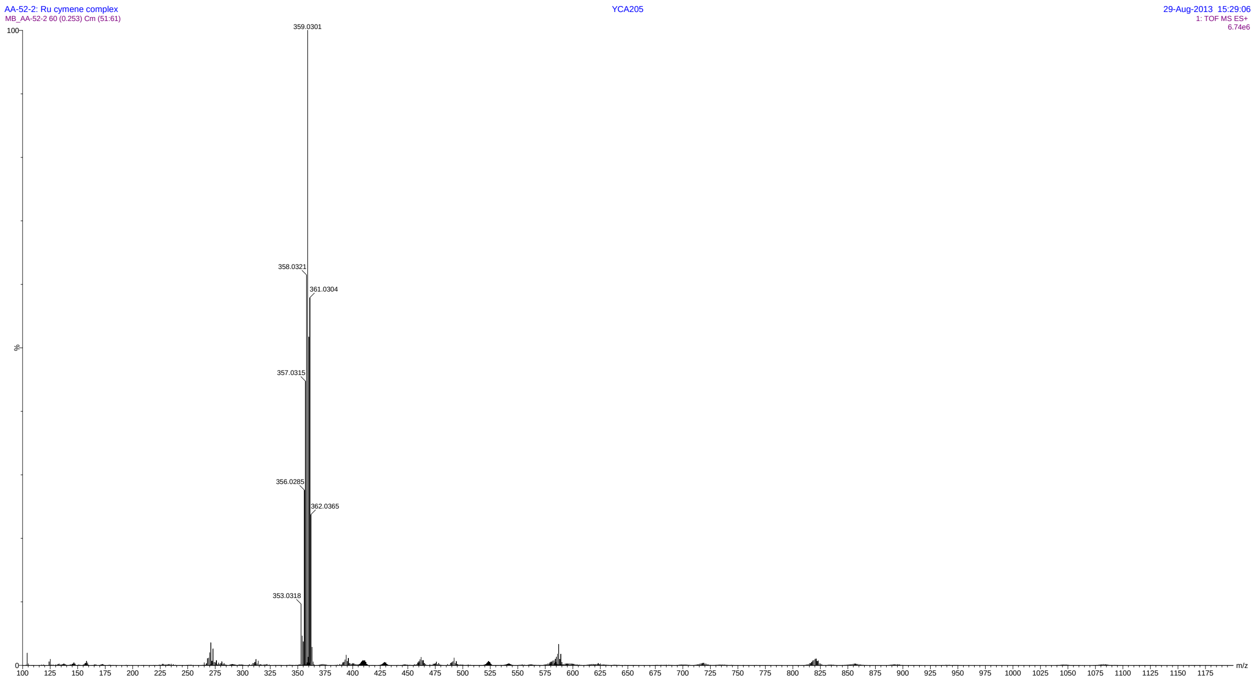

Figure S57. HRMS of **2a** (X = BF_4) signal 893 *m/z* (full); theoretical results above, experiment below – high energy ionization

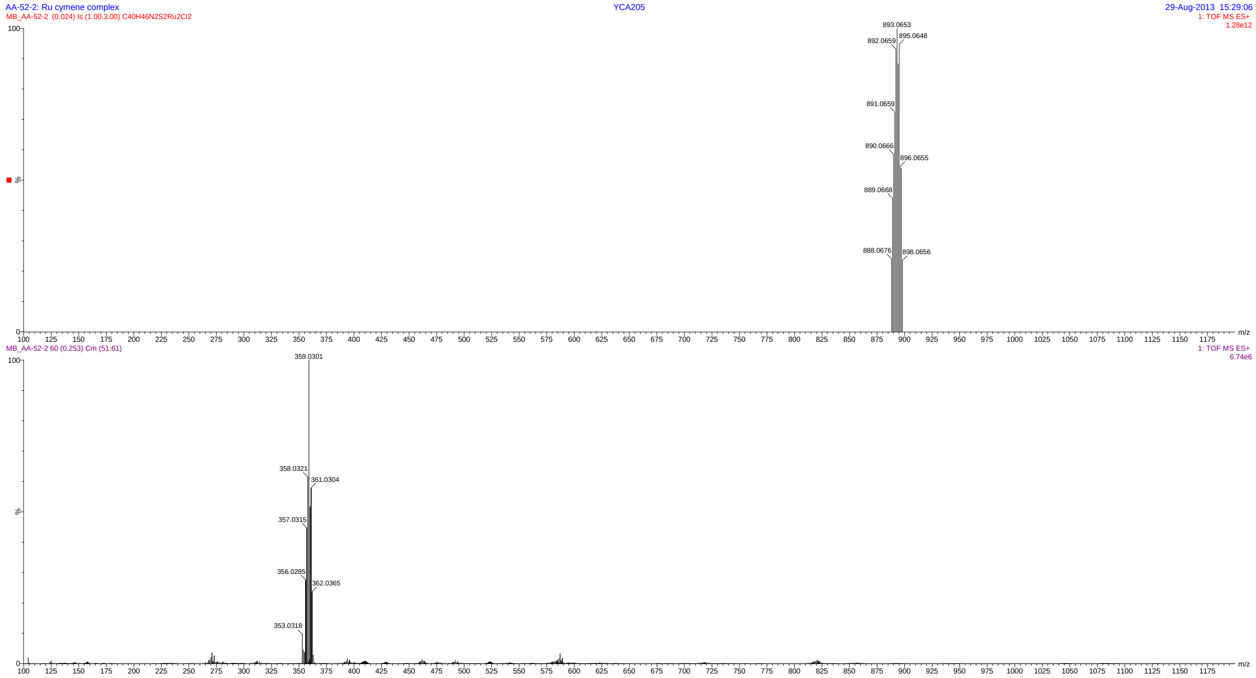

Figure S58. HRMS of **2a** (X = BF_4) signal 893 *m/z* (zoom); theoretical results above, experiment below – high energy ionization

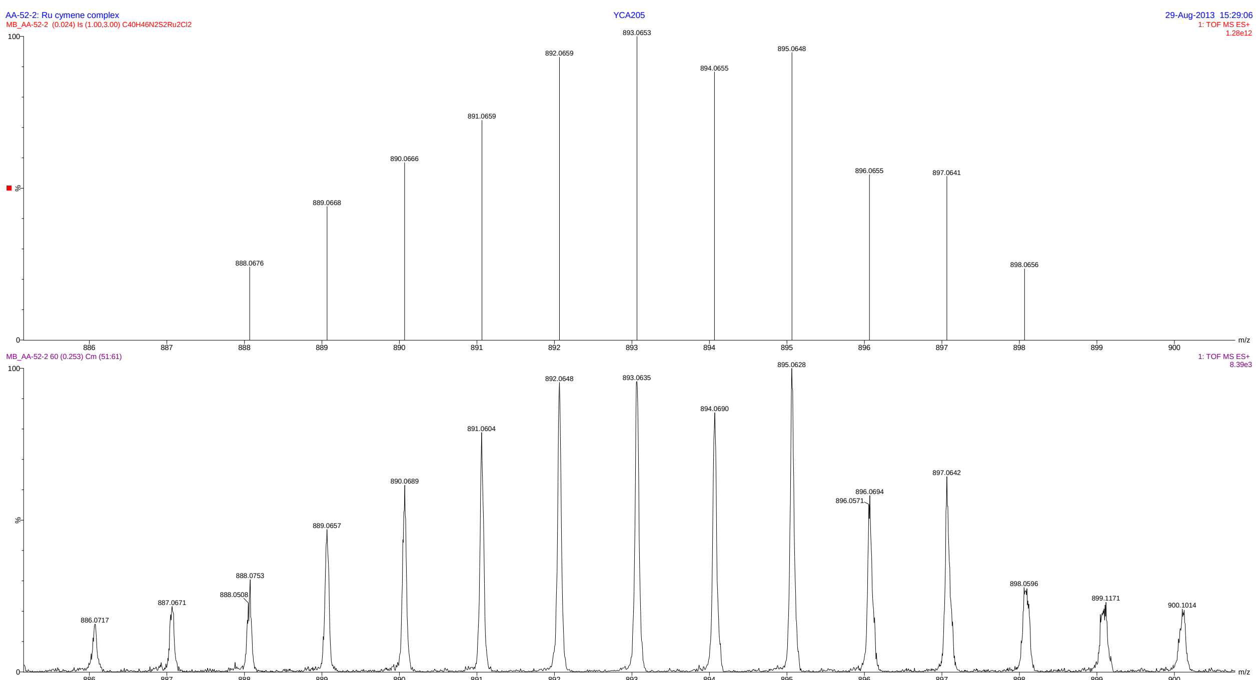

Figure S59. UPLC-MS chromatogram of **2b** (X = BF_4) – low energy ionization

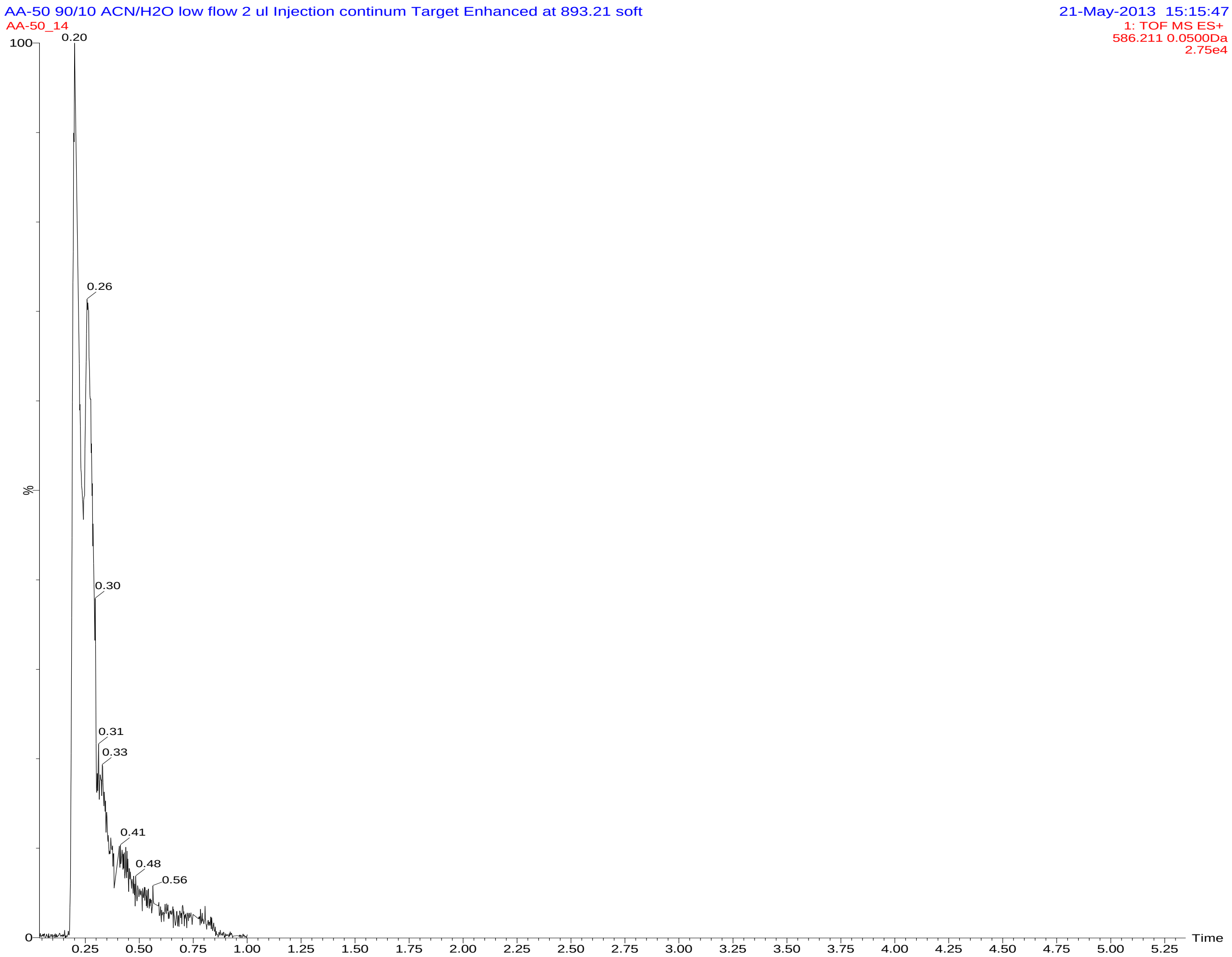

Figure S60. HRMS of **2b** (X = BF_4); spectrum for peak 0.20 min– low energy ionization

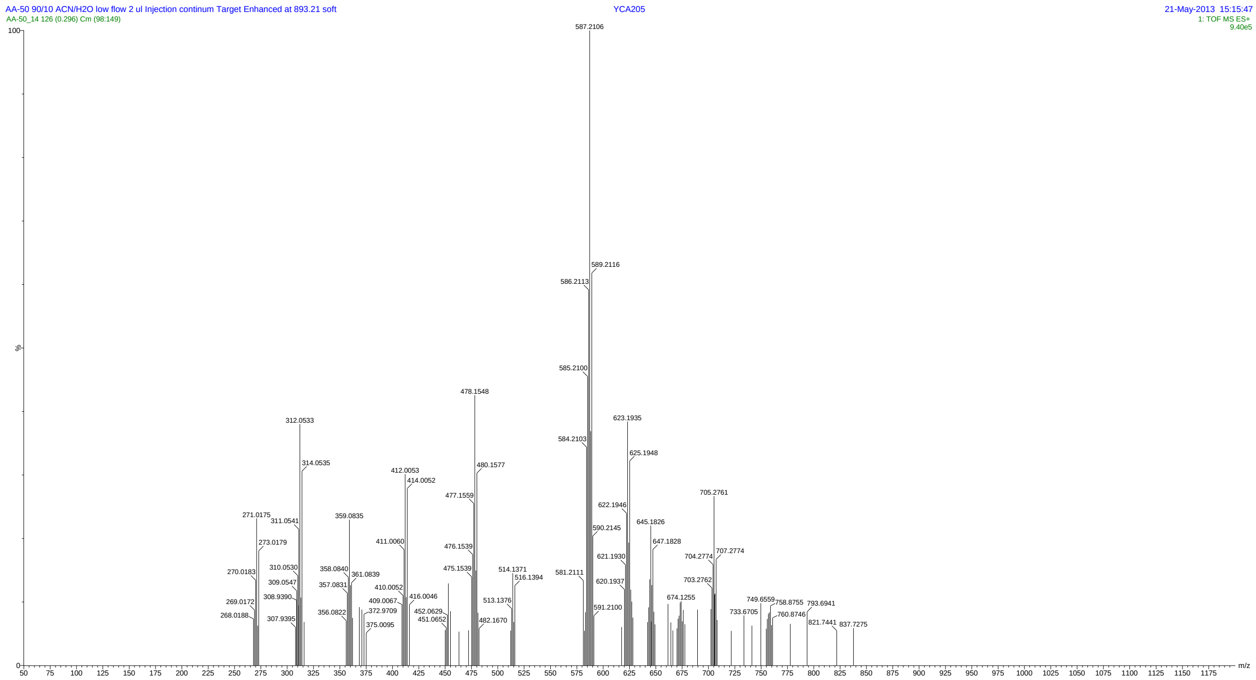

Figure S61. HRMS of **3** (X = BF_4); spectrum for peak 0.26 min– low energy ionization

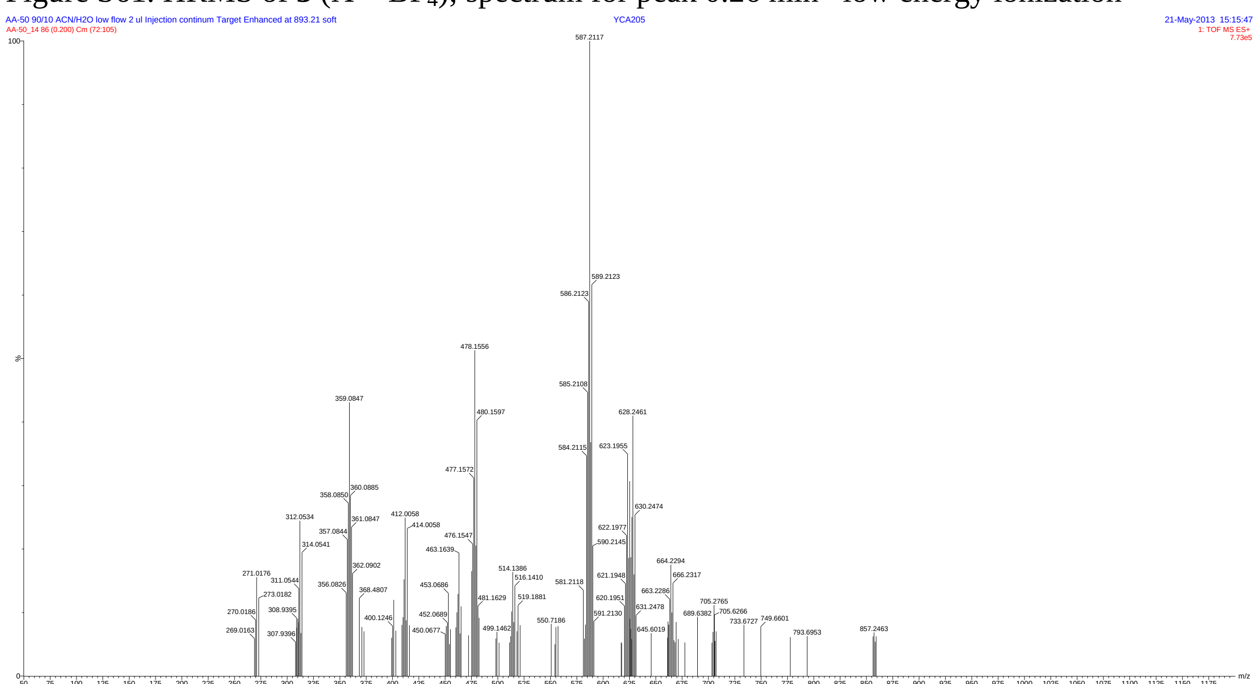

Figure S62. HRMS of **3** (X = BF_4) for peak 0.20 min; signal 893 *m/z* (full); theoretical results above, experiment below – low energy ionization

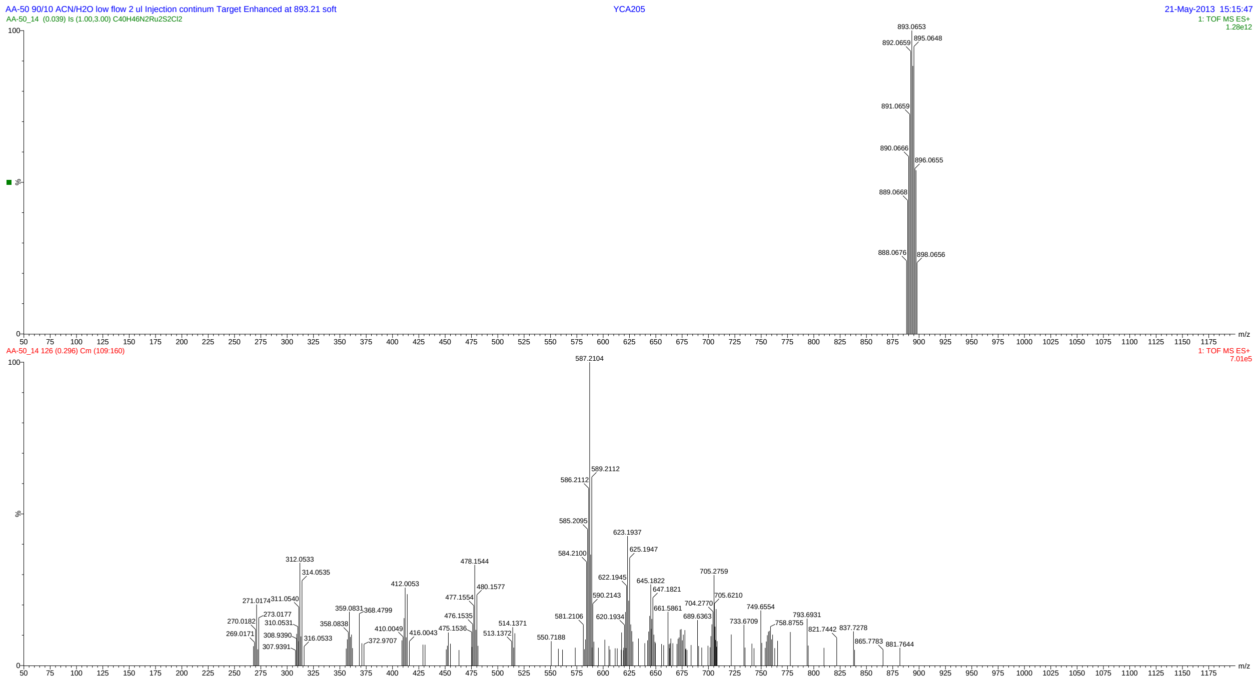

Figure S63. HRMS of **3** (X = BF_4) for peak 0.20 min; signal 893 *m/z* (zoom); theoretical results above, experiment below – low energy ionization

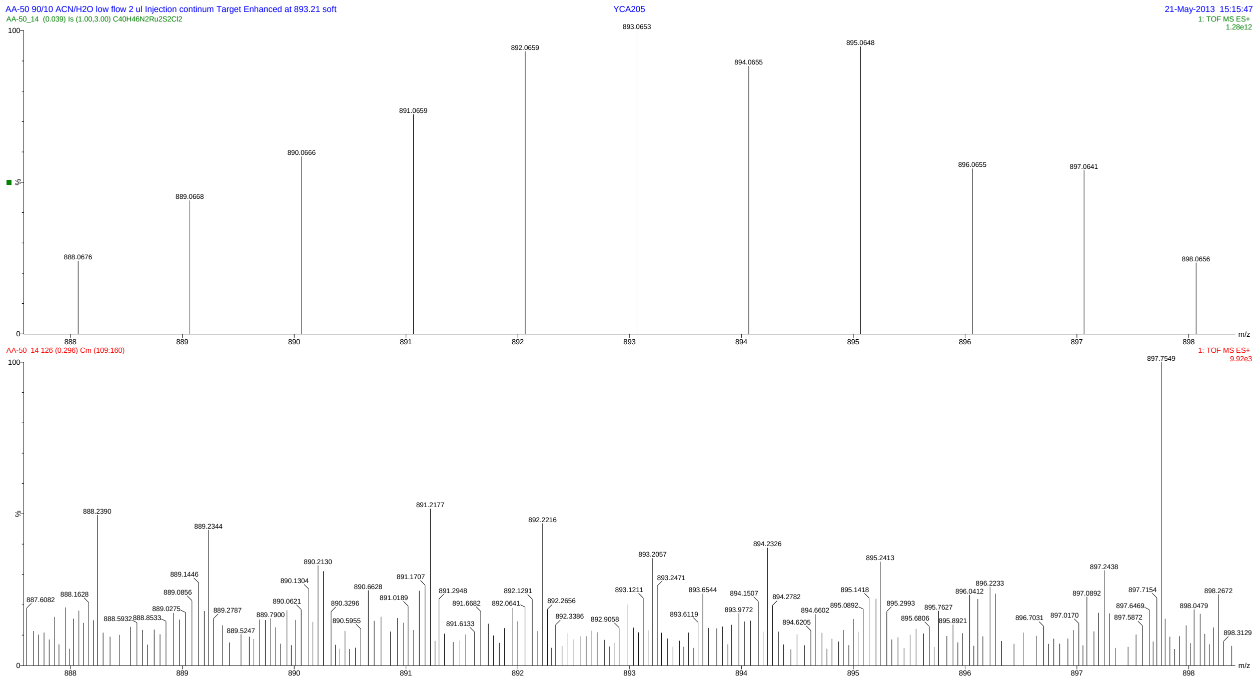

Figure S64. HRMS of **3** (X = BF_4) for peak 0.20 min; signal 623 *m/z* (full); theoretical results above, experiment below – low energy ionization

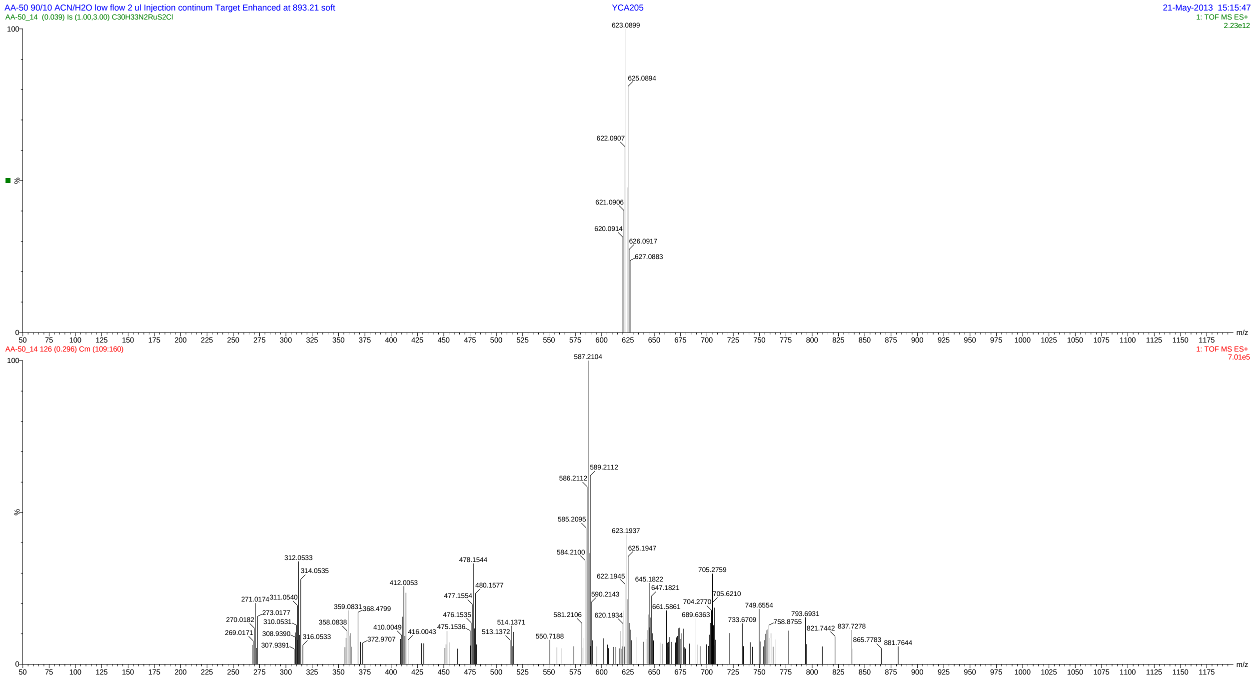

Figure S65. HRMS of **3** (X = BF_4) for peak 0.20 min; signal 623 *m/z* (zoom); theoretical results above, experiment below – low energy ionization

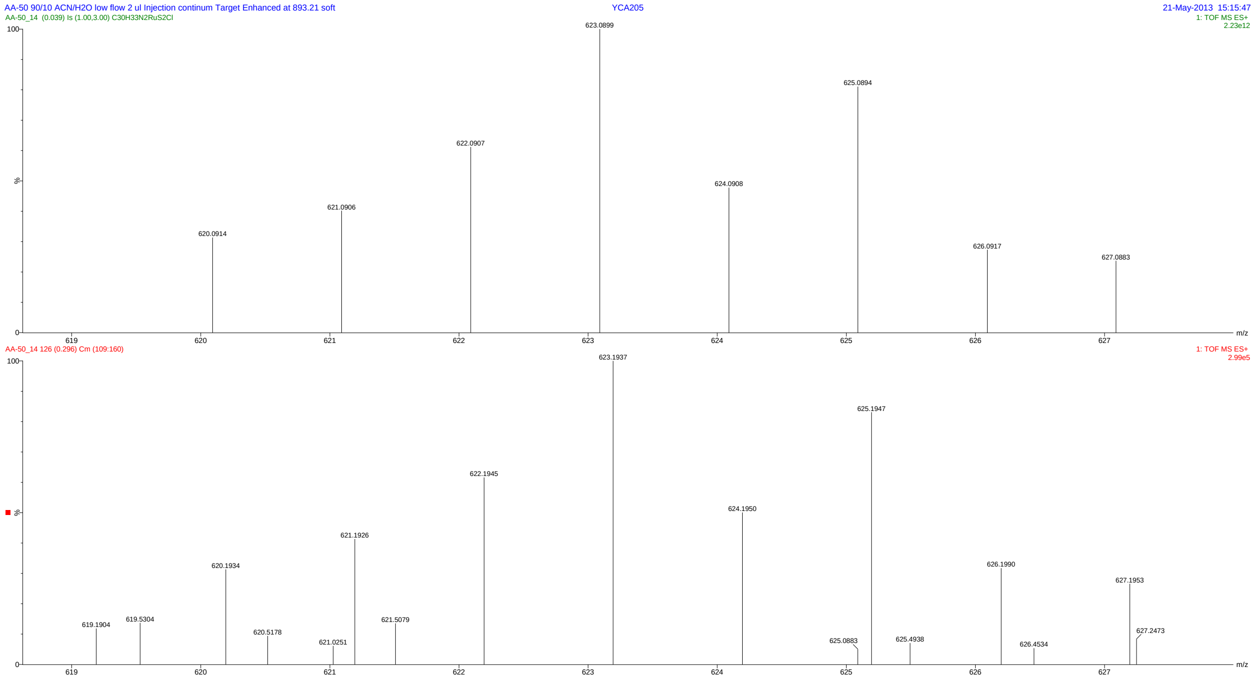

Figure S66. HRMS of **3** (X = BF_4) for peak 0.20 min; signal 587 *m/z* (full); theoretical results above, experiment below – low energy ionization

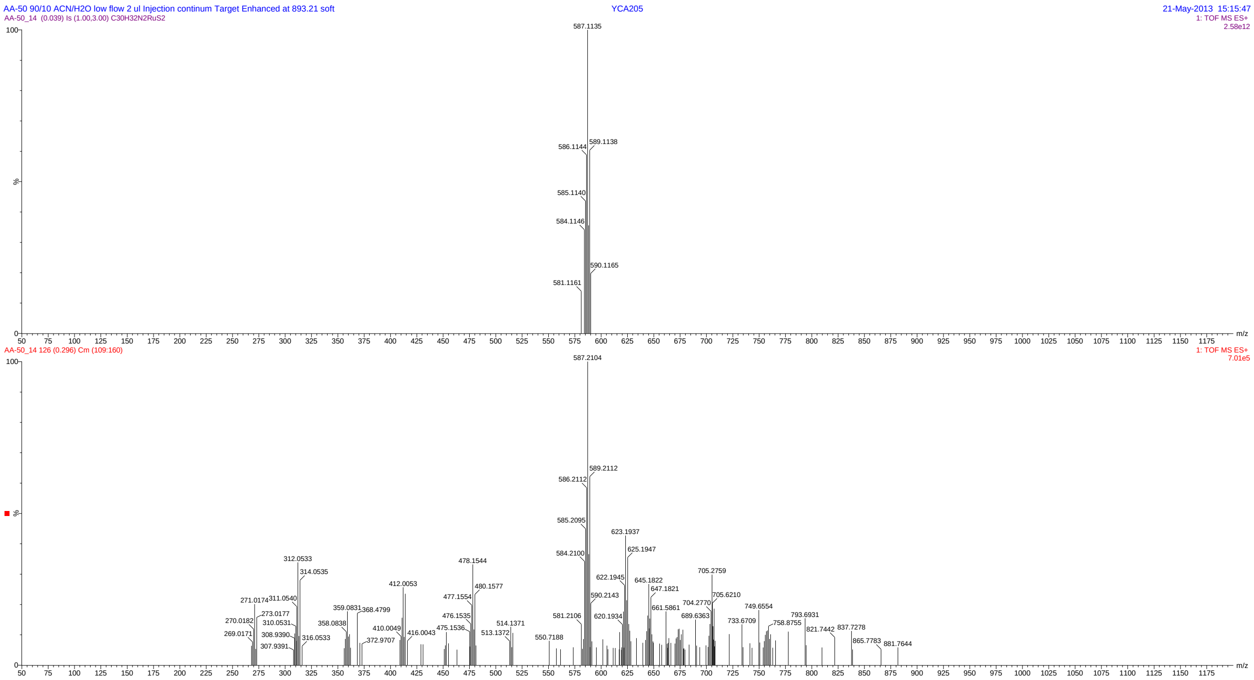

Figure S67. HRMS of **3** (X = BF_4) for peak 0.20 min; signal 587 *m/z* (zoom); theoretical results above, experiment below – low energy ionization

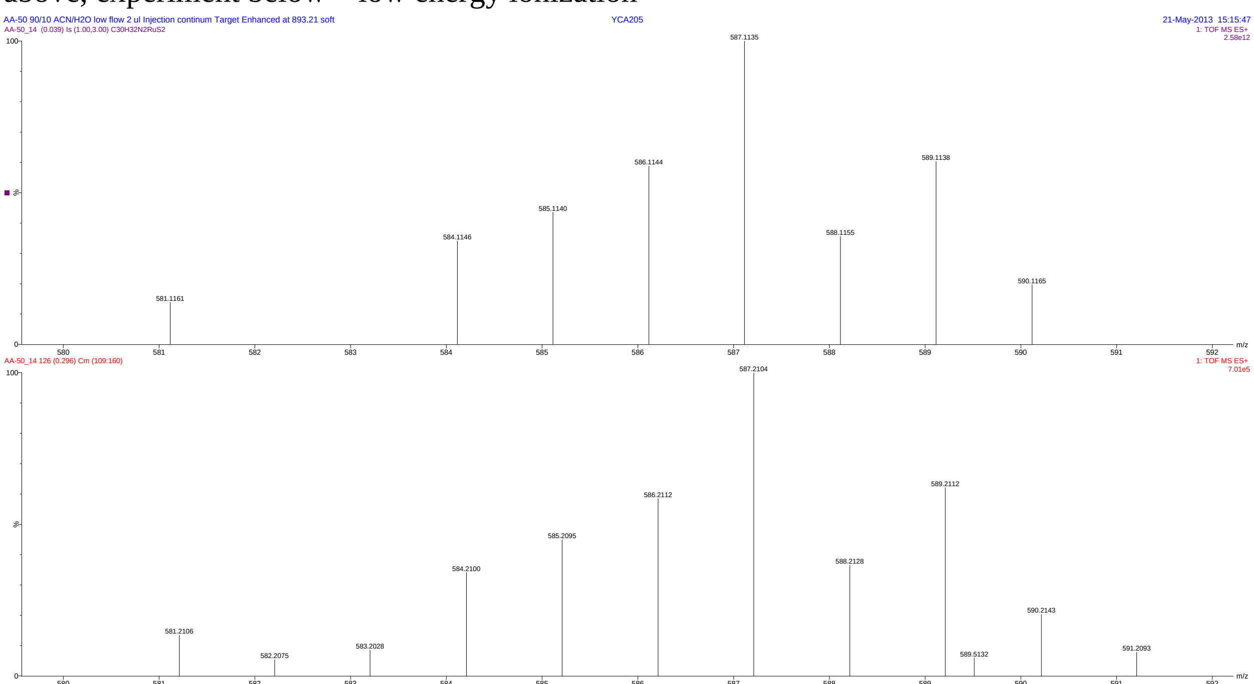

Figure S68. HRMS of **2b** (X = BF_4) for peak 0.26 min; signal 893 *m/z* (full); theoretical results above, experiment below – low energy ionization

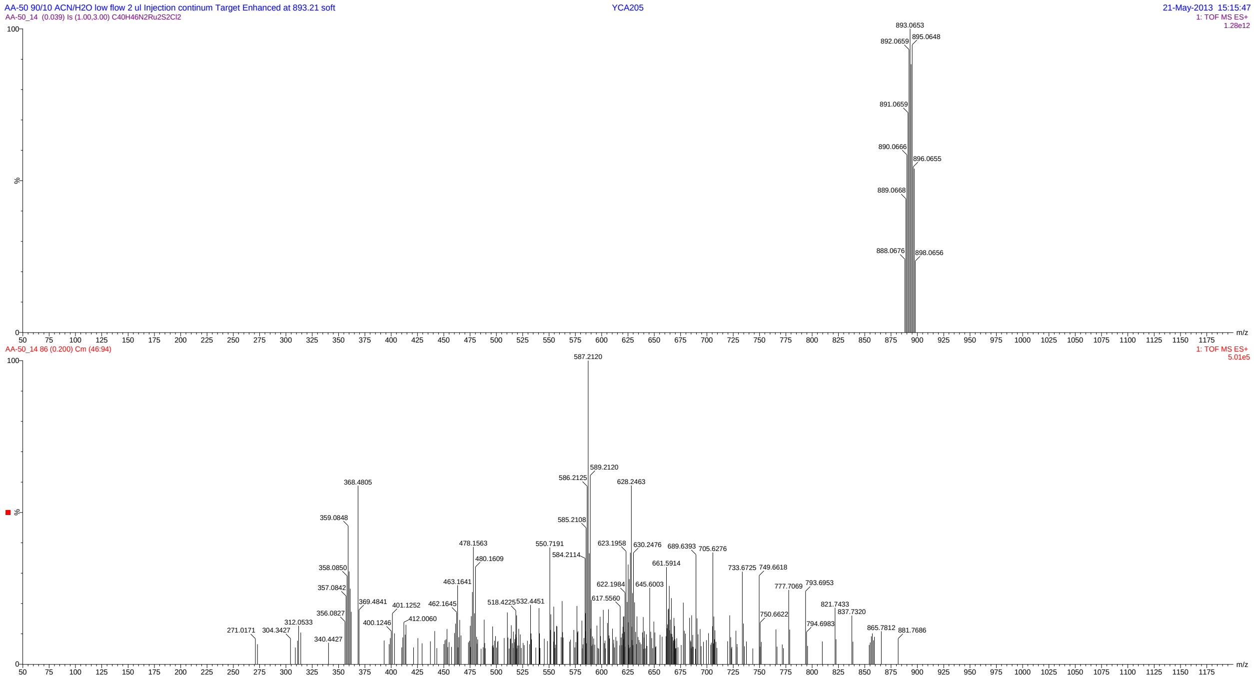

Figure S69. HRMS of **2b** (X = BF_4) for peak 0.26 min; signal 893 *m/z* (zoom); theoretical results above, experiment below – low energy ionization

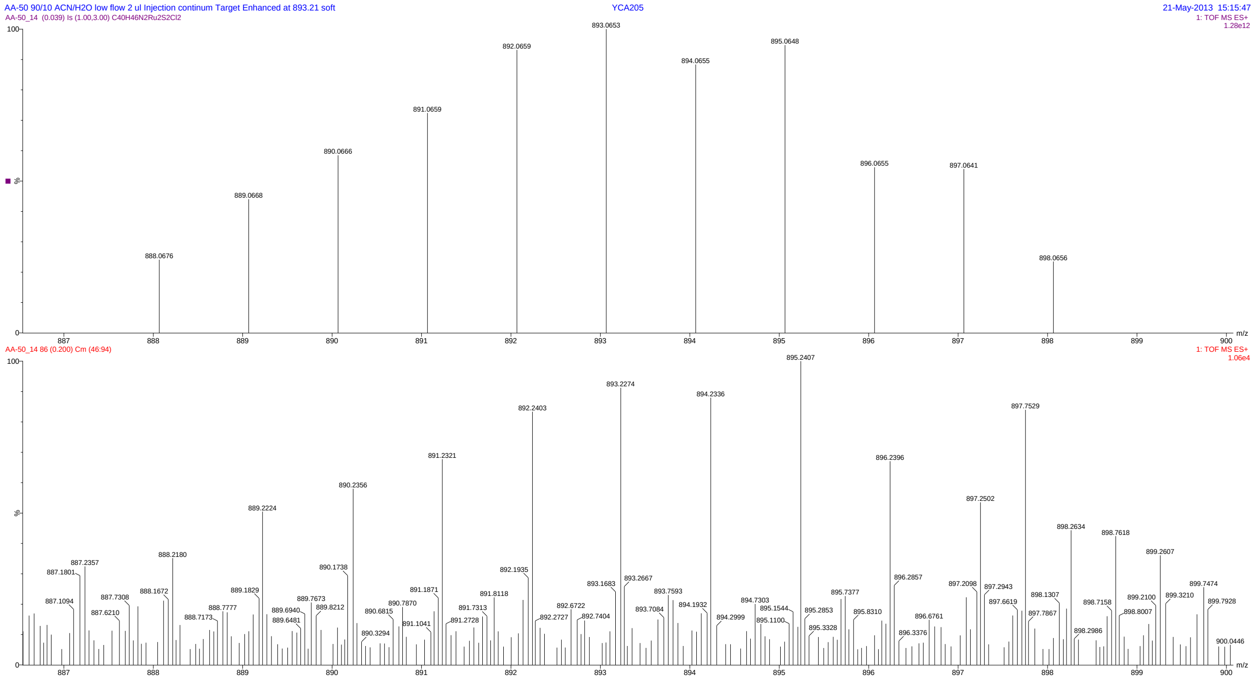

Electronic Supplementary Material (ESI) for Dalton Transactions

Figure S70. HRMS of **2b** (X = BF_4) for peak 0.26 min; signal 587 *m/z* (full); theoretical results above, experiment below – low energy ionization

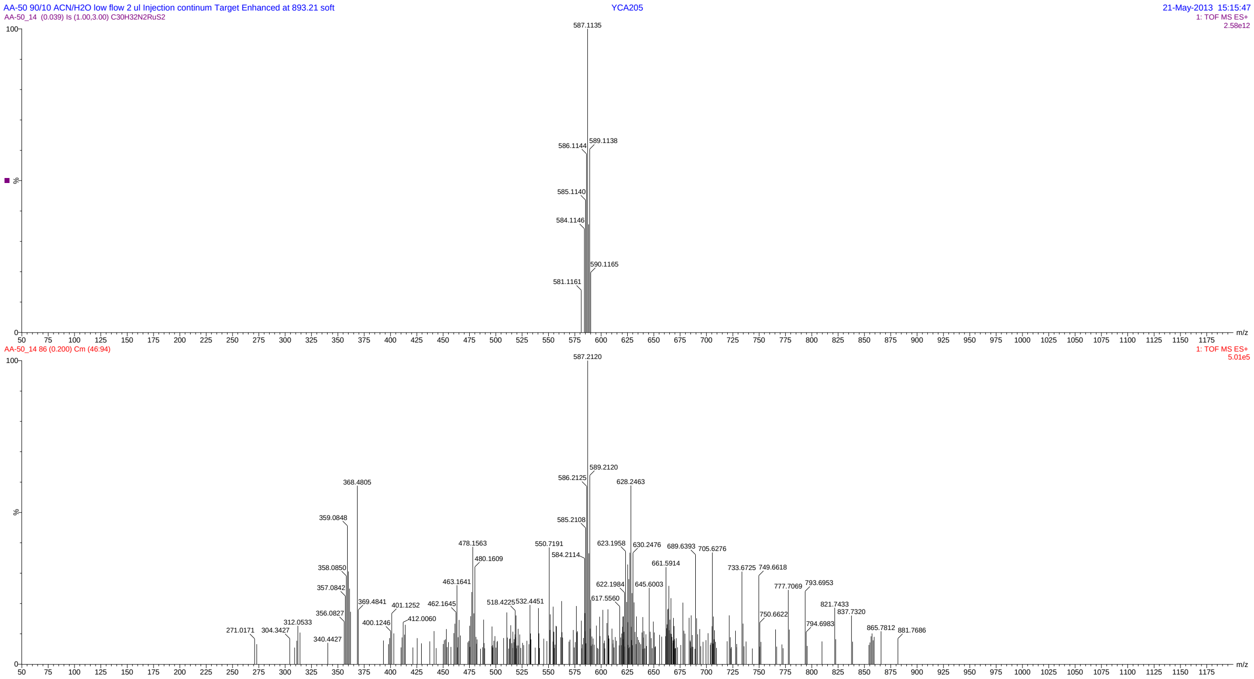

Figure S71. HRMS of **2b** (X = BF_4) for peak 0.26 min; signal 587 *m/z* (zoom); theoretical results above, experiment below – low energy ionization

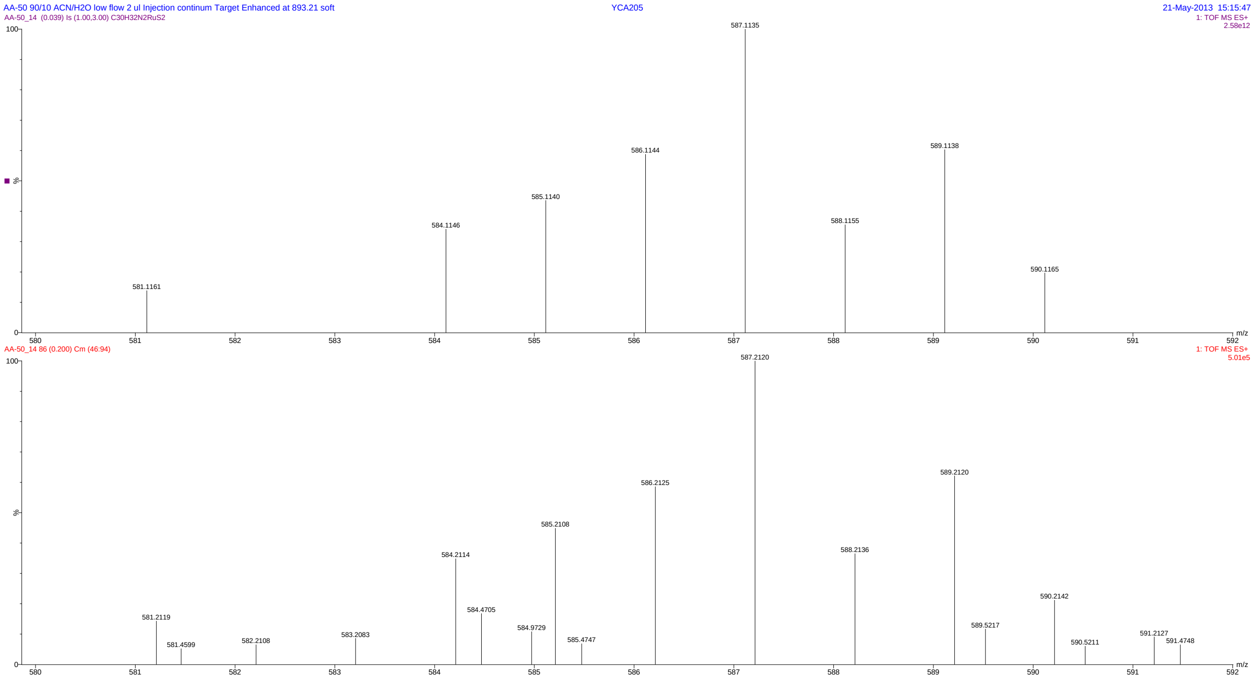

Figure S72. HRMS of **2b** (X = BF_4) for peak 0.26 min; signal 357 *m/z* (full); theoretical results above, experiment below – low energy ionization

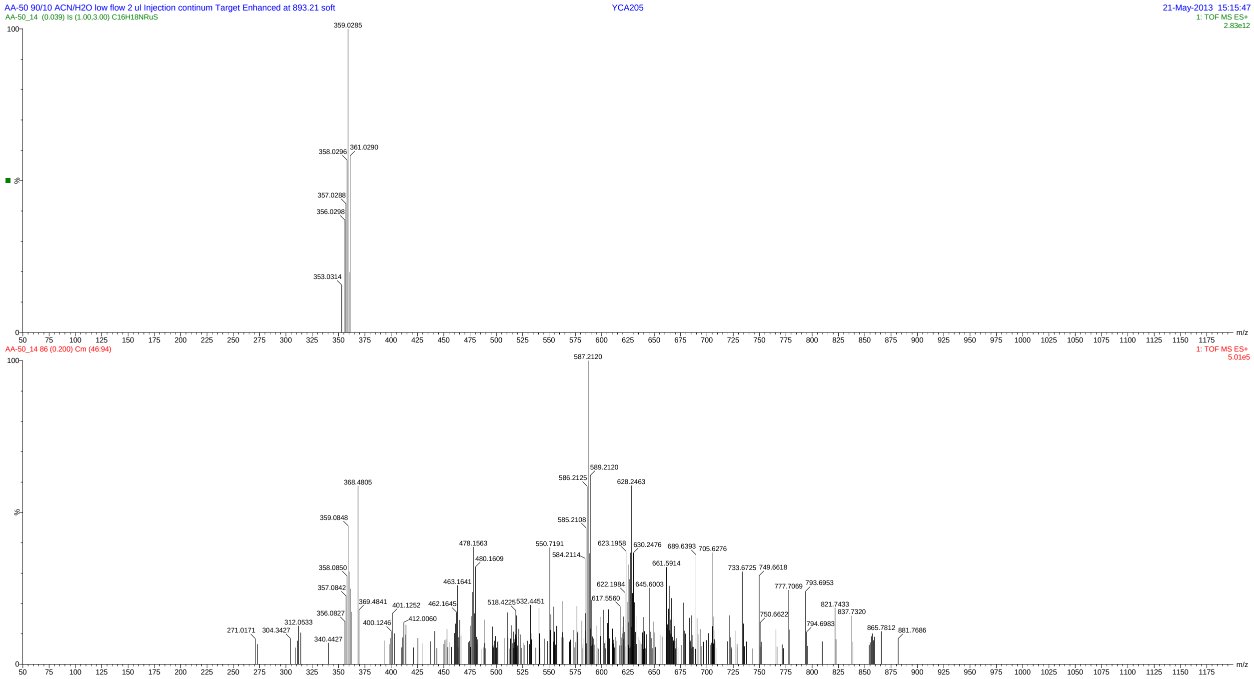

Figure S73. HRMS of **2b** (X = BF_4) for peak 0.26 min; signal 357 *m/z* (zoom); theoretical results middle and above (+1H), experiment below – low energy ionization

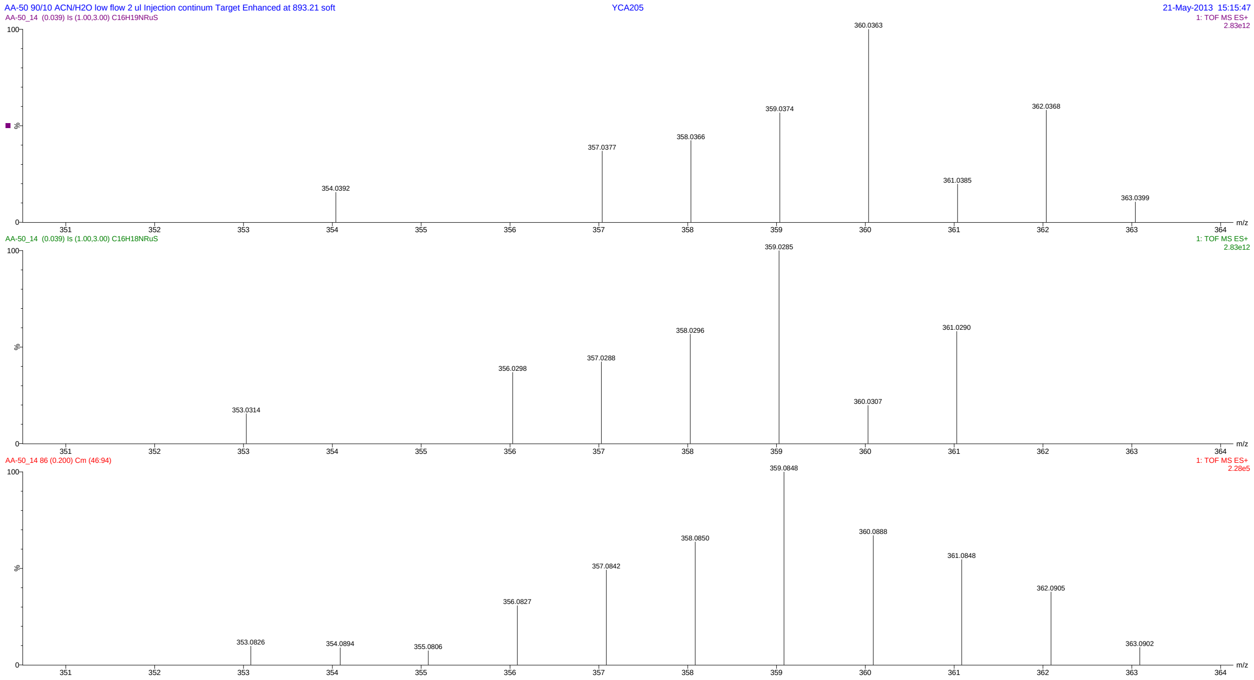

Figure S74. UPLC-MS chromatogram of **2b** (X = BF_4) – high energy ionization

Figure S75. HRMS of **2b** (X = BF_4) – high energy ionization

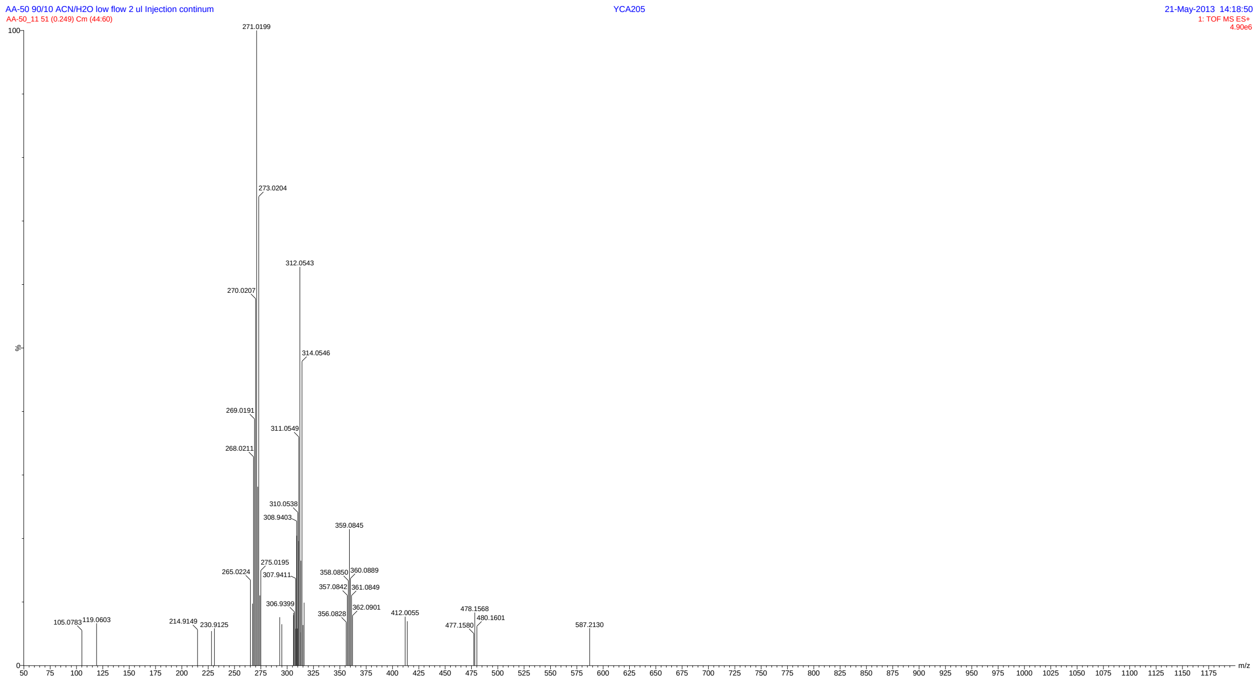

Figure S76. HRMS of **2b** (X = BF_4) signal 893 *m/z* (full); theoretical results above, experiment below – high energy ionization

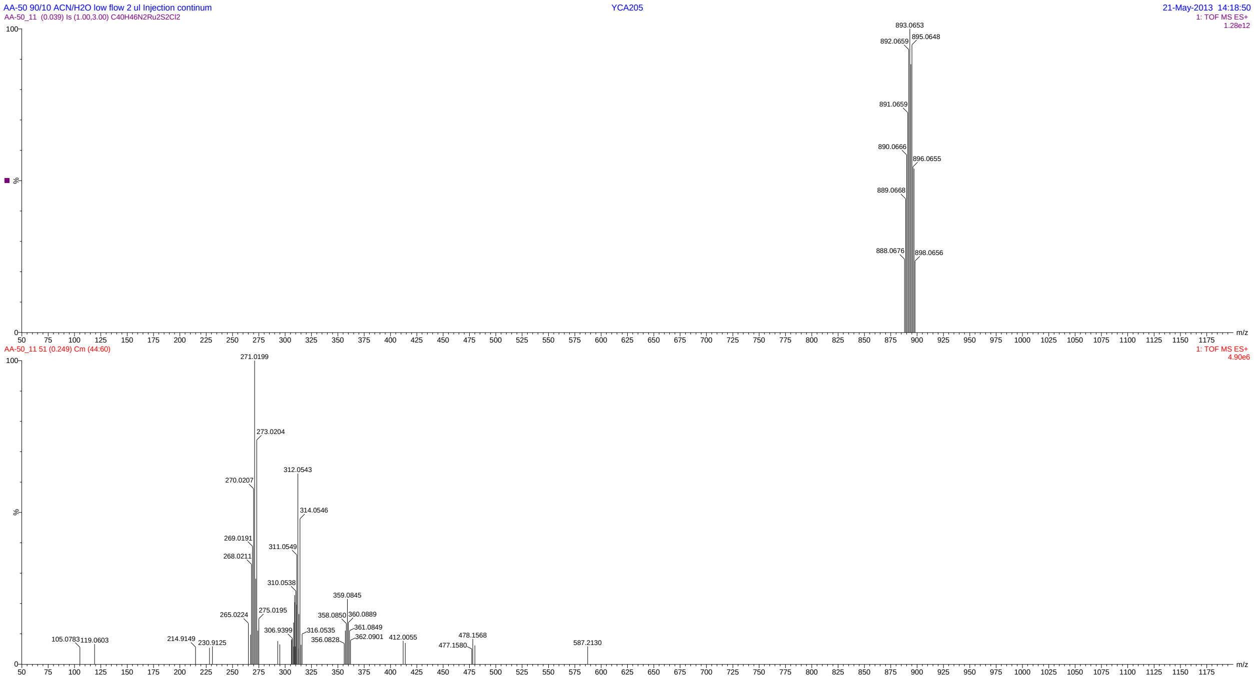

Figure S77. HRMS of **2b** (X = BF_4) signal 893 *m/z* (zoom); theoretical results above, experiment below – high energy ionization

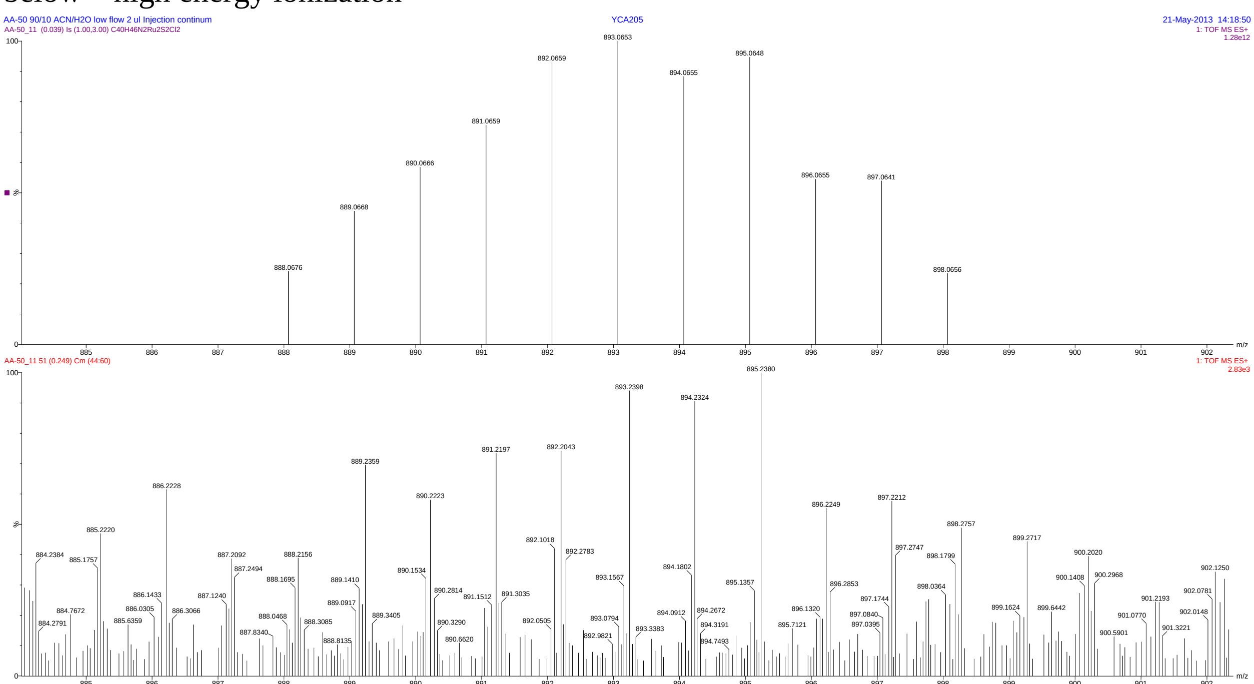

Figure S78. HRMS of **2b** (X = BF_4) signal 587 *m/z* (full); theoretical results above, experiment below – high energy ionization

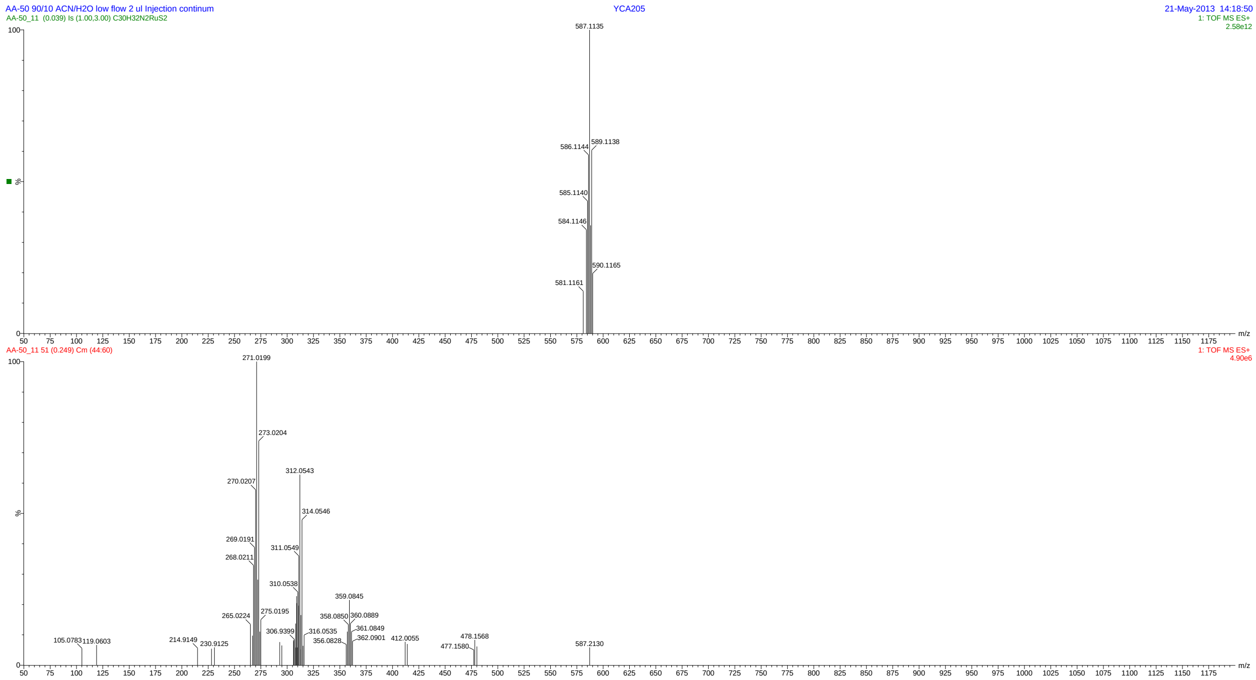

Figure S79. HRMS of **2b** (X = BF_4) signal 587 *m/z* (zoom); theoretical results above, experiment below – high energy ionization

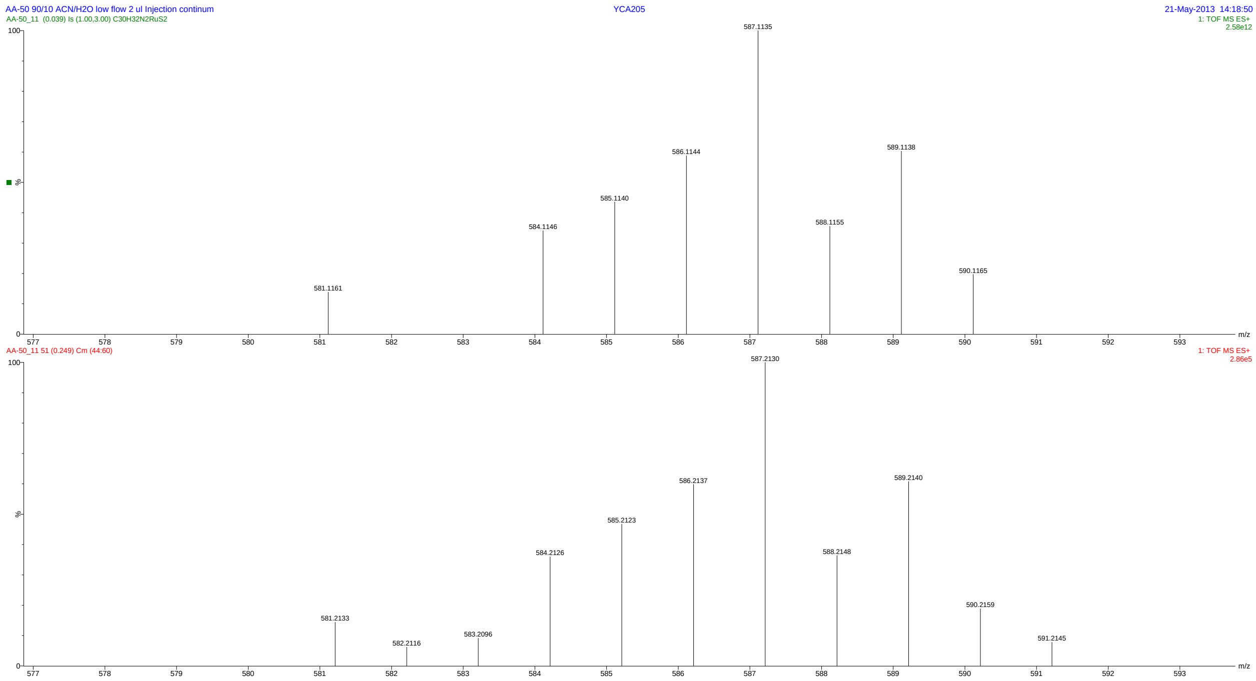

Electronic Supplementary Material (ESI) for Dalton Transactions
This journal is © The Royal Society of Chemistry 2013

Figure S80. HRMS of **2b** (X = BF_4) signal 359 *m/z* (full); theoretical results above, experiment below – high energy ionization

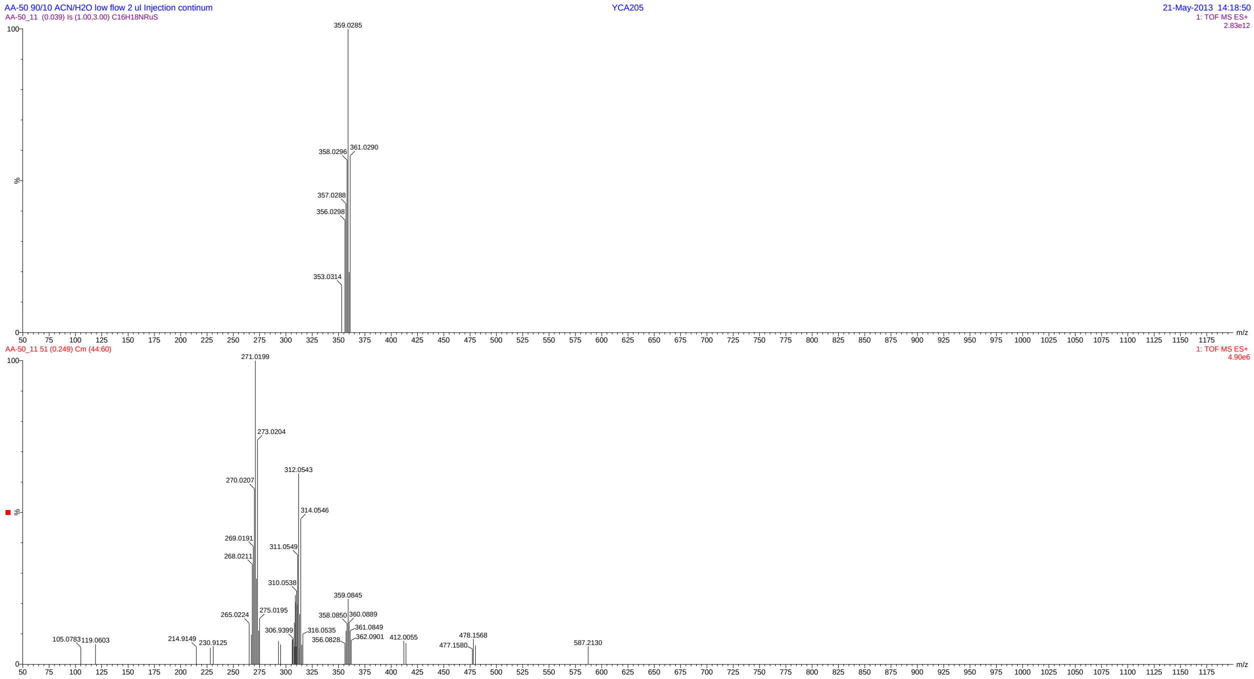

Figure S81. HRMS of **2b** (X = BF_4) signal 359 *m/z* (zoom); theoretical results middle and above (+1H), experiment below – low energy ionization

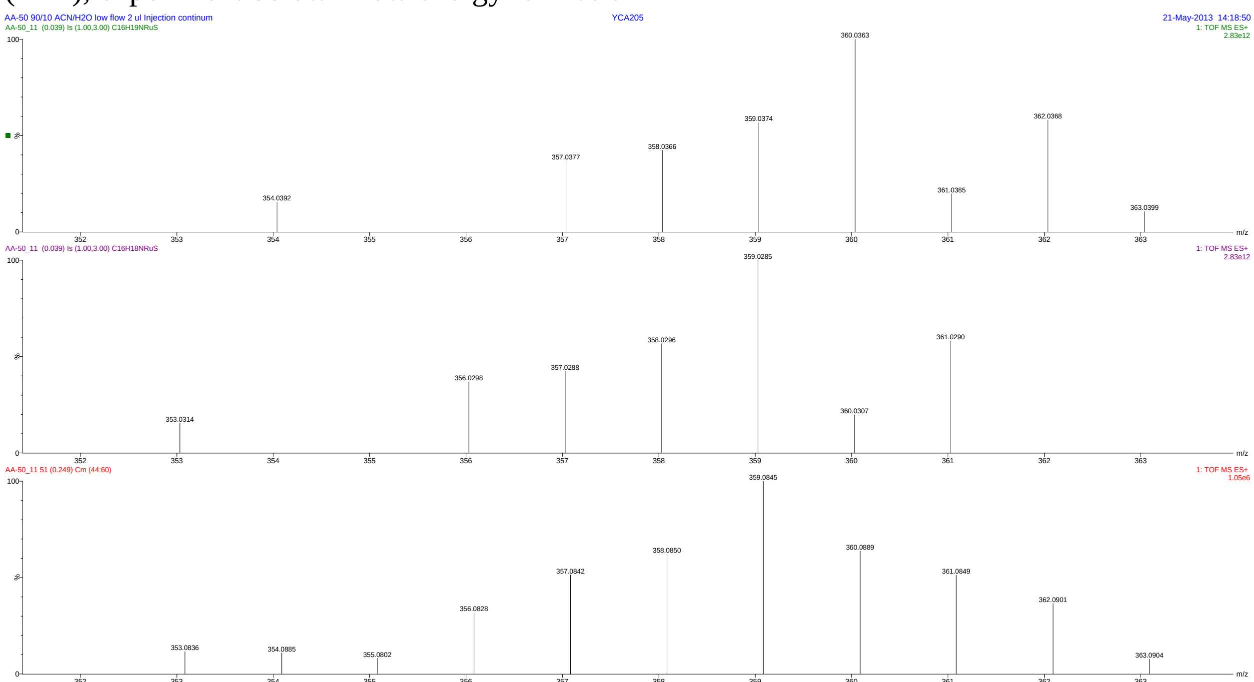

Figure S82. HRMS of **2b** (X = BF_4) signal 312 *m/z* (full); theoretical results above, experiment below – high energy ionization

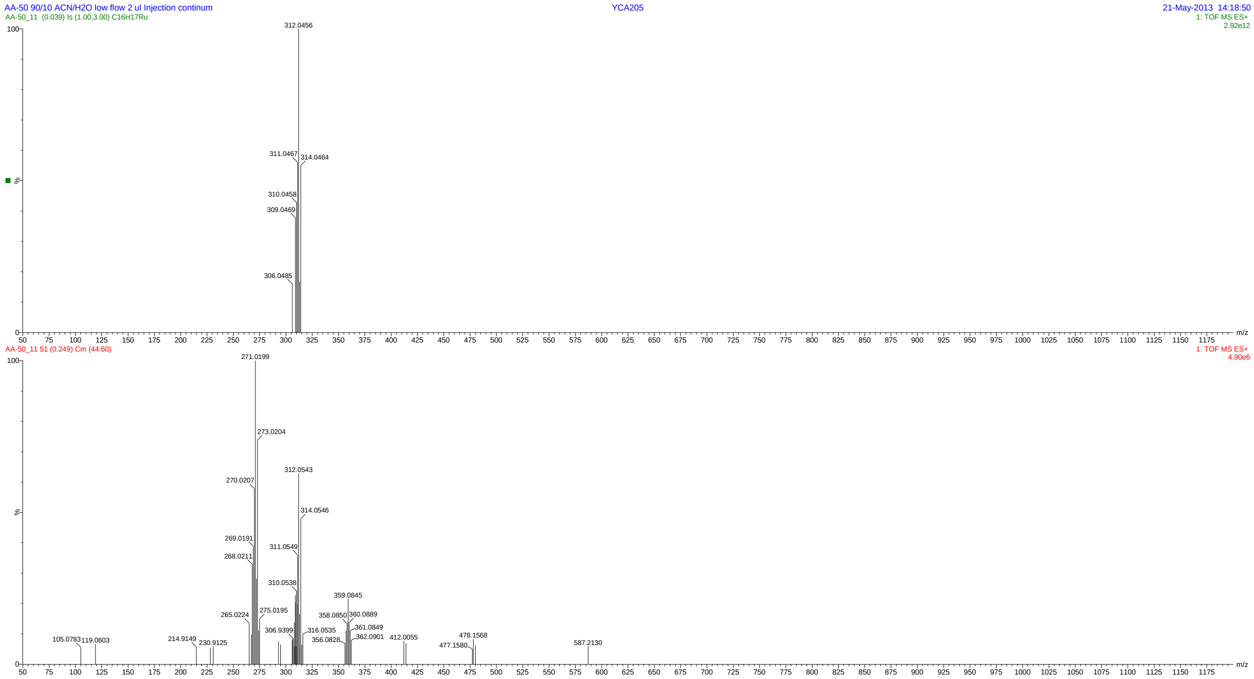

Figure S83. HRMS of **2b** (X = BF_4) signal 312 *m/z* (zoom); theoretical results above, experiment below – high energy ionization

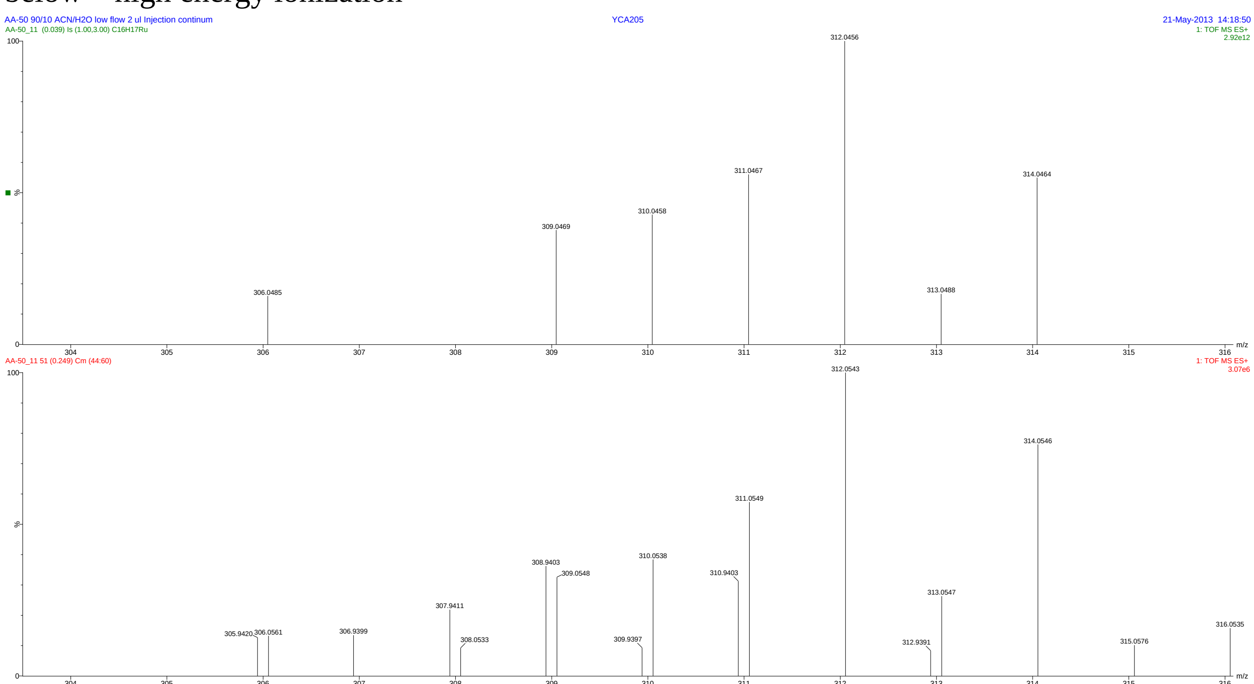

Electronic Supplementary Material (ESI) for Dalton Transactions
This journal is © The Royal Society of Chemistry 2013

Figure S84. HRMS of **2b** (X = BF_4) signal 270 *m/z* (full); theoretical results above, experiment below – high energy ionization

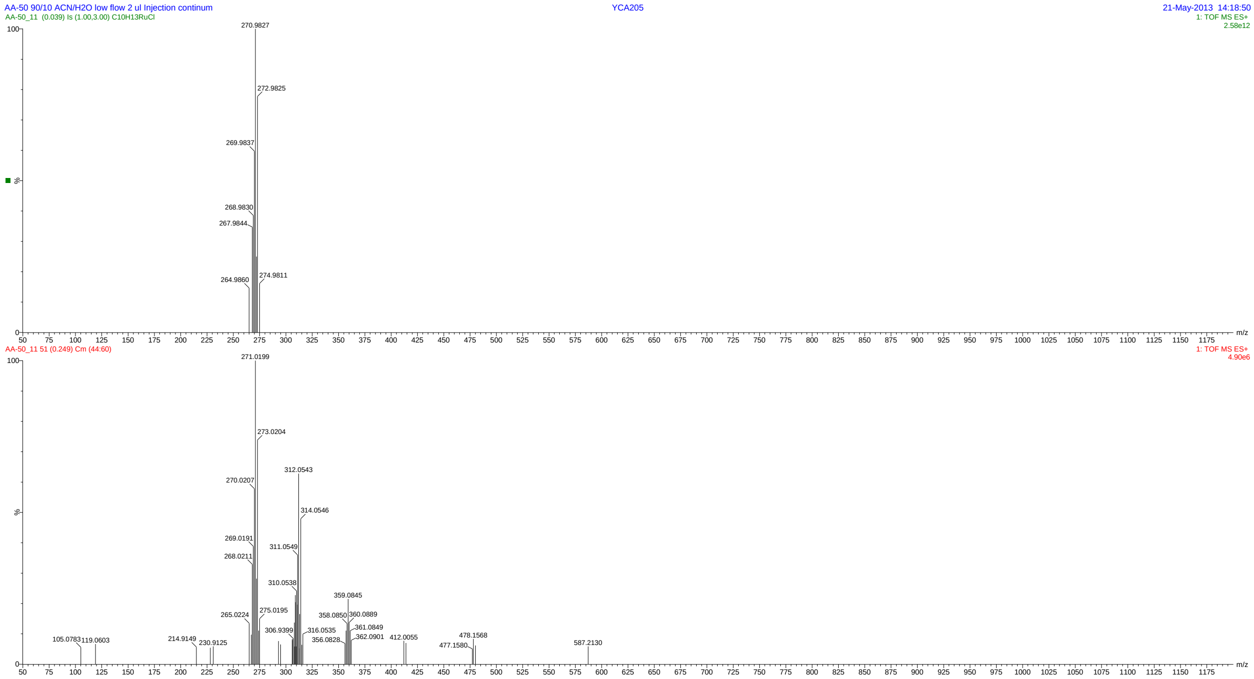

Figure S85. HRMS of **2b** (X = BF_4) signal 270 *m/z* (zoom); theoretical results above, experiment below – high energy ionization

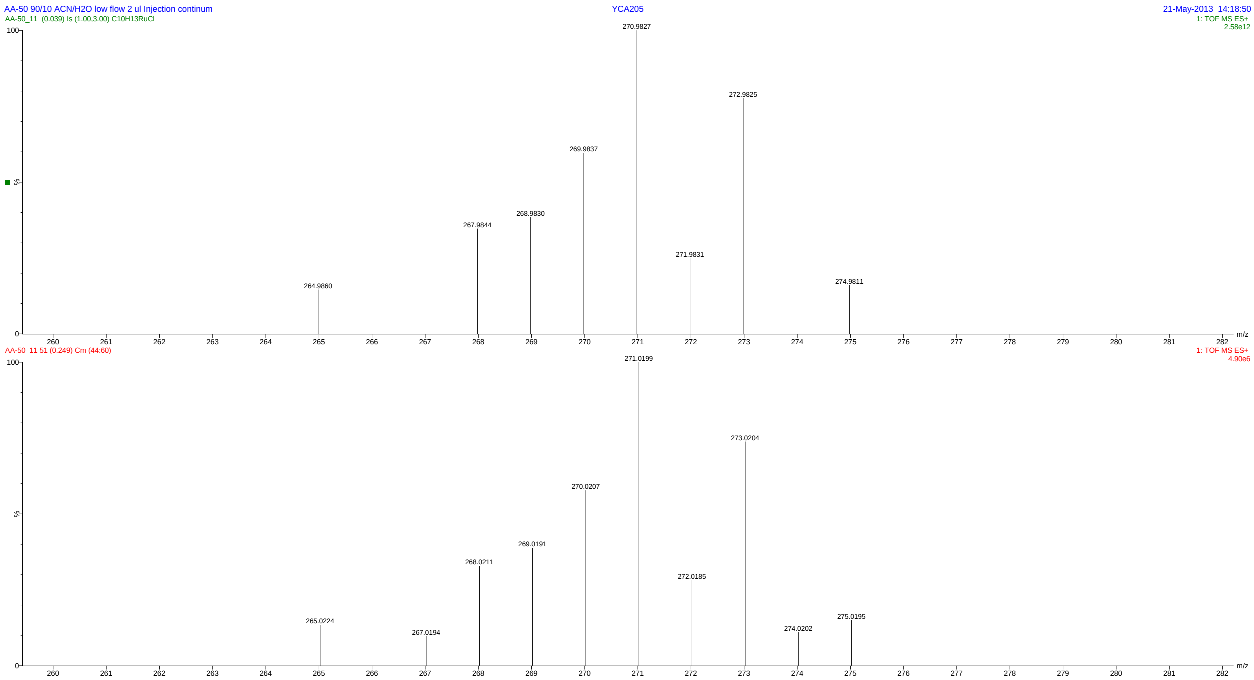

Figure S86. UPLC-MS chromatogram of **2b** (X = PF_6) – medium energy ionization

Figure S87. HRMS of **2b** (X = PF_6) – medium energy ionization

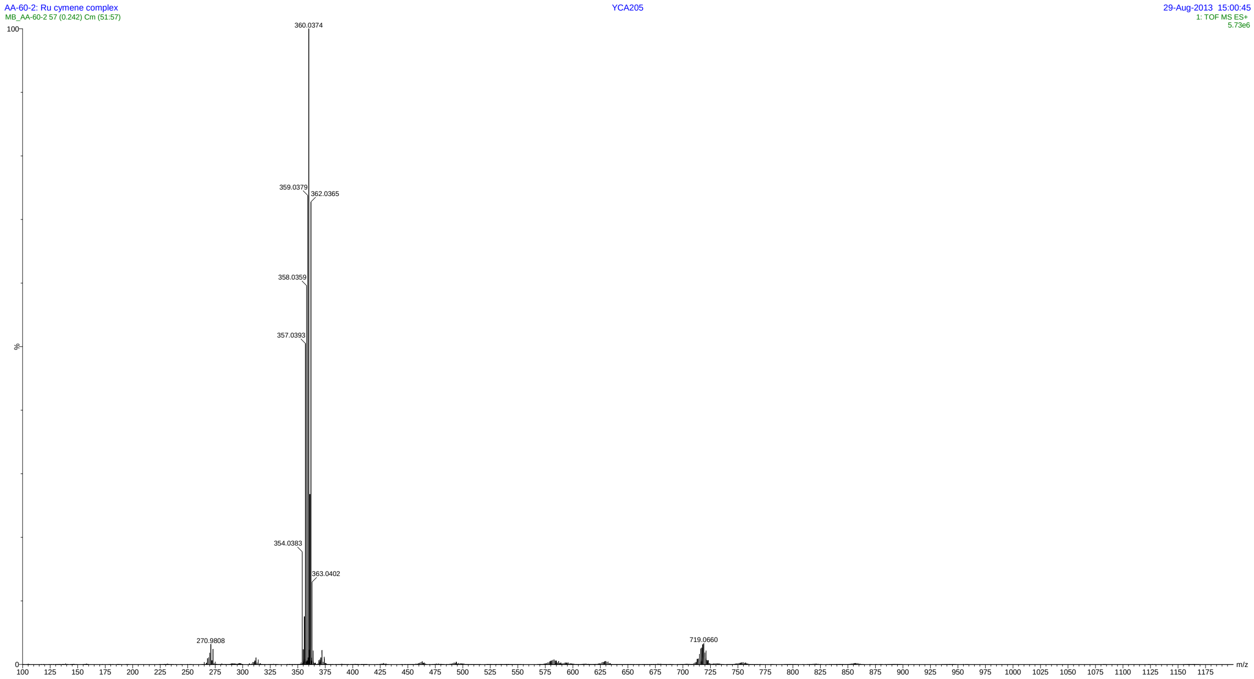

Figure S88. HRMS of **2b** (X = PF_6); 50-fold magnification – medium energy ionization

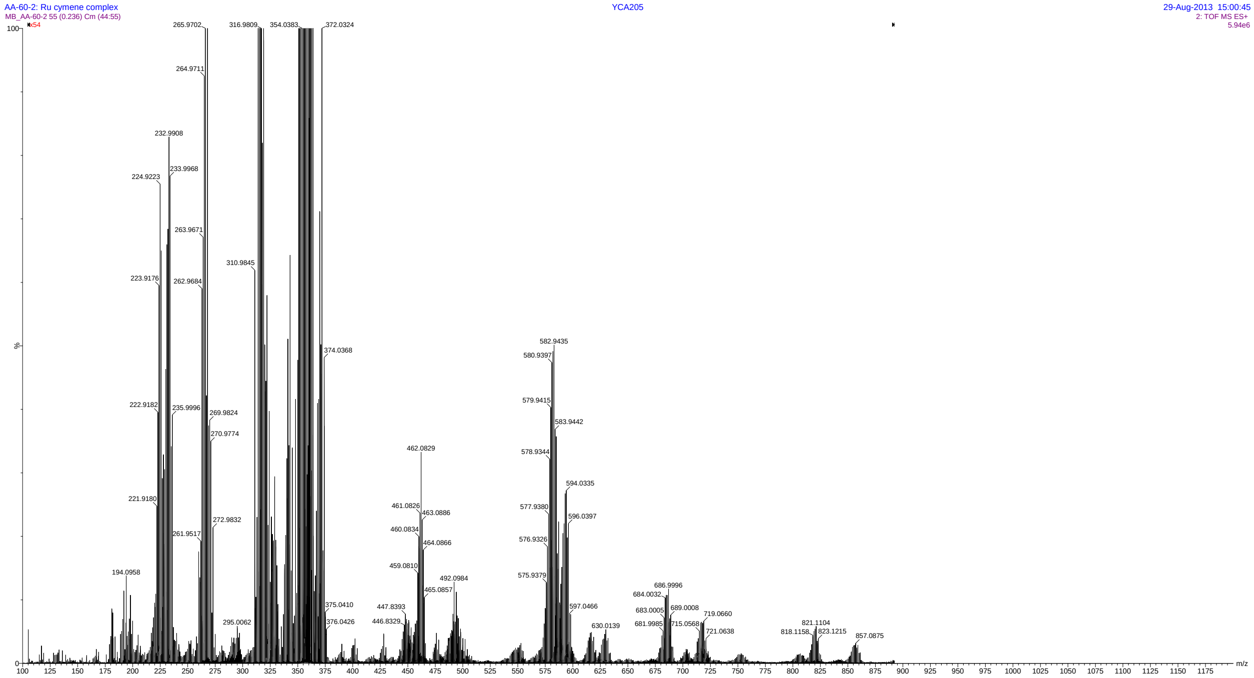

Figure S89. HRMS of **2b** (X = PF_6); signal 893 *m/z* (full); theoretical results above, experiment below – low energy ionization

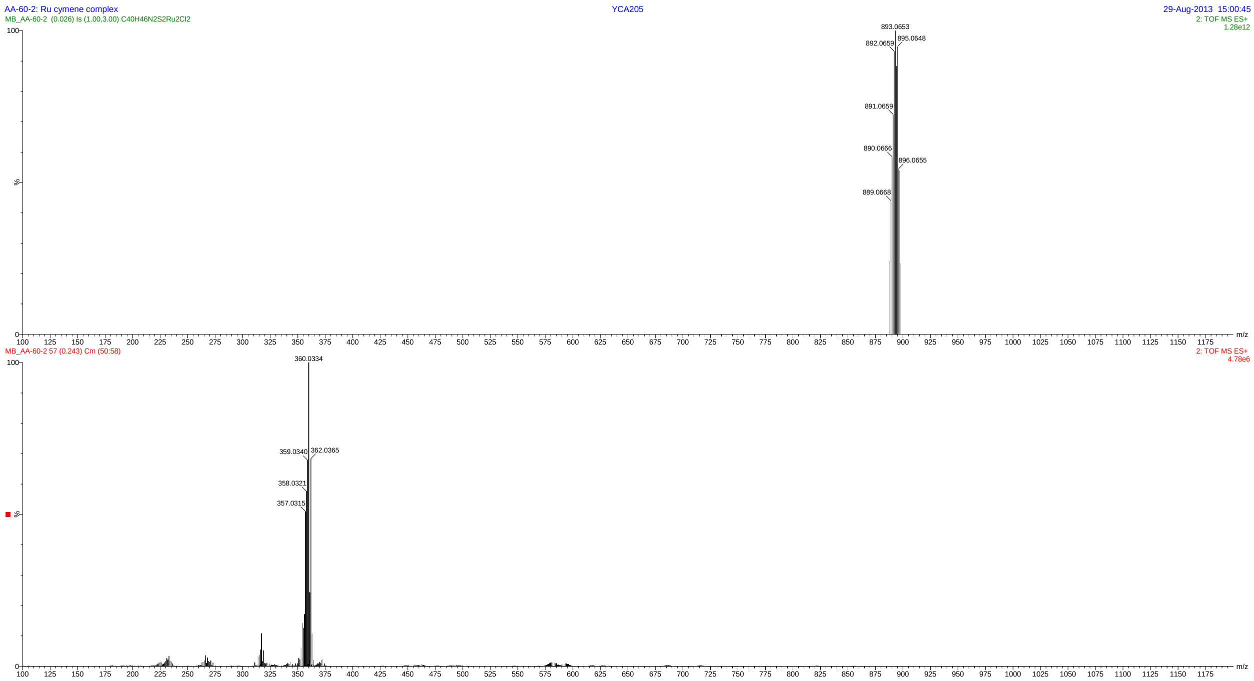

Figure S90. HRMS of **2b** (X = PF_6); signal 893 *m/z* (zoom); theoretical results above, experiment below – low energy ionization

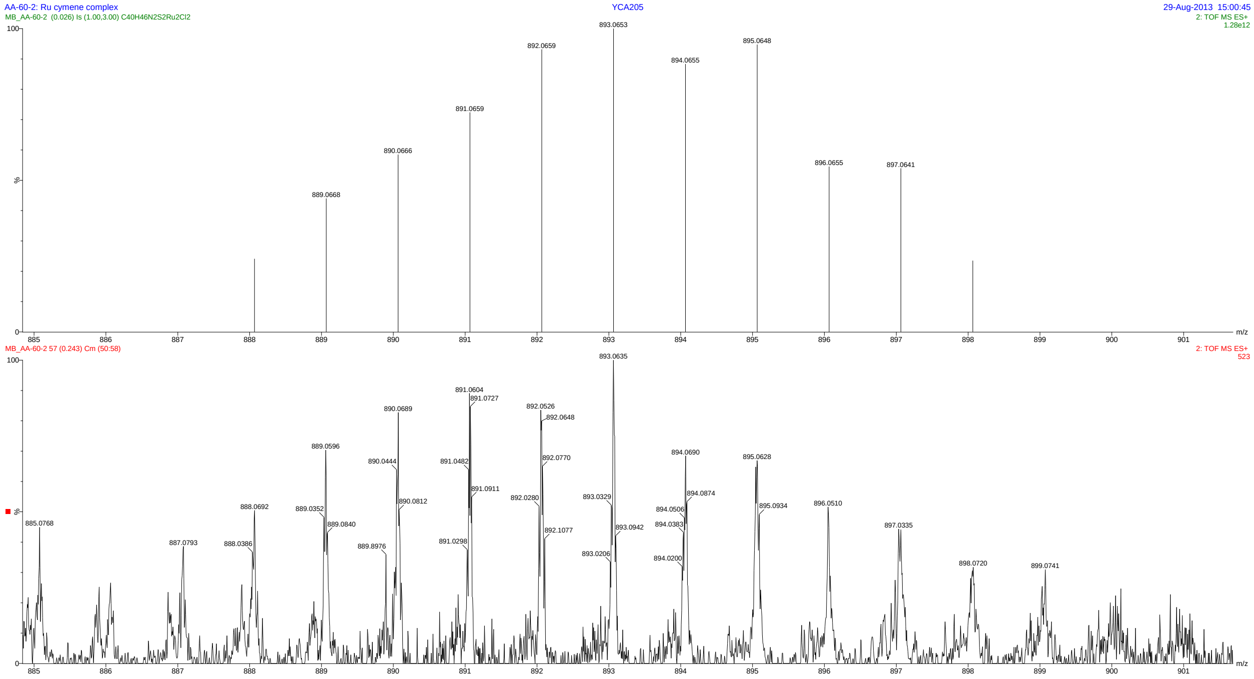

Figure S91. UPLC-MS chromatogram of **2c** (X = BF_4) – low energy ionization

Figure S92. HRMS of **2c** (X = BF_4) – low energy ionization

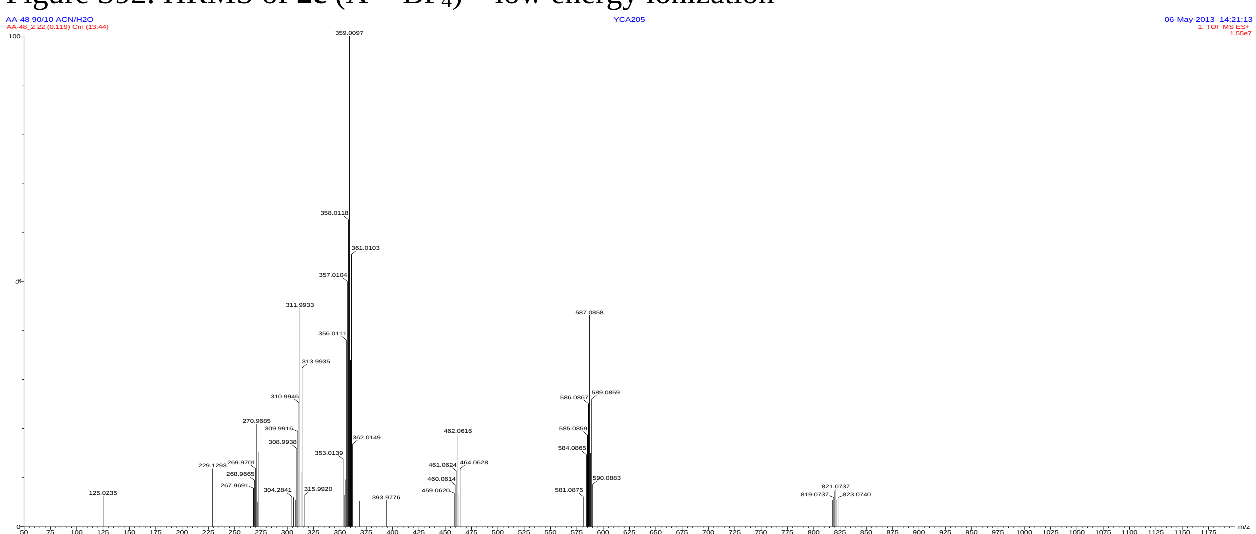

Figure S93. HRMS of **2c** (X = BF_4) signal 893 *m/z* (full); theoretical results above, experiment below – low energy ionization

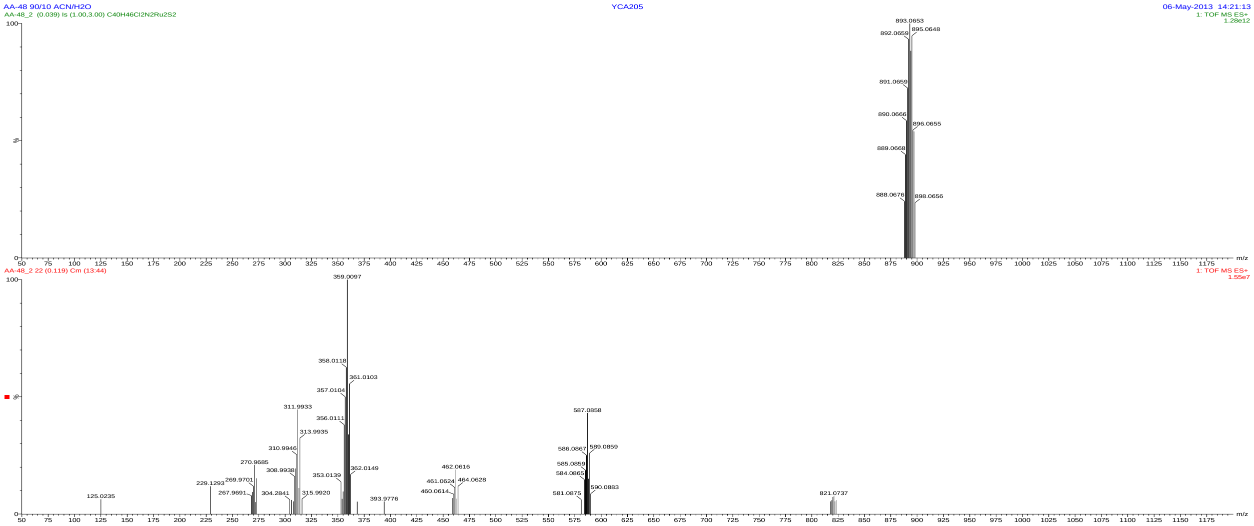

Figure S94. HRMS of **2c** (X = BF_4) signal 893 *m/z* (zoom); theoretical results above, experiment below – low energy ionization

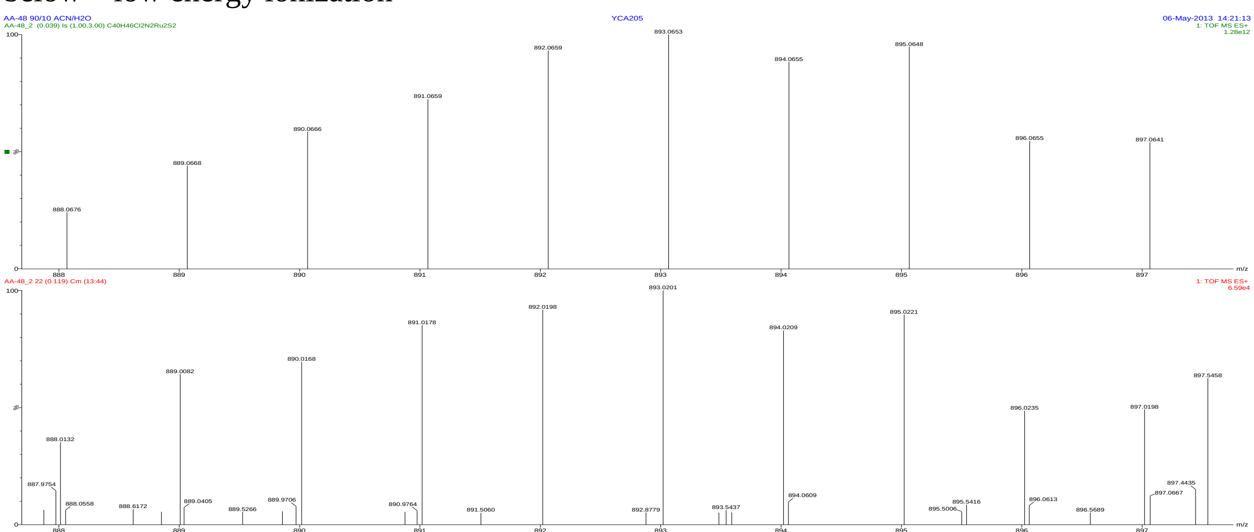

Figure S95. HRMS of **2c** (X = BF_4) signal 857 *m/z* (full); theoretical results above, experiment below – low energy ionization

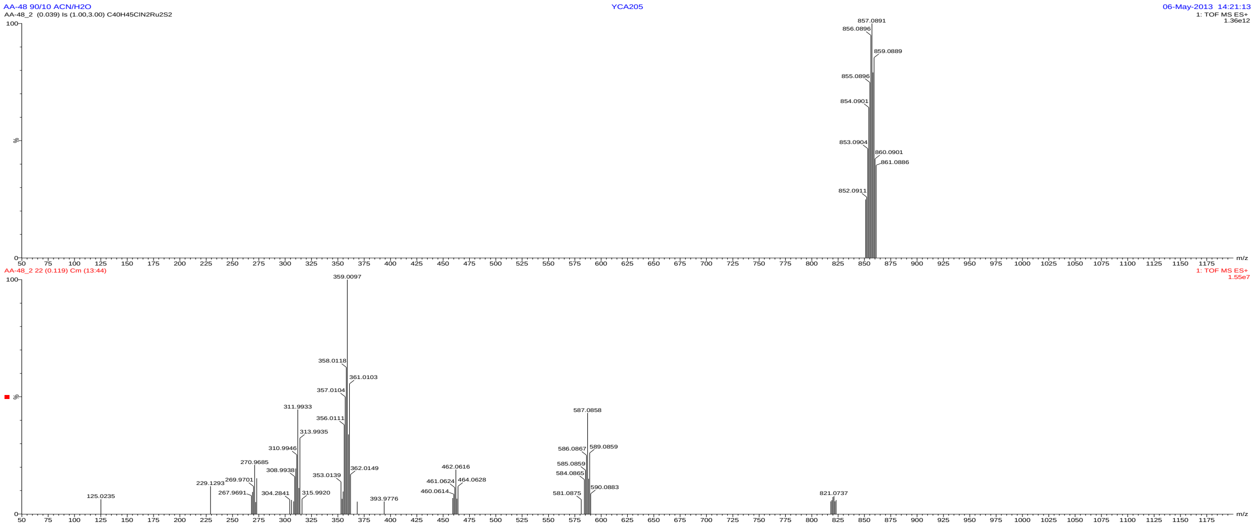

Figure S96. HRMS of **2c** (X = BF_4) signal 857 *m/z* (zoom); theoretical results above, experiment below – low energy ionization

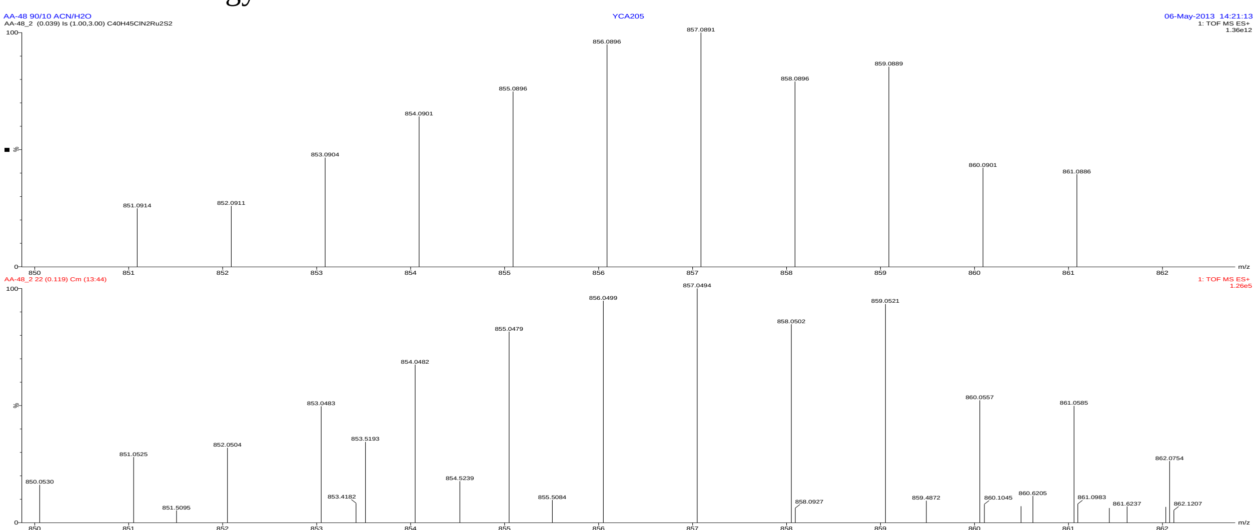

Electronic Supplementary Material (ESI) for Dalton Transactions

Figure S97. HRMS of **2c** (X = BF_4) signal 821 *m/z* (full); theoretical results above, experiment below – low energy ionization

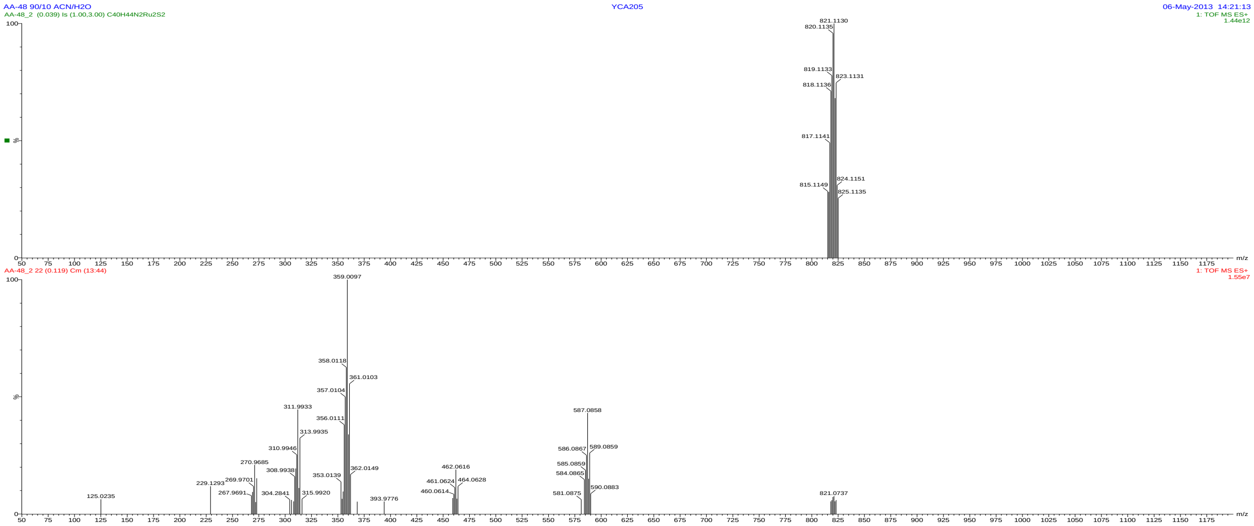

Figure S98. HRMS of **2c** (X = BF_4) signal 821 *m/z* (zoom); theoretical results above, experiment below – low energy ionization

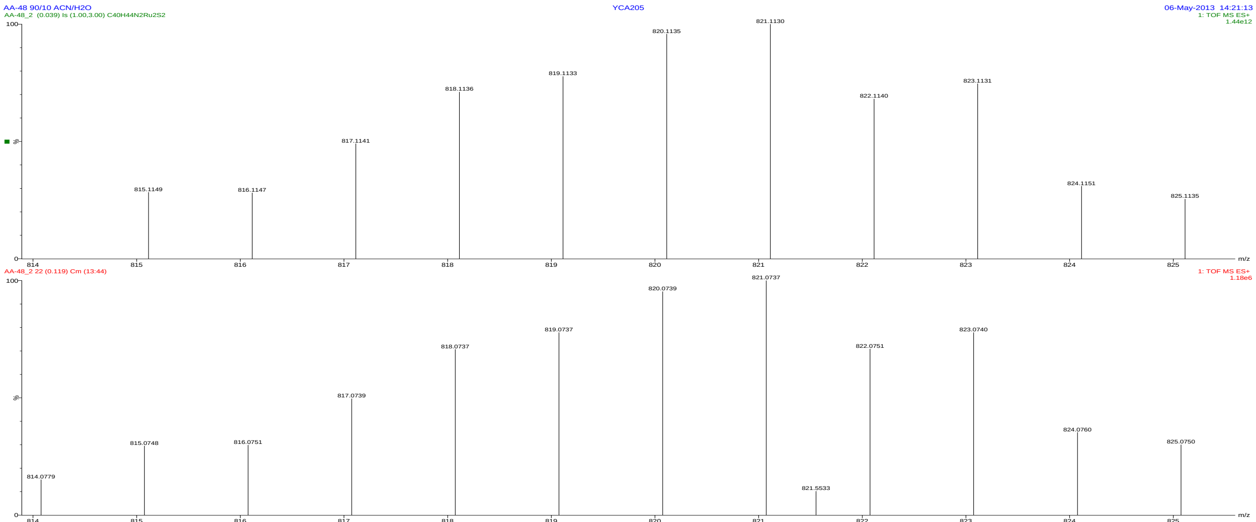

Figure S99. HRMS of **2c** (X = BF_4) signal 587 *m/z* (full); theoretical results above, experiment below – low energy ionization

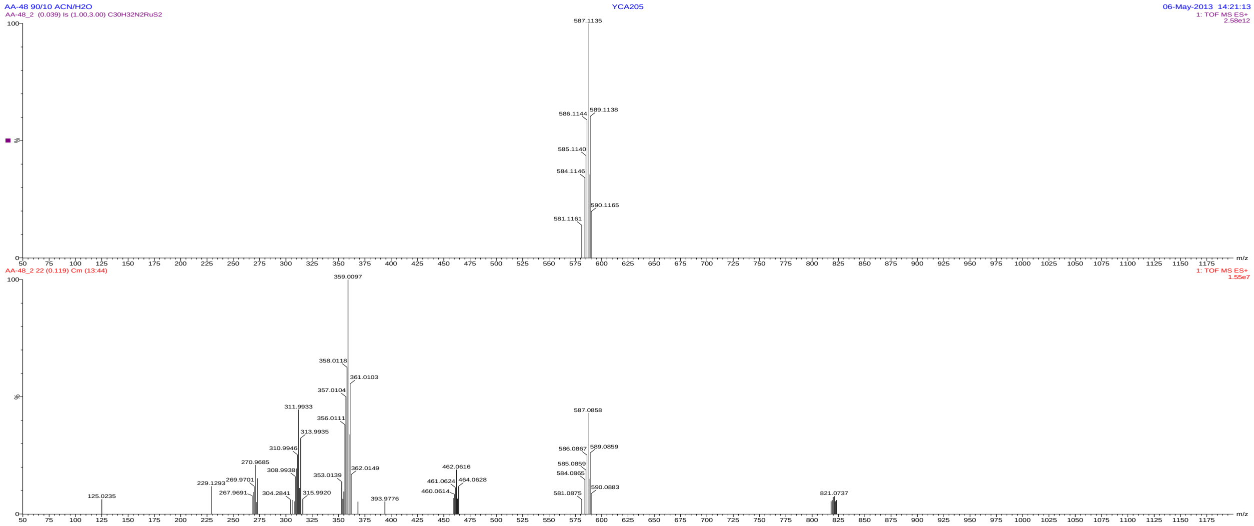

Figure S100. HRMS of **2c** (X = BF_4) signal 587 *m/z* (zoom); theoretical results above, experiment below – low energy ionization

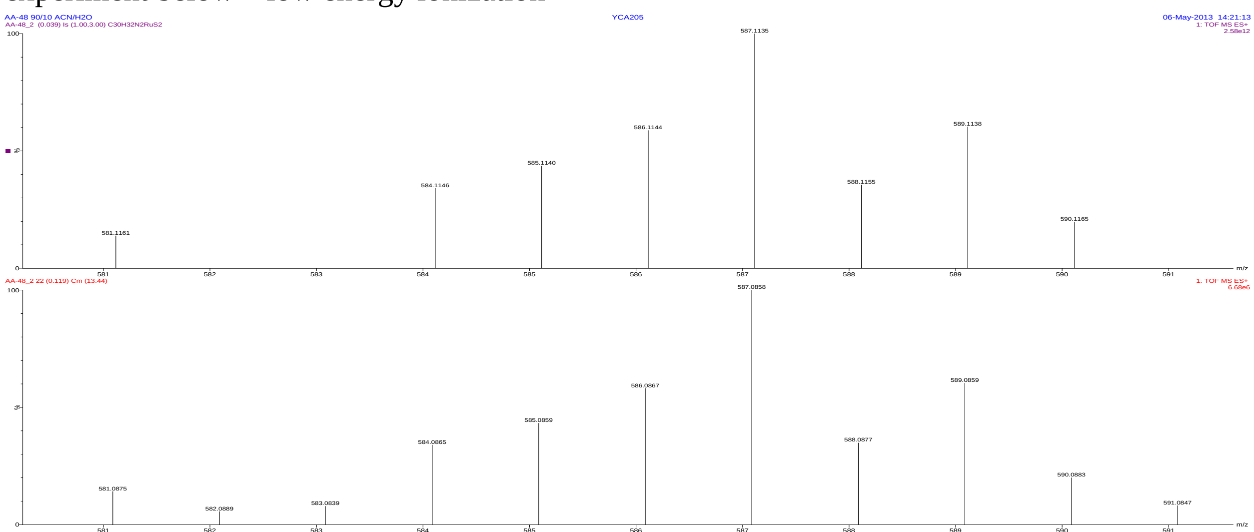

Figure S101. HRMS of **2c** (X = BF_4) signal 462 *m/z* (full); theoretical results above, experiment below – low energy ionization

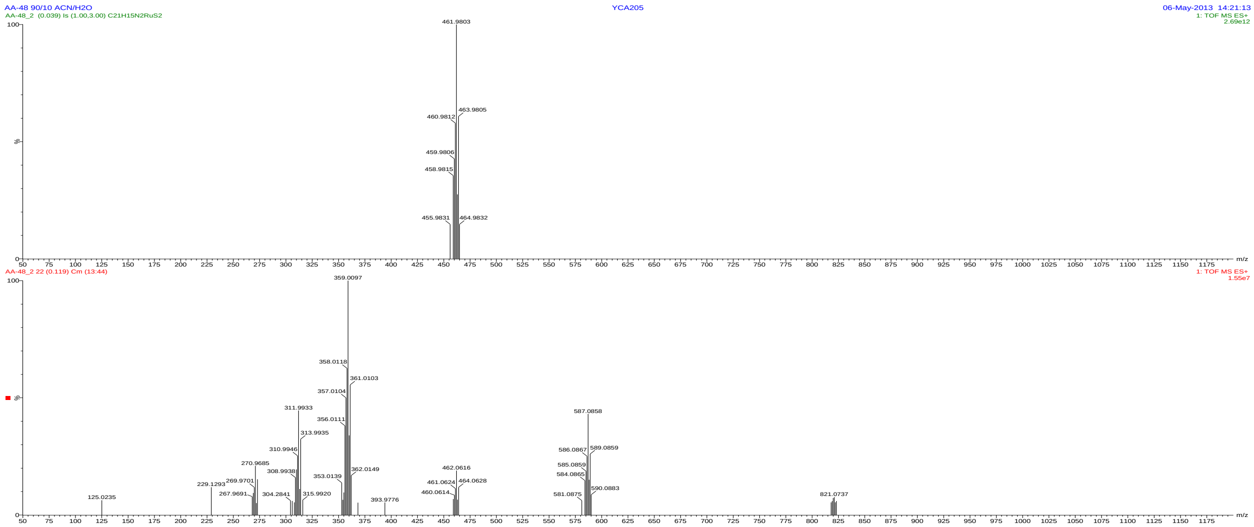

Figure S102. HRMS of **2c** (X = BF_4) signal 462 *m/z* (zoom); theoretical results above, experiment below – low energy ionization

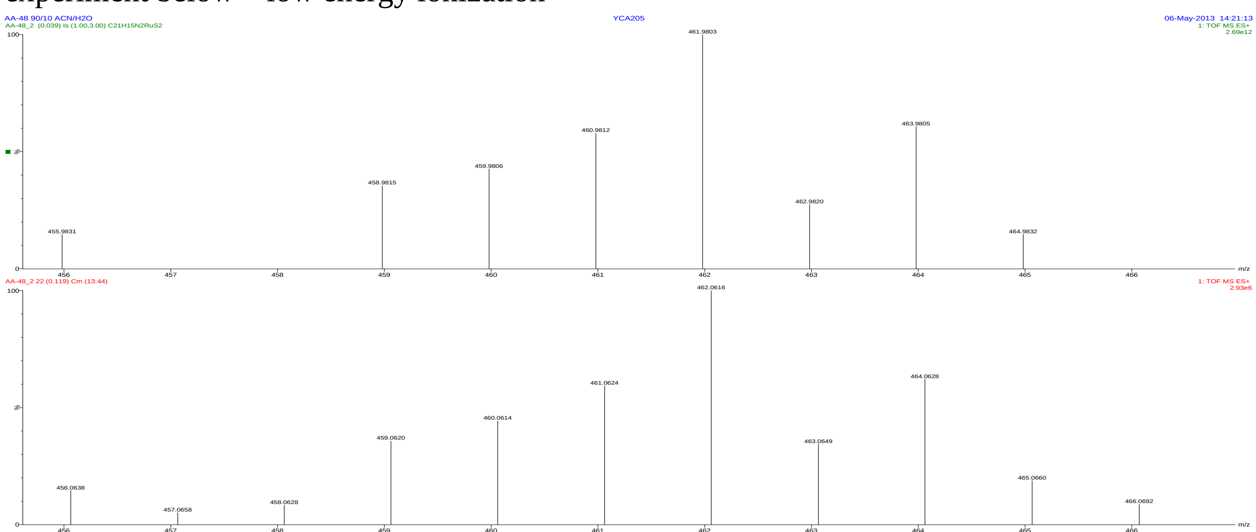

Figure S103. HRMS of **2c** (X = BF_4) signal 359 *m/z* (full); theoretical results above, experiment below – low energy ionization

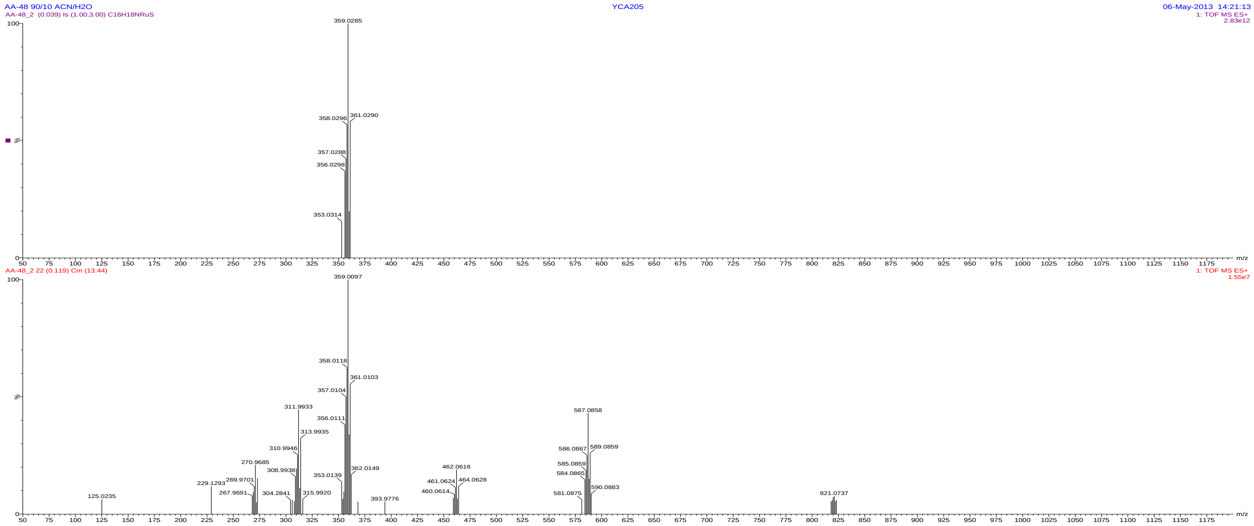

Figure S104. HRMS of **2c** (X = BF_4) signal 359 *m/z* (zoom); theoretical results above, experiment below – low energy ionization

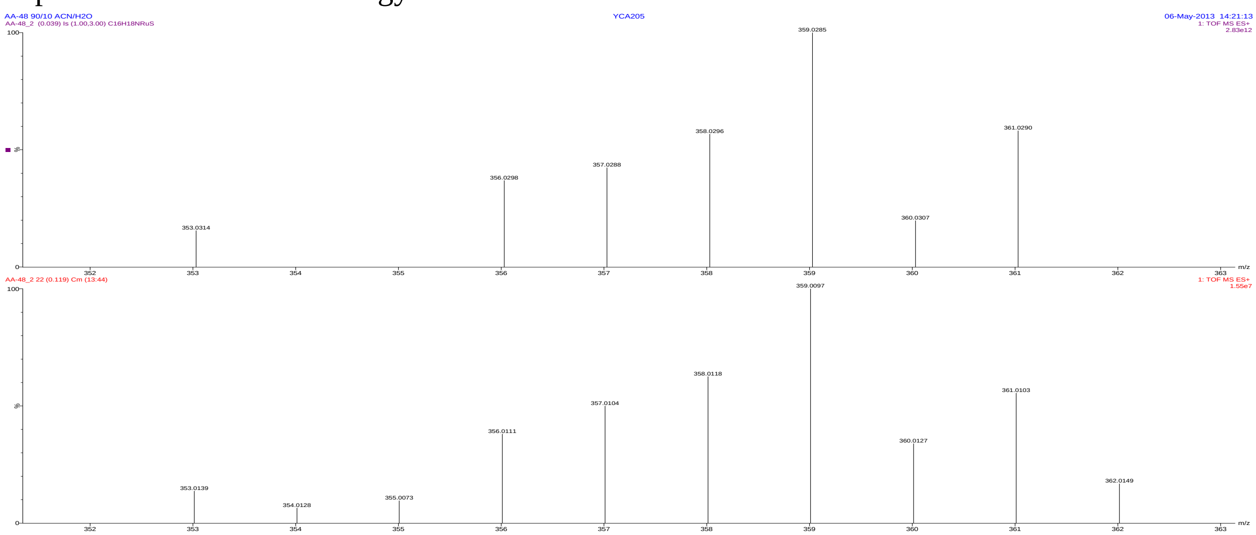

Figure S105. HRMS of **2c** (X = BF_4) signal 312 *m/z* (full); theoretical results above, experiment below – low energy ionization

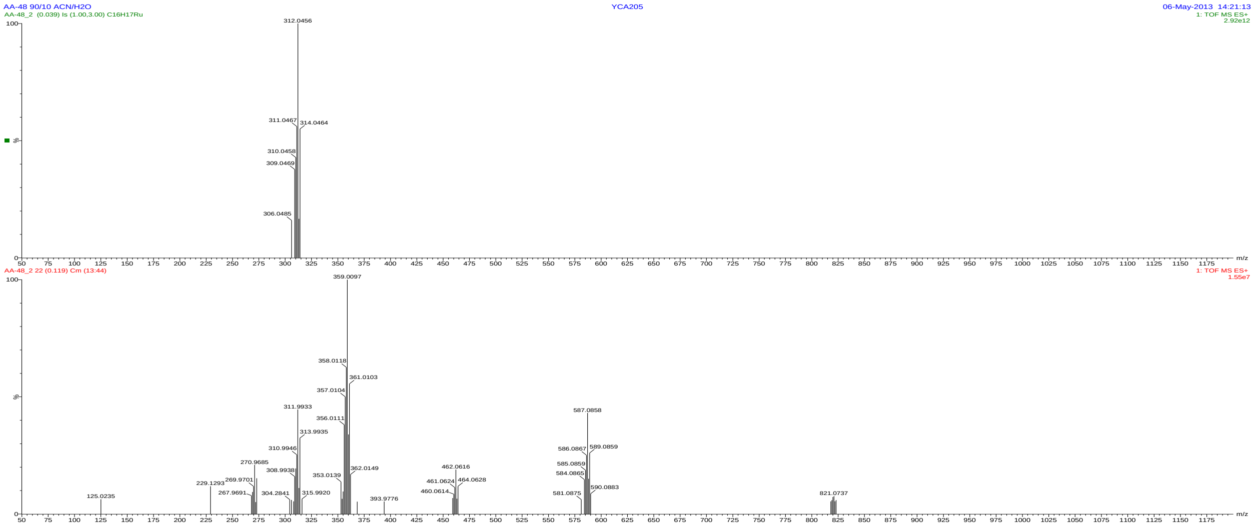

Figure S106. HRMS of **2c** (X = BF_4) signal 312 *m/z* (zoom); theoretical results above, experiment below – low energy ionization

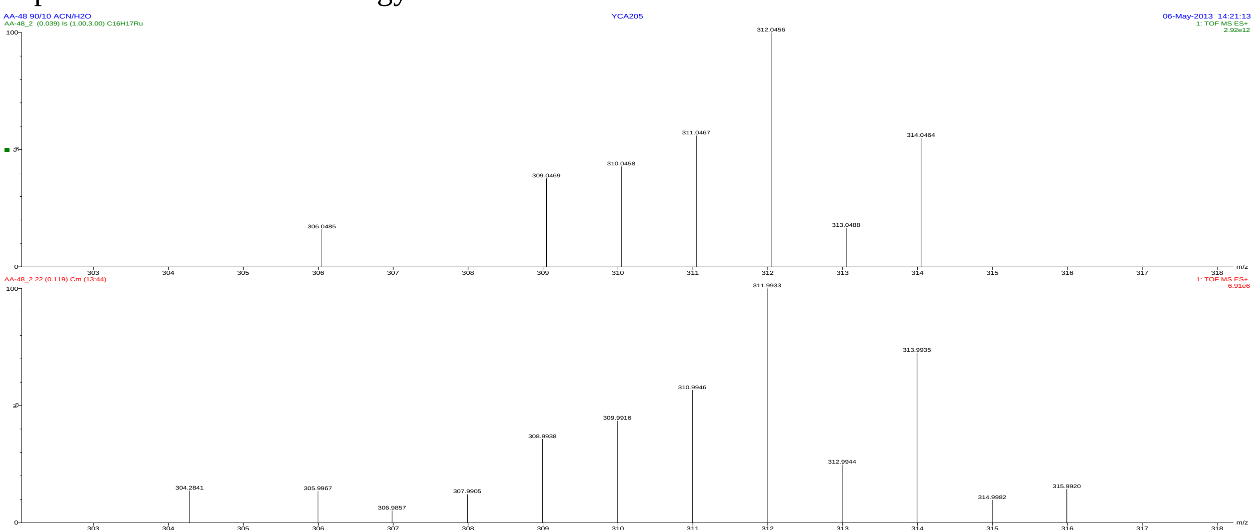

Figure S107. HRMS of **2c** (X = BF_4) signal 270 *m/z* (full); theoretical results above, experiment below – low energy ionization

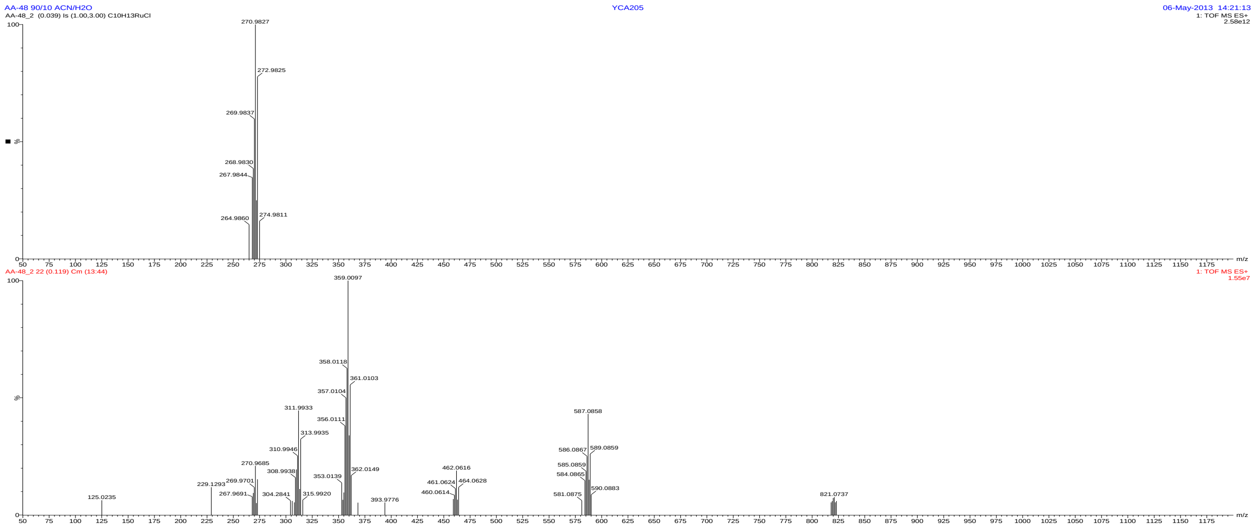

Figure S108. HRMS of **2c** (X = BF_4) signal 270 *m/z* (zoom); theoretical results above, experiment below – low energy ionization

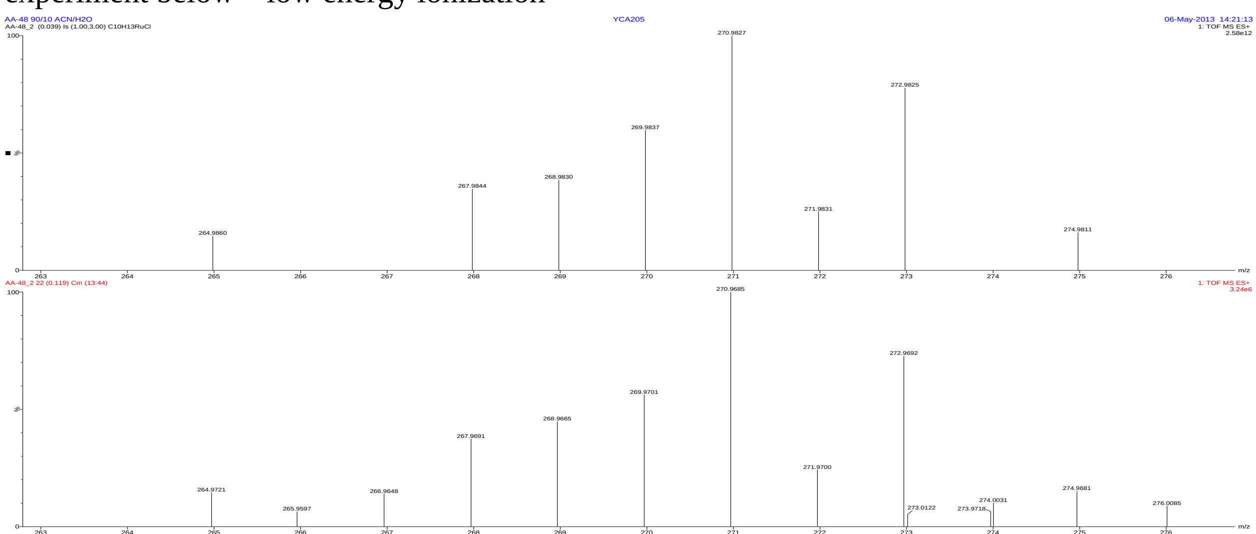

Figure S109. UPLC-MS chromatogram of **2c** (X = BF_4) – high energy ionization

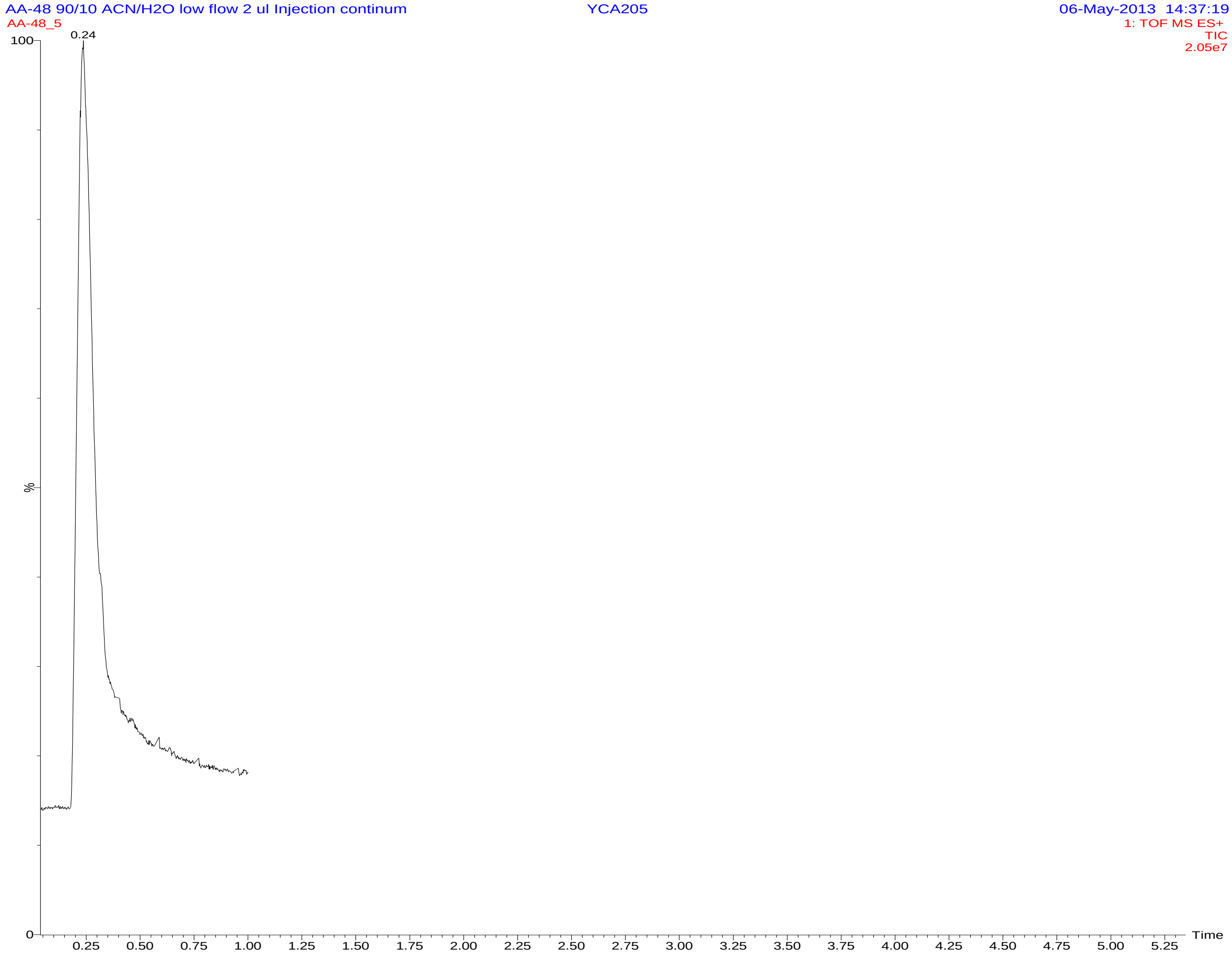

Figure S110. HRMS of **2c** (X = BF_4) – high energy ionization

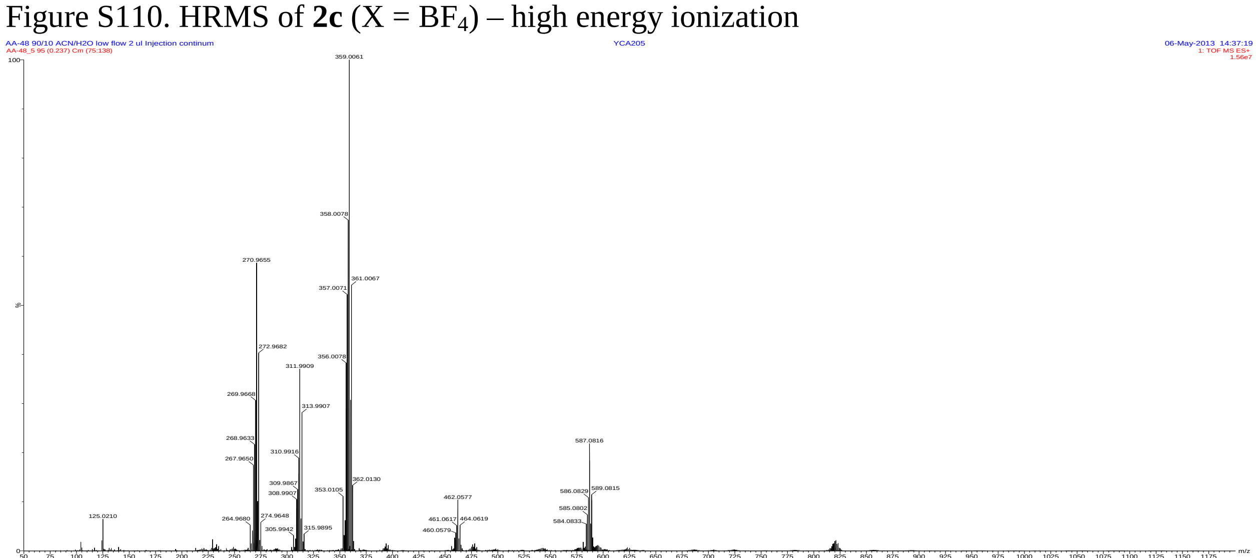

Figure S111. HRMS of **2c** (X = BF_4) signal 893 *m/z* (full); theoretical results above, experiment below – high energy ionization

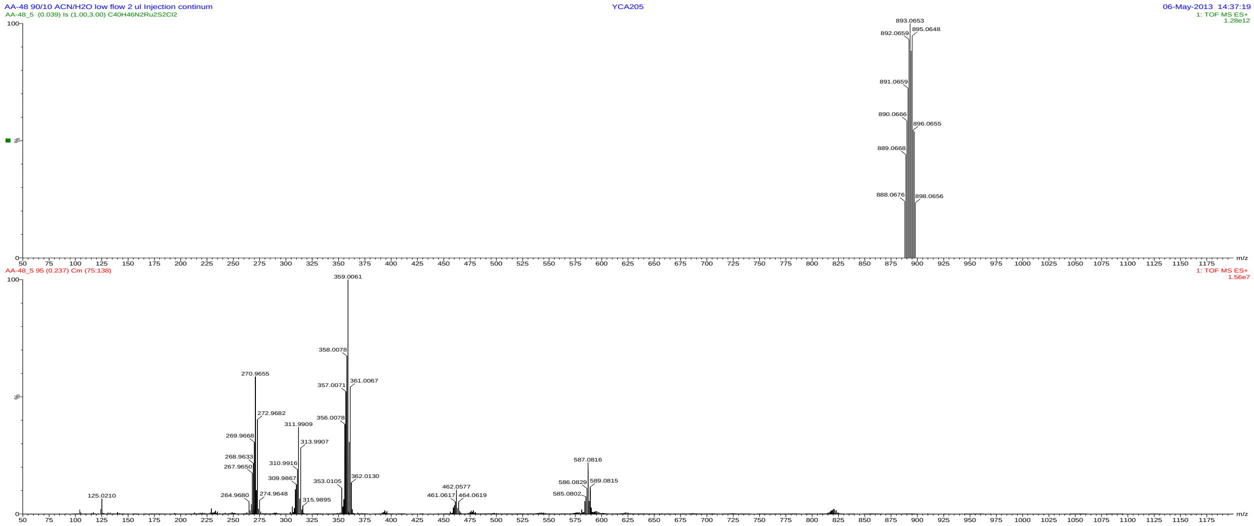

Figure S112. HRMS of **2c** (X = BF_4) signal 893 *m/z* (zoom); theoretical results above, experiment below – high energy ionization

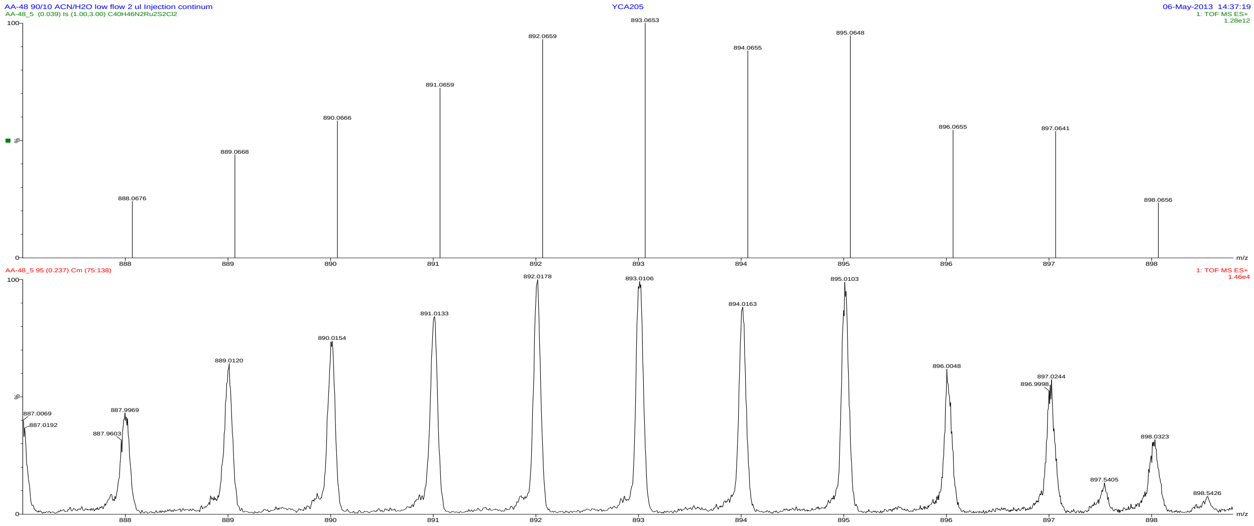

Figure S113. HRMS of **2c** (X = BF_4) signal 857 *m/z* (full); theoretical results above, experiment below – high energy ionization

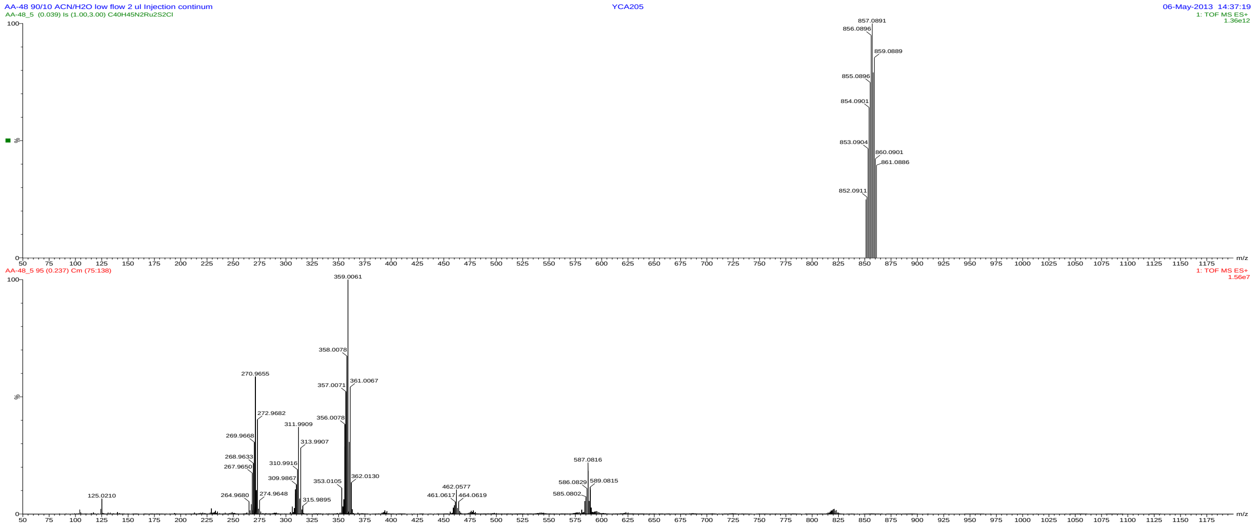

Figure S114. HRMS of **2c** (X = BF_4) signal 857 *m/z* (zoom); theoretical results above, experiment below – high energy ionization

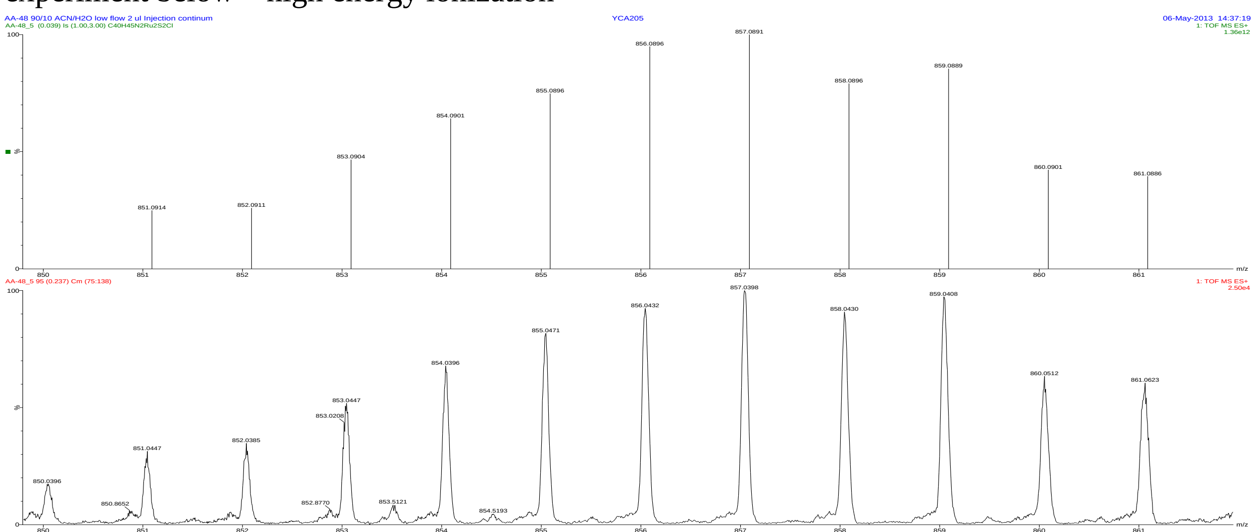

Figure S115. HRMS of **2c** (X = BF_4) signal 821 *m/z* (full); theoretical results above, experiment below – high energy ionization

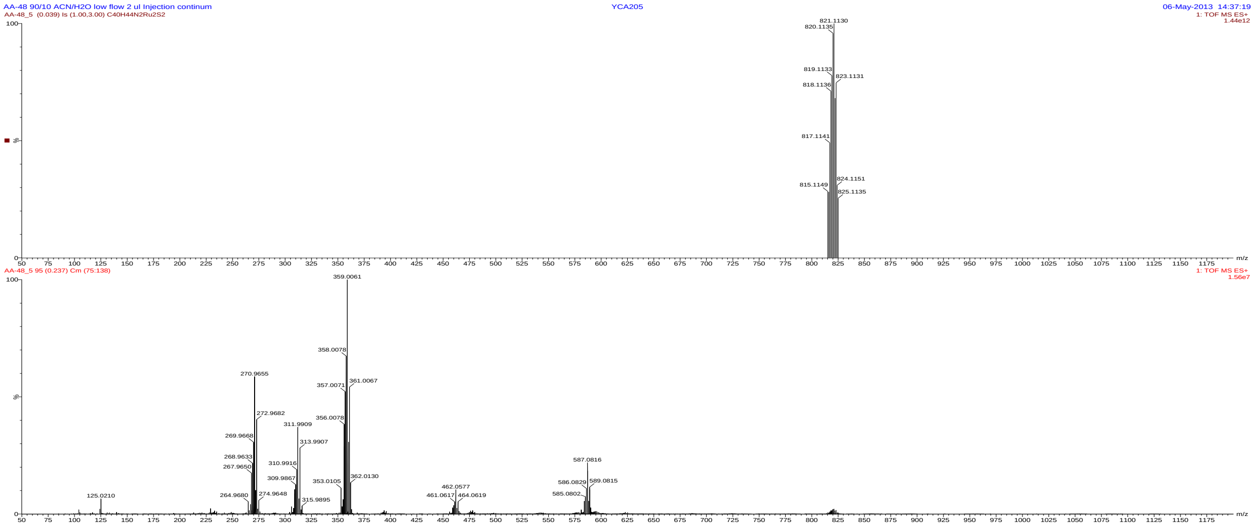

Figure S116. HRMS of **2c** (X = BF_4) signal 821 *m/z* (zoom); theoretical results above, experiment below – high energy ionization

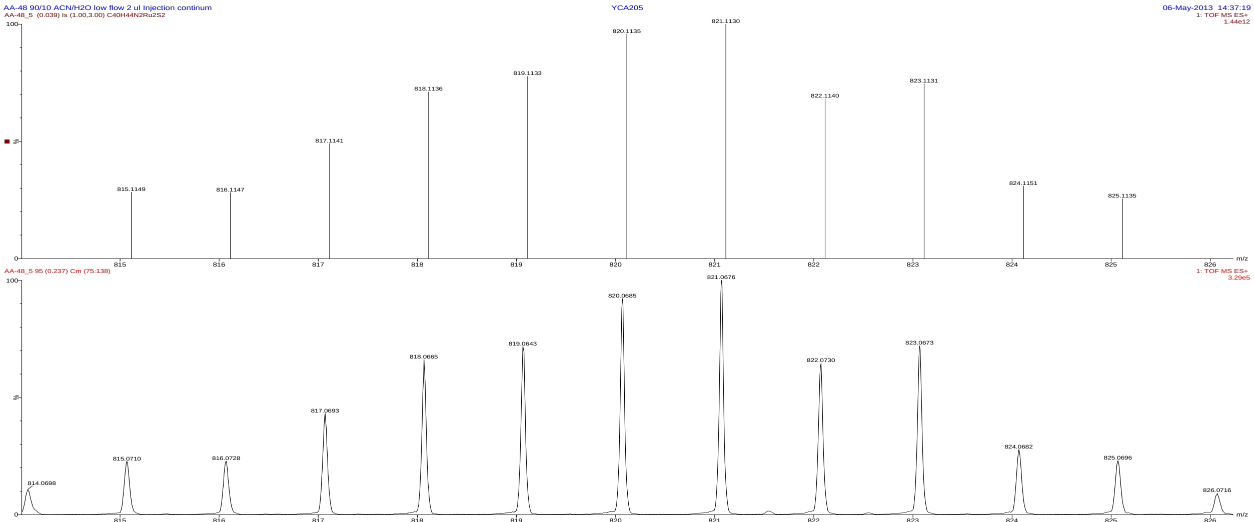

Figure S117. HRMS of **2c** (X = BF_4) signal 587 *m/z* (full); theoretical results above, experiment below – high energy ionization

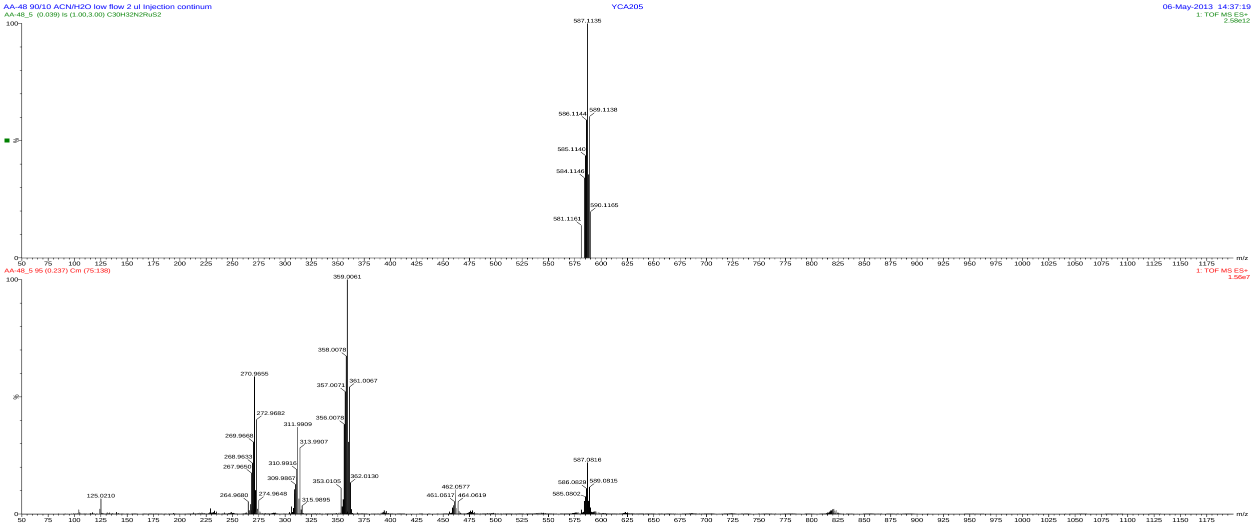

Figure S118. HRMS of **2c** (X = BF_4) signal 587 *m/z* (zoom); theoretical results above, experiment below – high energy ionization

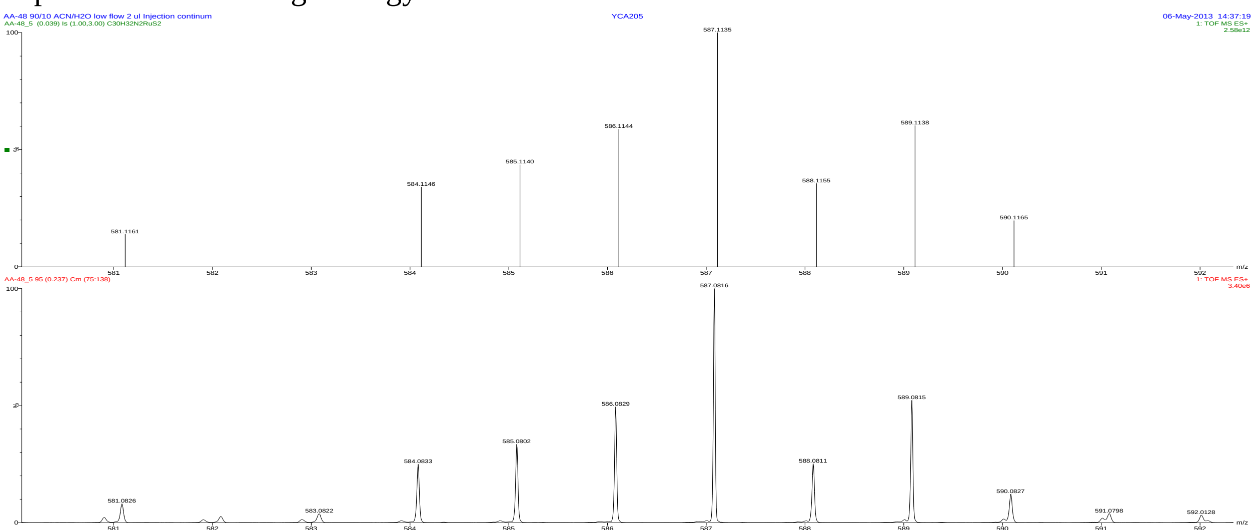

Figure S119. HRMS of **2c** (X = BF_4) signal 462 *m/z* (full); theoretical results above, experiment below – high energy ionization

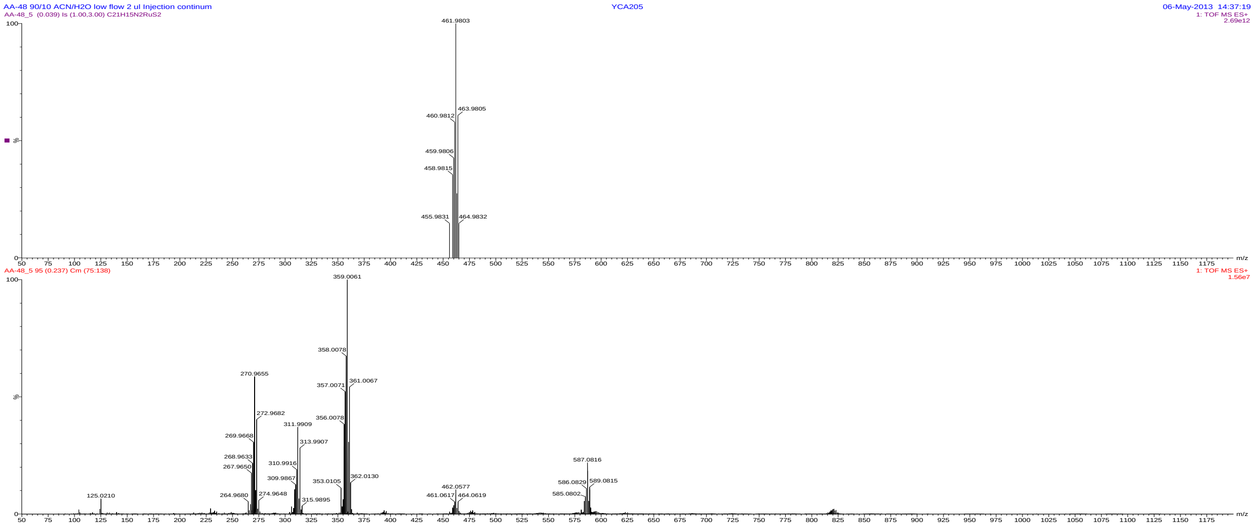

Figure S120. HRMS of **2c** (X = BF_4) signal 462 *m/z* (zoom); theoretical results above, experiment below – high energy ionization

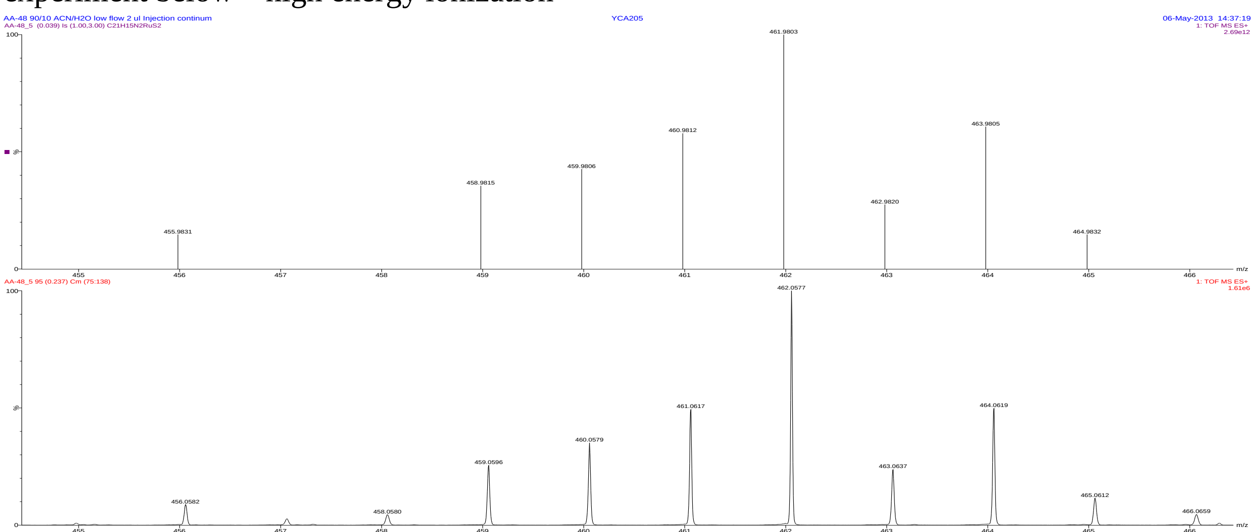

Figure S121. HRMS of **2c** (X = BF_4) signal 359 *m/z* (full); theoretical results above, experiment below – high energy ionization

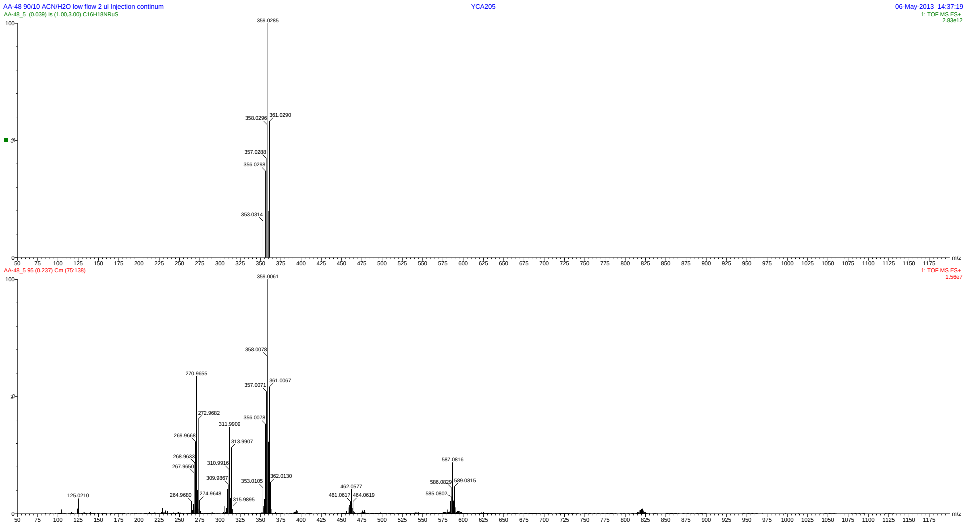

Figure S122. HRMS of **2c** (X = BF_4) signal 359 *m/z* (zoom); theoretical results above, experiment below – high energy ionization

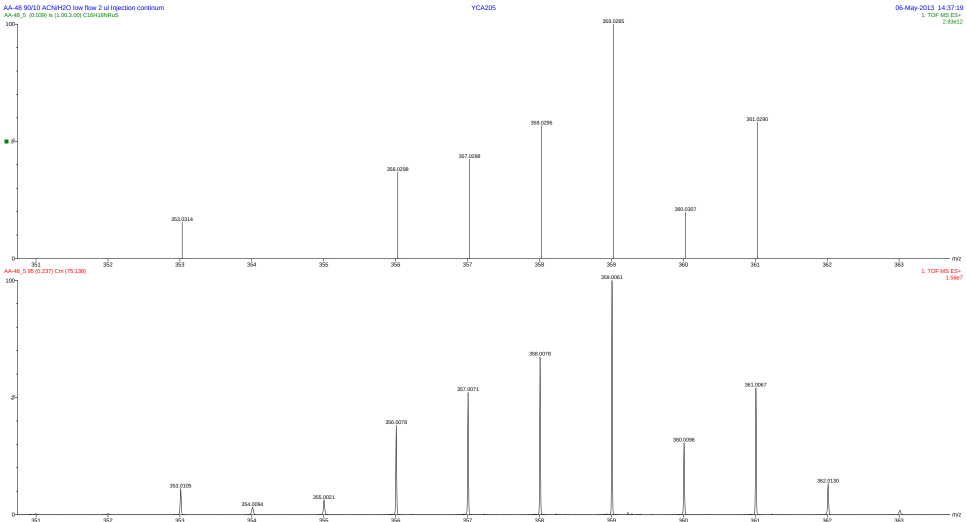

Figure S123. HRMS of **2c** (X = BF_4) signal 312 *m/z* (full); theoretical results above, experiment below – high energy ionization

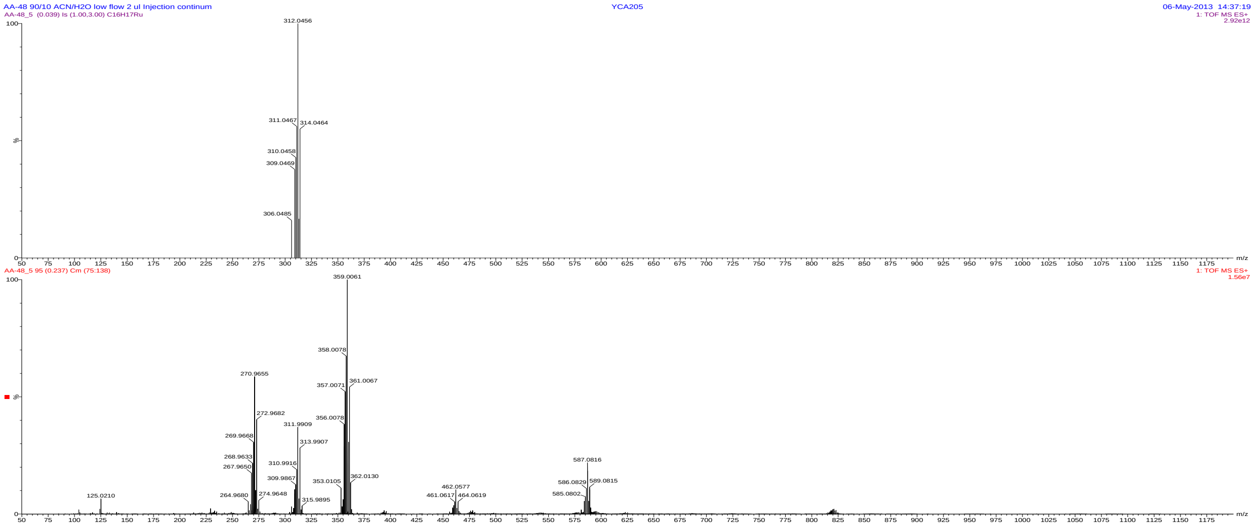

Figure S124. HRMS of **2c** (X = BF_4) signal 312 *m/z* (zoom); theoretical results above, experiment below – high energy ionization

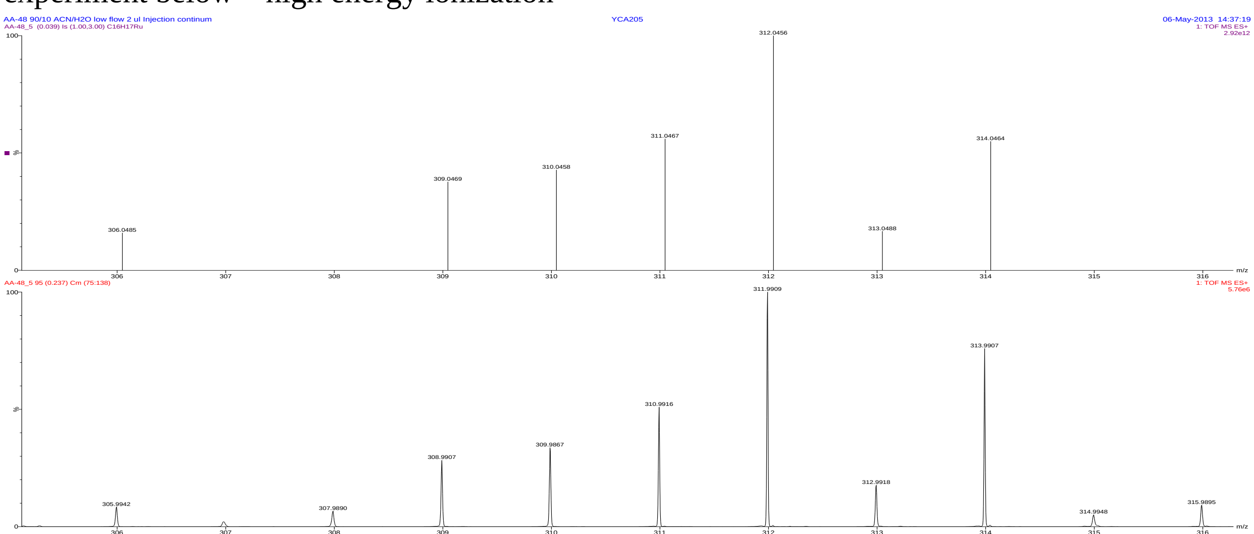

Figure S125. HRMS of **2c** (X = BF_4) signal 270 *m/z* (full); theoretical results above, experiment below – high energy ionization

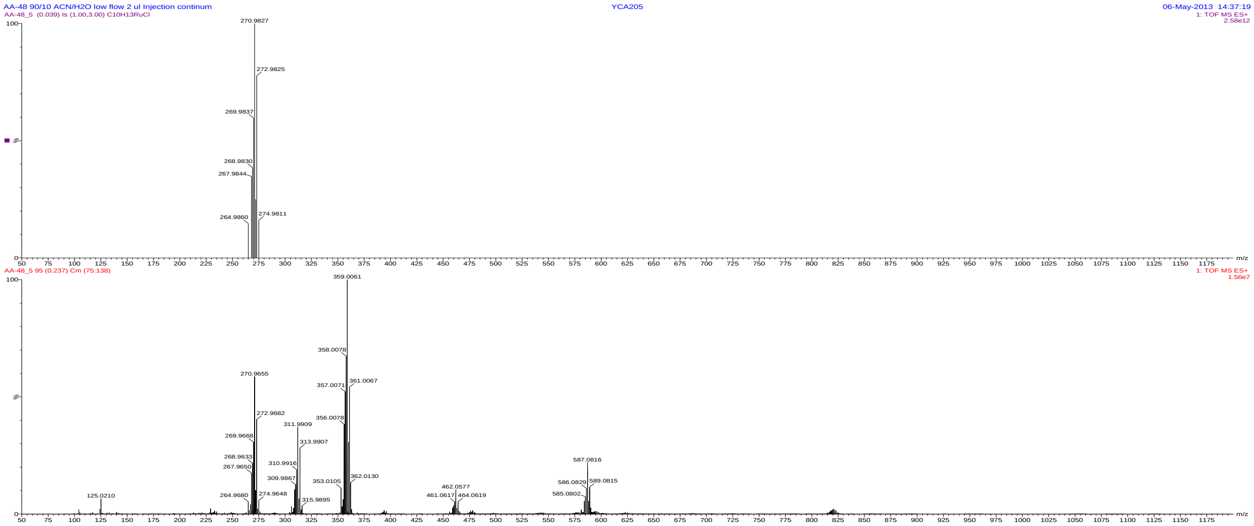

Figure S126. HRMS of **2c** (X = BF_4) signal 270 *m/z* (zoom); theoretical results above, experiment below – high energy ionization

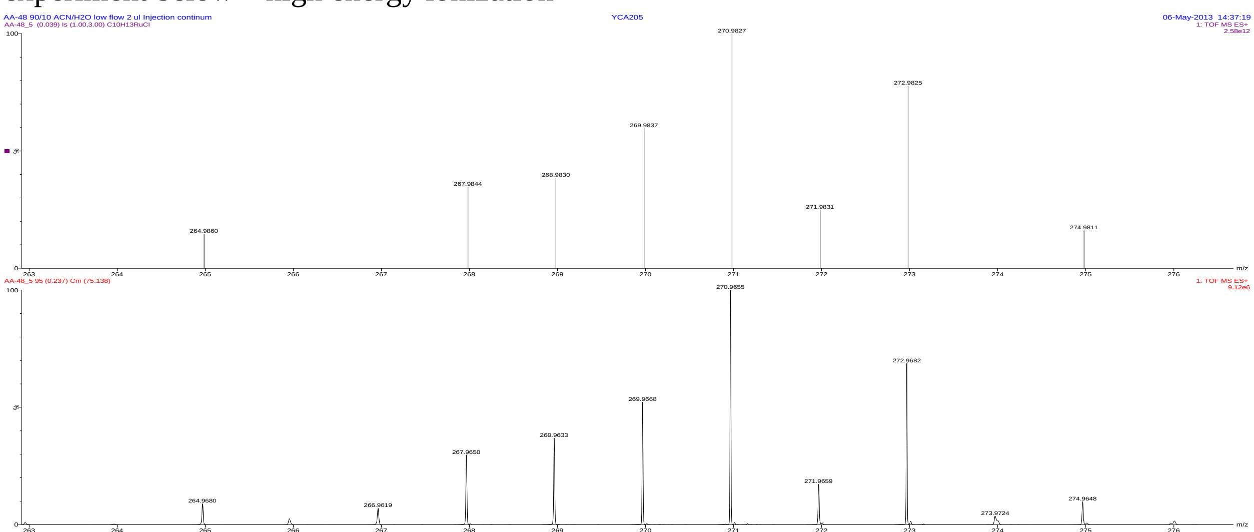

Figure S127. UPLC-MS chromatogram of **2c** (X = PF_6) – low energy ionization

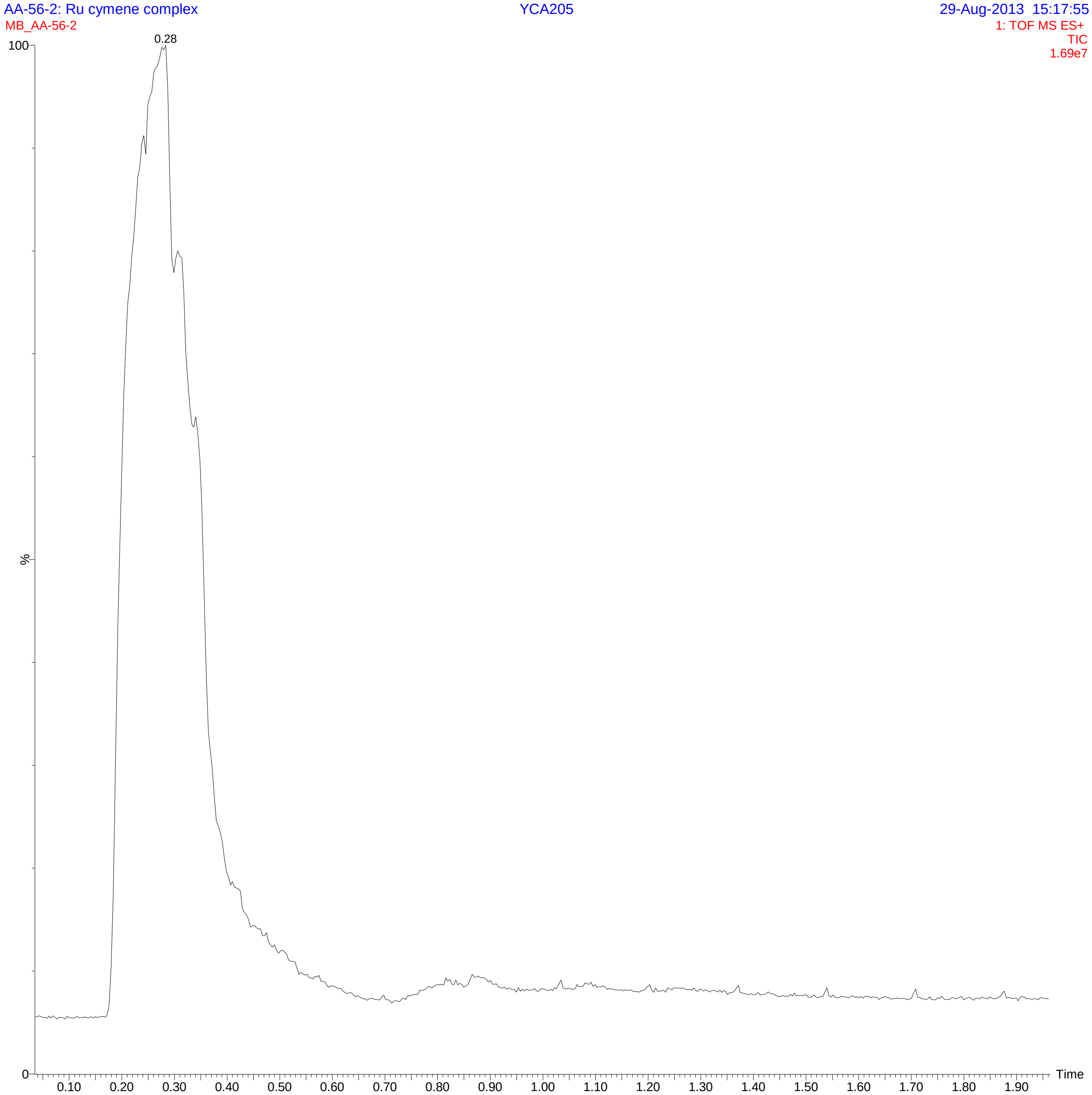

Figure S128. HRMS of **2c** (X = PF_6) – high energy ionization

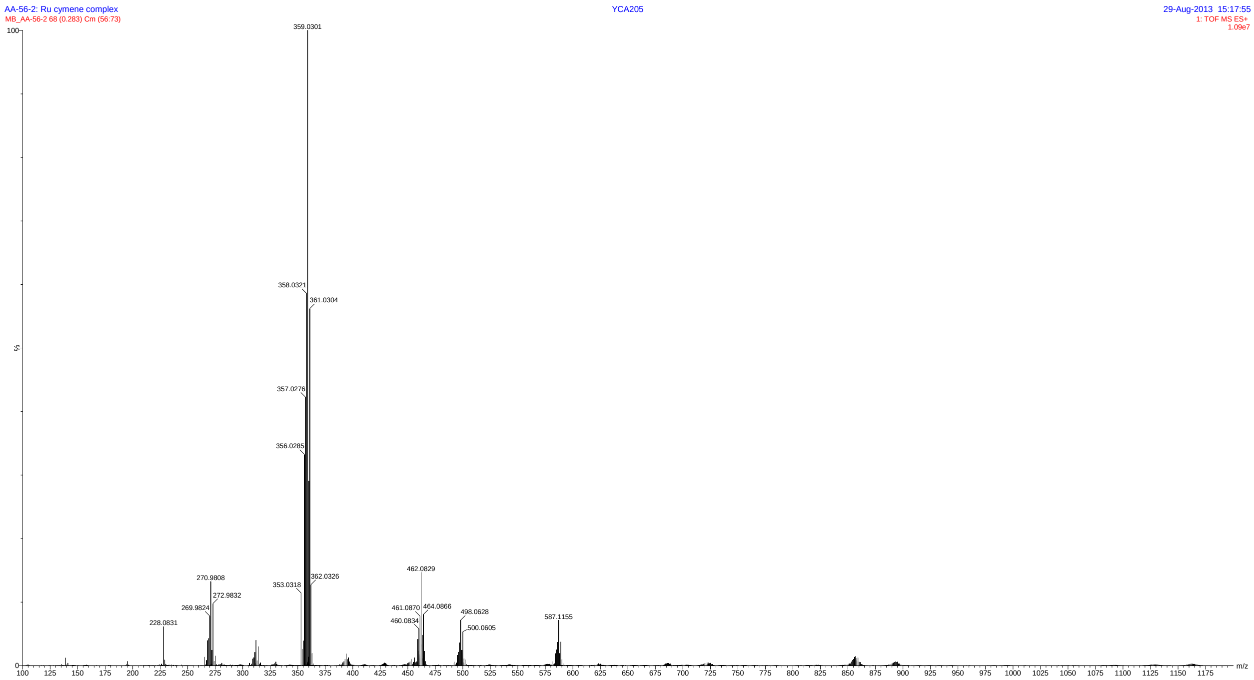

Figure S129. HRMS of **2c** (X = PF_6) signal 893 *m/z* (full); theoretical results above, experiment below – low energy ionization

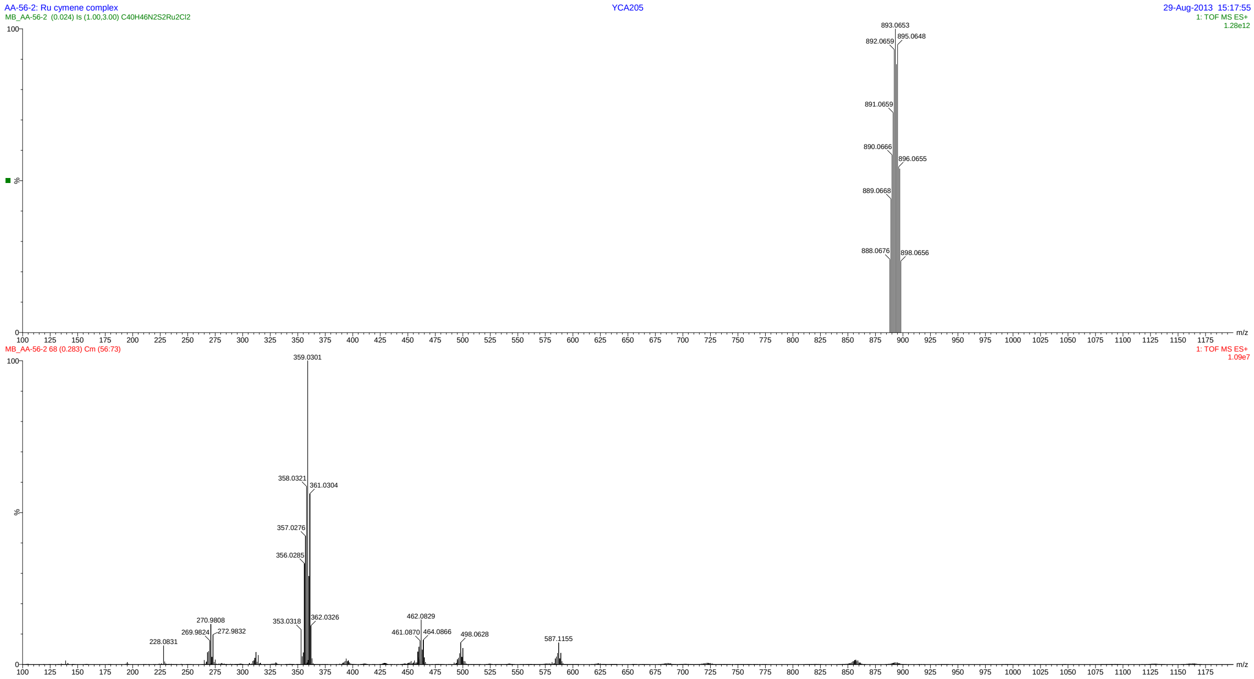

Figure S130. HRMS of **2c** (X = PF_6) signal 893 *m/z* (zoom); theoretical results above, experiment below – low energy ionization

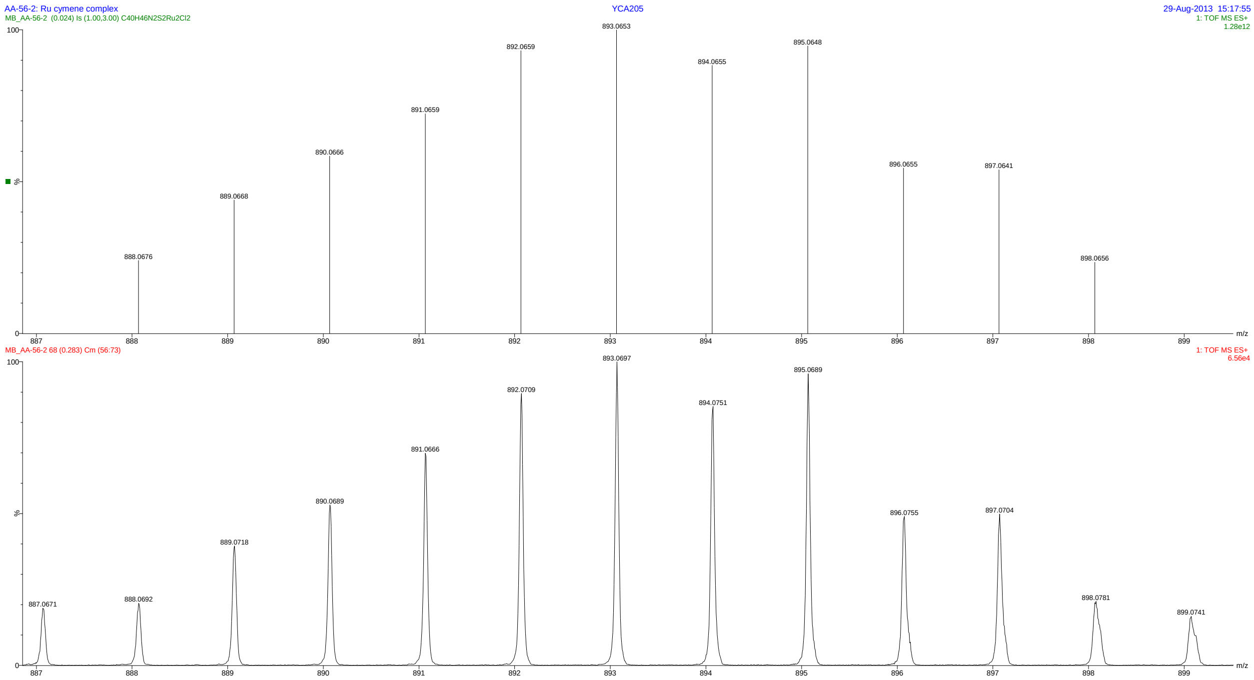

Table S1. Crystallographic Experimental Details

A. Crystal Data	
formula	$C_{20}H_{20}N_2S_2$
formula weight	352.50
crystal dimensions (mm)	0.39 × 0.33 × 0.24
crystal system	orthorhombic
space group	*Pbcn* (No. 60)
unit cell parameters[a]	
a (Å)	8.4685 (3)
b (Å)	12.1683 (4)
c (Å)	17.2063 (5)
V (Å^3)	1773.06 (10)
Z	4
ρ_{calcd} (g cm^{-3})	1.321
μ (mm^{-1})	0.304
B. Data Collection and Refinement Conditions	
diffractometer	Bruker D8/APEX II CCD[b]
radiation (λ [Å])	graphite-monochromated Mo Kα (0.71073)
temperature (°C)	–100
scan type	ω scans (0.3°) (15 s exposures)
data collection 2θ limit (deg)	55.02
total data collected	14660 ($-11 \le h \le 11$, $-15 \le k \le 15$, $-22 \le l \le 22$)
independent reflections	2038 (R_{int} = 0.0173)
number of observed reflections (*NO*)	1841 [$F_o^2 \ge 2\sigma(F_o^2)$]
structure solution method	direct methods (*SHELXD*[c])
refinement method	full-matrix least-squares on F^2 (*SHELXL–97*[d])
absorption correction method	Gaussian integration (face-indexed)
range of transmission factors	0.9313–0.8918
data/restraints/parameters	2038 / 0 / 117
goodness-of-fit (S)[e] [all data]	1.068
final R indices[f]	
R_1 [$F_o^2 \ge 2\sigma(F_o^2)$]	0.0284
wR_2 [all data]	0.0788
largest difference peak and hole	0.279 and –0.189 e Å^{-3}

[a]Obtained from least-squares refinement of 7053 reflections with 5.86° < 2θ < 54.56°.

[b]Programs for diffractometer operation, data collection, data reduction and absorption correction were those supplied by Bruker.

(continued)

Table 1. Crystallographic Experimental Details (continued)

[c]Schneider, T. R.; Sheldrick, G. M. *Acta Crystallogr*. **2002**, *D58*, 1772-1779.

[d]Sheldrick, G. M. *Acta Crystallogr*. **2008**, *A64*, 112–122.

[e]$S = [\Sigma w(F_o^2 - F_c^2)^2/(n - p)]^{1/2}$ (n = number of data; p = number of parameters varied; $w = [\sigma^2(F_o^2) + (0.0374P)^2 + 0.6253P]^{-1}$ where $P = [\mathrm{Max}(F_o^2, 0) + 2F_c^2]/3$).

[f]$R_1 = \Sigma||F_o| - |F_c||/\Sigma|F_o|$; $wR_2 = [\Sigma w(F_o^2 - F_c^2)^2/\Sigma w(F_o^4)]^{1/2}$.

Table S2. Atomic Coordinates and Equivalent Isotropic Displacement Parameters

Atom	x	y	z	U_{eq}, Å^2
S	-0.08559(4)	0.06451(2)	0.378101(18)	0.03134(11)*
N	0.15774(16)	0.15458(11)	0.49234(7)	0.0426(3)*
C1	0.03910(14)	-0.09762(9)	0.28579(7)	0.0278(2)*
C2	0.07503(15)	-0.19776(11)	0.32107(8)	0.0349(3)*
C3	0.03709(17)	-0.29651(10)	0.28569(9)	0.0399(3)*
C10	0.08518(14)	0.00839(10)	0.32520(7)	0.0314(3)*
C11	-0.02919(14)	0.20340(9)	0.39152(6)	0.0267(2)*
C12	0.07829(14)	0.23289(10)	0.45021(7)	0.0295(3)*
C13	0.10865(16)	0.34527(11)	0.46173(8)	0.0349(3)*
C14	0.03833(16)	0.42377(10)	0.41528(8)	0.0365(3)*
C15	-0.06340(16)	0.39462(11)	0.35613(8)	0.0372(3)*
C16	-0.09756(15)	0.28428(10)	0.34474(7)	0.0324(3)*
H1NA	0.115(2)	0.0908(16)	0.4951(10)	0.052(5)
H1NB	0.204(2)	0.1776(14)	0.5348(11)	0.056(5)

Anisotropically-refined atoms are marked with an asterisk (*). The form of the anisotropic displacement parameter is: $\exp[-2\pi^2(h^2a^{*2}U_{11} + k^2b^{*2}U_{22} + l^2c^{*2}U_{33} + 2klb^*c^*U_{23} + 2hla^*c^*U_{13} + 2hka^*b^*U_{12})]$.

Table S3. Selected Interatomic Distances (Å)

Atom1	Atom2	Distance	Atom1	Atom2	Distance
S	C10	1.8402(13)	C2	C3	1.3849(19)
S	C11	1.7714(12)	C3	C3’	1.379(3)
N	C12	1.3733(17)	C11	C12	1.4061(16)
N	H1NA	0.859(19)	C11	C16	1.3970(17)
N	H1NB	0.877(19)	C12	C13	1.4055(17)
C1	C1’	1.399(2)	C13	C14	1.3806(19)
C1	C2	1.3949(17)	C14	C15	1.380(2)
C1	C10	1.5086(16)	C15	C16	1.3873(18)

Primed atoms are related to unprimed ones via the crystallographic twofold axis (0, y, $^1/4$).

Table 4. Selected Interatomic Angles (deg)

Atom1	Atom2	Atom3	Angle	Atom1	Atom2	Atom3	Angle
C10	S	C11	101.92(5)	S	C11	C12	120.77(9)
C12	N	H1NA	116.6(12)	S	C11	C16	119.03(9)
C12	N	H1NB	116.0(11)	C12	C11	C16	120.16(11)
H1NA	N	H1NB	115.8(16)	N	C12	C11	121.28(11)
C1’	C1	C2	119.11(7)	N	C12	C13	120.73(12)
C1’	C1	C10	121.22(7)	C11	C12	C13	117.90(11)
C2	C1	C10	119.67(11)	C12	C13	C14	120.85(12)
C1	C2	C3	121.07(12)	C13	C14	C15	121.23(12)
C2	C3	C3’	119.81(8)	C14	C15	C16	118.89(12)
S	C10	C1	109.66(8)	C11	C16	C15	120.93(12)

Primed atoms are related to unprimed ones via the crystallographic twofold axis (0, *y*, $^{1}/_{4}$).

Table 5. Torsional Angles (deg)

Atom1	Atom2	Atom3	Atom4	Angle	Atom1	Atom2	Atom3	Atom4	Angle
C11	S	C10	C1	-161.66(8)	S	C11	C12	N	8.27(16)
C10	S	C11	C12	-78.72(10)	S	C11	C12	C13	-175.13(9)
C10	S	C11	C16	103.65(10)	C16	C11	C12	N	-174.13(12)
C2	C1	C1’	C2’	-1.8(3)	C16	C11	C12	C13	2.47(17)
C2	C1	C1’	C10’	178.08(8)	S	C11	C16	C15	176.41(10)
C10	C1	C1’	C10’	-2.0(2)	C12	C11	C16	C15	-1.23(18)
C1’	C1	C2	C3	1.2(2)	N	C12	C13	C14	174.81(12)
C10	C1	C2	C3	-178.73(12)	C11	C12	C13	C14	-1.80(18)
C1’	C1	C10	S	82.09(16)	C12	C13	C14	C15	-0.2(2)
C2	C1	C10	S	-98.00(12)	C13	C14	C15	C16	1.4(2)
C1	C2	C3	C3’	0.2(2)	C14	C15	C16	C11	-0.75(19)

Primed atoms are related to unprimed ones via the crystallographic twofold axis (0, *y*, 1/4).

Table S6. Anisotropic Displacement Parameters (U_{ij}, Å^2)

Atom	U_{11}	U_{22}	U_{33}	U_{23}	U_{13}	U_{12}
S	0.03392(18)	0.02513(17)	0.03497(19)	-0.00366(11)	0.00228(12)	-0.00570(11)
N	0.0529(7)	0.0348(6)	0.0401(6)	0.0037(5)	-0.0164(6)	-0.0038(5)
C1	0.0279(5)	0.0228(5)	0.0328(6)	-0.0008(5)	-0.0017(5)	0.0007(4)
C2	0.0371(6)	0.0303(6)	0.0372(7)	0.0056(5)	-0.0031(5)	0.0032(5)
C3	0.0423(7)	0.0221(6)	0.0553(8)	0.0082(5)	0.0042(6)	0.0036(5)
C10	0.0300(6)	0.0275(6)	0.0368(6)	-0.0054(5)	-0.0042(5)	-0.0003(5)
C11	0.0291(6)	0.0239(5)	0.0272(5)	-0.0019(4)	0.0035(4)	-0.0012(4)
C12	0.0326(6)	0.0287(6)	0.0271(6)	-0.0011(5)	0.0022(5)	-0.0013(5)
C13	0.0377(6)	0.0317(6)	0.0352(6)	-0.0076(5)	0.0032(5)	-0.0060(5)
C14	0.0431(7)	0.0244(6)	0.0420(7)	-0.0040(5)	0.0149(6)	-0.0014(5)
C15	0.0422(7)	0.0294(6)	0.0402(7)	0.0064(5)	0.0105(6)	0.0080(5)
C16	0.0334(6)	0.0329(6)	0.0309(6)	0.0004(5)	0.0020(5)	0.0037(5)

The form of the anisotropic displacement parameter is:
$\exp[-2\pi^2(h^2a^{*2}U_{11} + k^2b^{*2}U_{22} + l^2c^{*2}U_{33} + 2klb^*c^*U_{23} + 2hla^*c^*U_{13} + 2hka^*b^*U_{12})]$

Table S7. Derived Atomic Coordinates and Displacement Parameters for Hydrogen Atoms

Atom	x	y	z	U_{eq}, Å^2
H2	0.1264	-0.1982	0.3702	0.042
H3	0.0621	-0.3641	0.3105	0.048
H10A	0.1216	0.0621	0.2859	0.038
H10B	0.1731	-0.0052	0.3619	0.038
H13	0.1785	0.3675	0.5020	0.042
H14	0.0604	0.4993	0.4242	0.044
H15	-0.1093	0.4492	0.3237	0.045
H16	-0.1685	0.2634	0.3046	0.039

Figure S131. UV-vis spectrum of **2a** (X = BF_4)

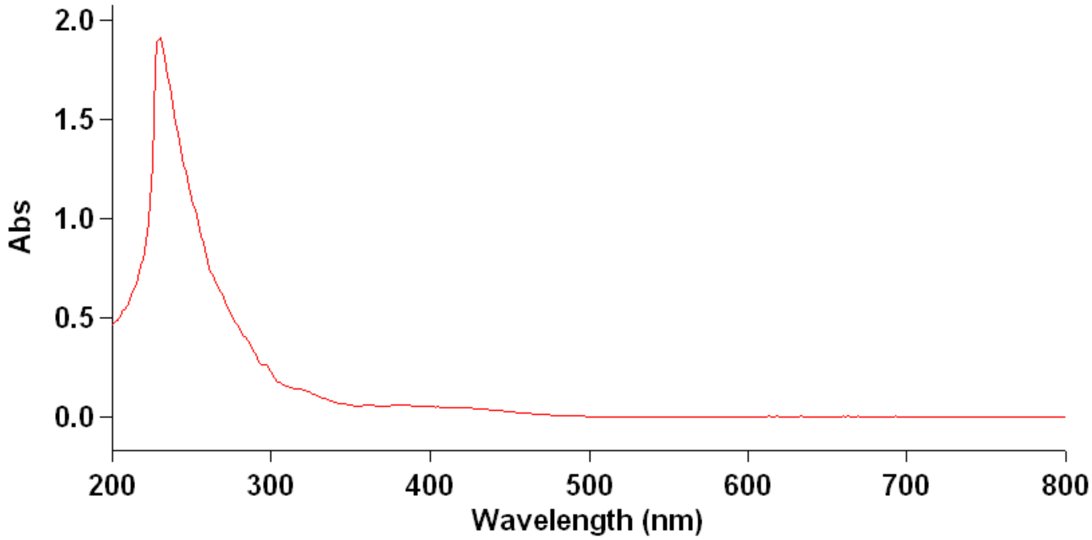

Solvent: CH_2Cl_2; Concentration: 0.025 mg/mL

λ_{max}/nm for **2a** (X = BF_4, CH_2Cl_2) 230 (ε/$dm^3mol^{-1}cm^{-1}$ 81 500) and 260 (sh).

Figure S132. UV-vis spectrum of **2b** (X = PF_6)

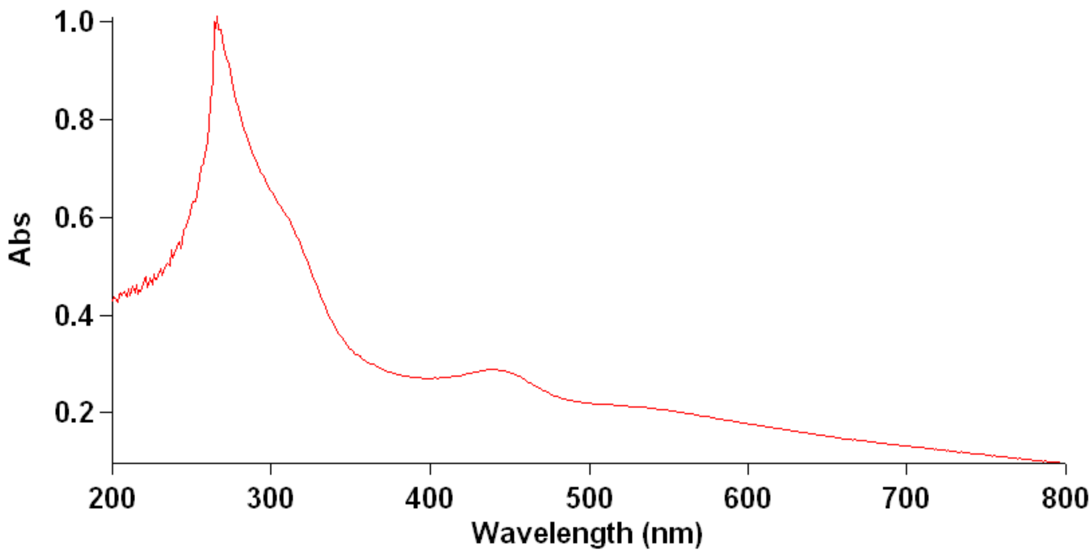

Solvent: DMF; Concentration: 0.07 mg/mL

λ_{max}/nm for **2b** (X = PF_6, DMF) 266 (ε/dm^3 mol^{-1} cm^{-1} 17 100), 303 (sh) and 439 (4 900).

Figure S133. UV-vis spectrum of **2c** (X = BF_4)

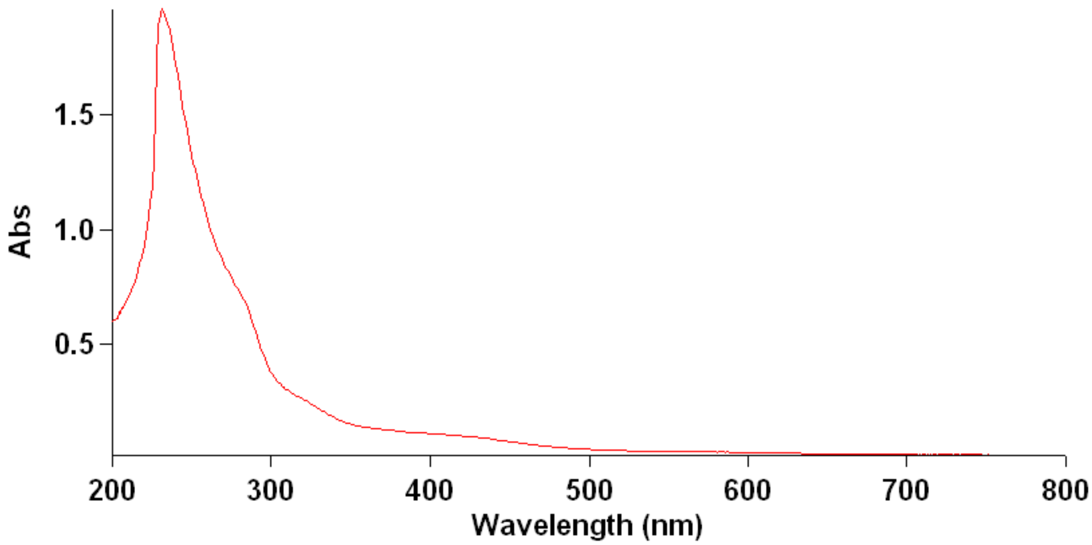

Solvent: CH_2Cl_2; Concentration: 0.025 mg/mL

λ_{max}/nm for **2c** (X = BF_4, CH_2Cl_2) 231 (ε/dm^3 mol^{-1} cm^{-1} 53 200) and 278 (sh).

Figure S134. UV-vis spectrum of **2c** (X = PF_6)

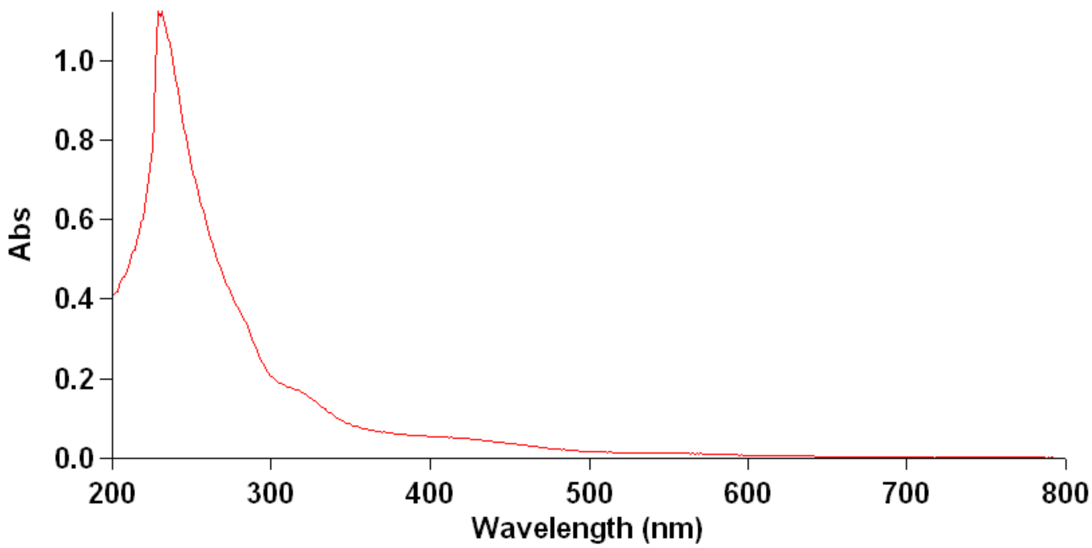

Solvent: CH_2Cl_2; Concentration: 0.025 mg/mL

λ_{max}/nm for **2c** (X = PF_6, CH_2Cl_2) 230 (ε/dm^3 mol^{-1} cm^{-1} 81 500), 270 (sh) and 312 (8 300).

Figure S135. UV-vis spectrum of **3** and mixture with **2b** (X = PF_6).

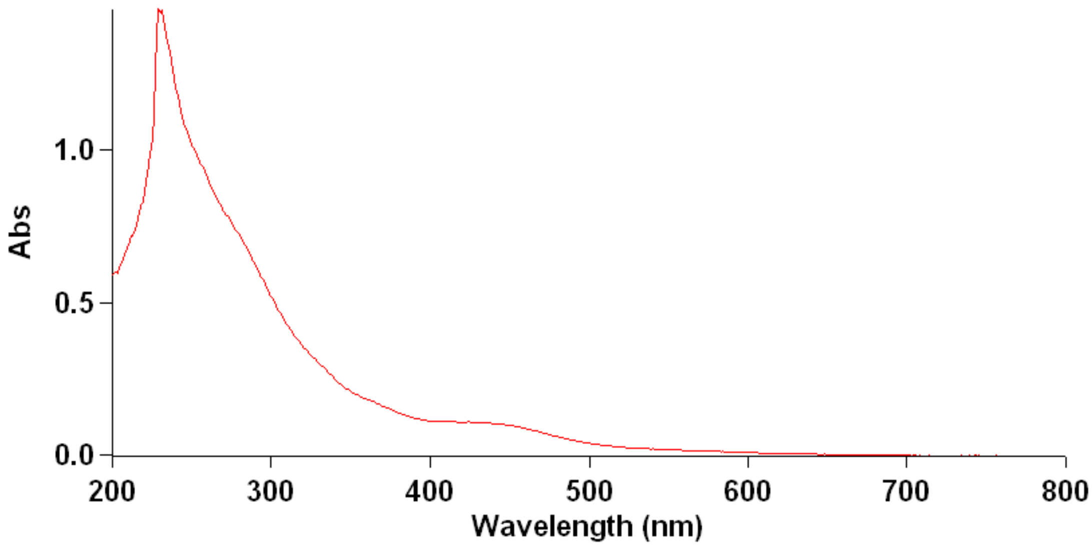

Solvent: DMF; Concentration: 0.038 mg/mL

λ_{max}/nm for **3** (DMF) 229, 270 and 440.

Electronic Supplementary Material (ESI) for Dalton Transactions

Figure S136. FTIR spectrum of **2a** (X = BF_4).

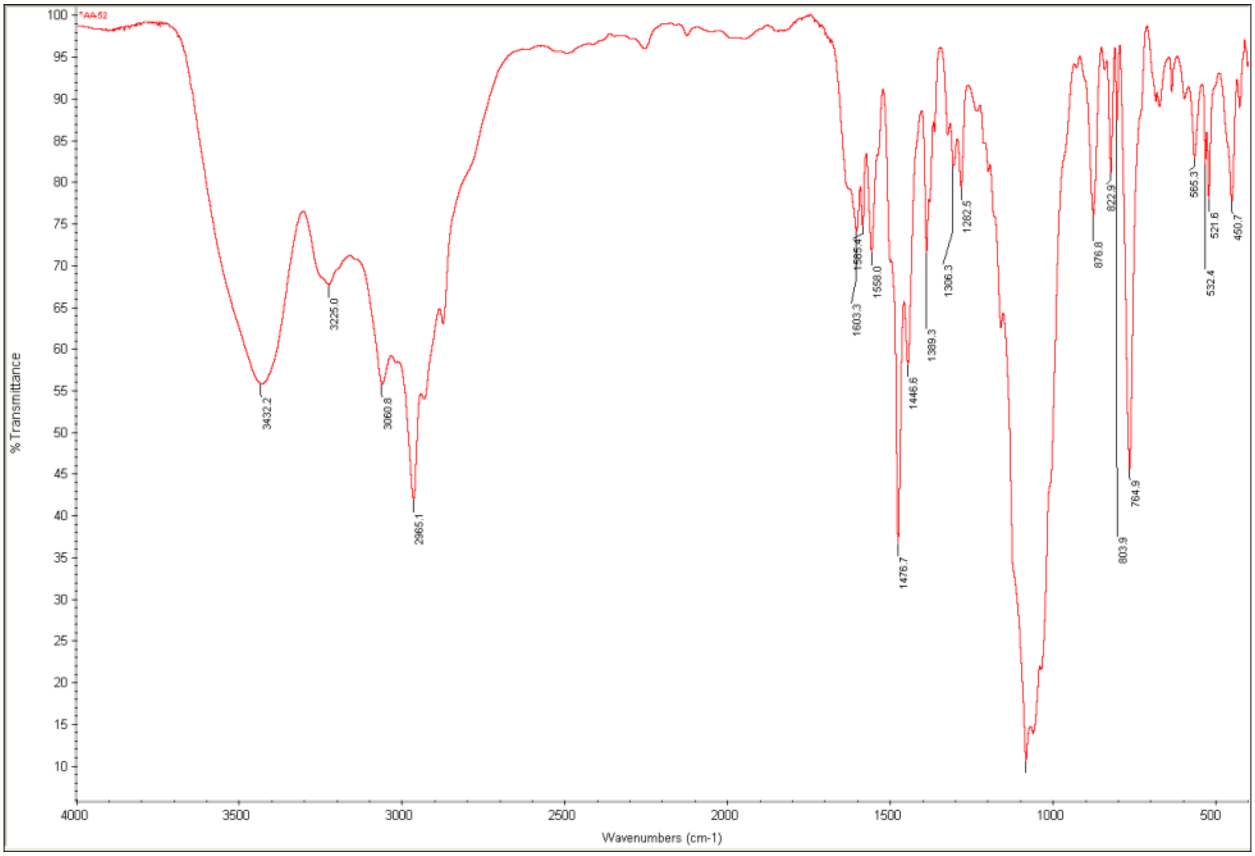

KBr pellet (approx. 1.5 mg in 300 mg KBr), 64 scan, 2 cm^{-1} resolution

Electronic Supplementary Material (ESI) for Dalton Transactions

Figure S137. FTIR spectrum of **2b** (X = PF_6).

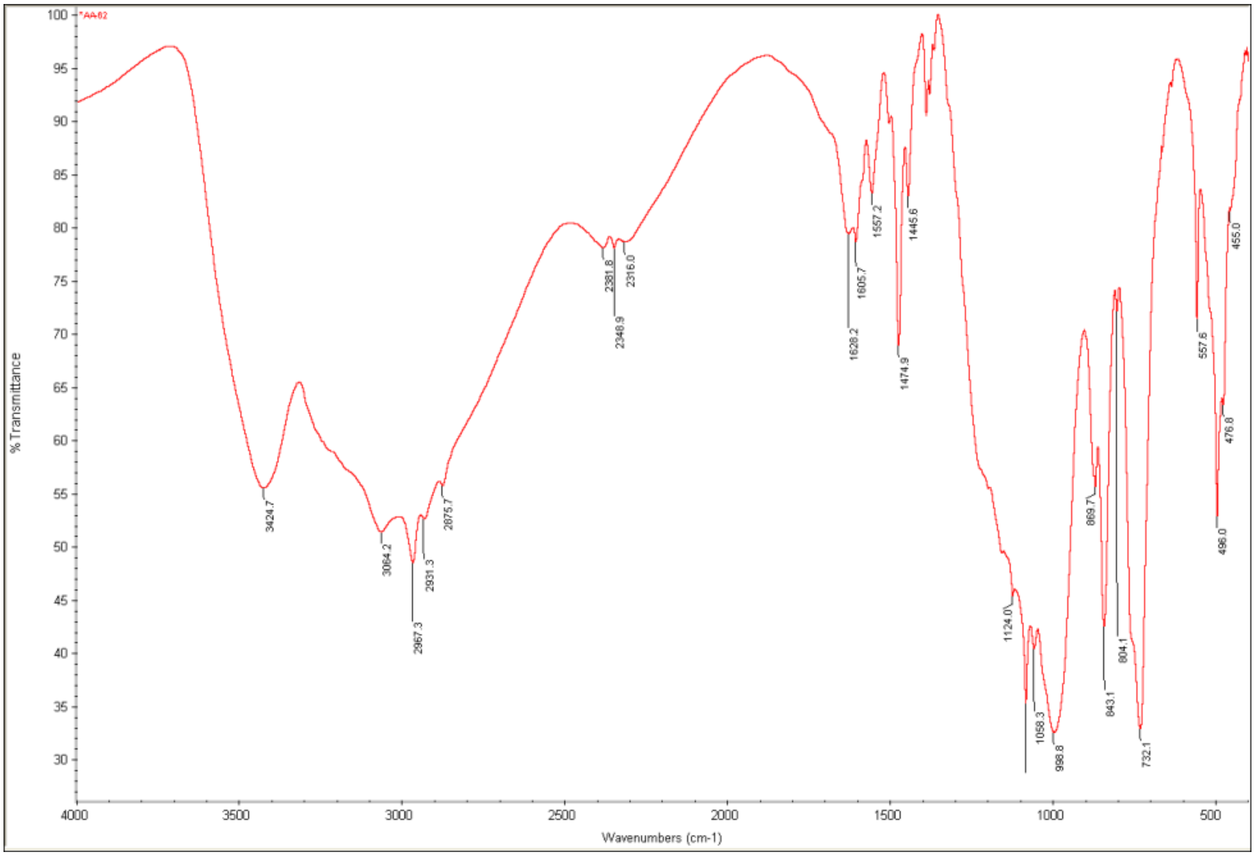

KBr pellet (approx. 1.5 mg in 300 mg KBr), 64 scan, 2 cm^{-1} resolution

Figure S138. FTIR spectrum of **2c** (X = BF_4).

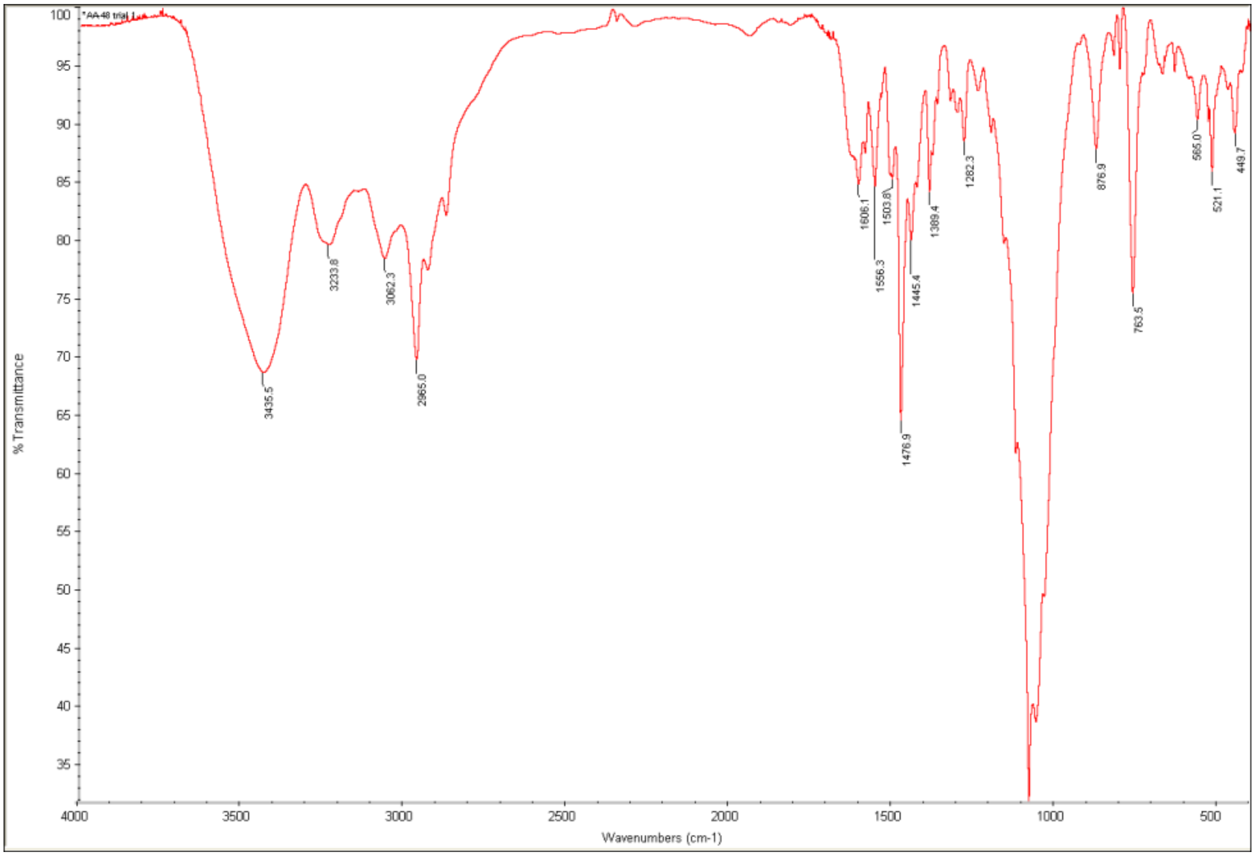

KBr pellet (approx. 1.5 mg in 300 mg KBr), 64 scan, 2 cm^{-1} resolution

Figure S139. FTIR spectrum of **2c** (X = PF_6).

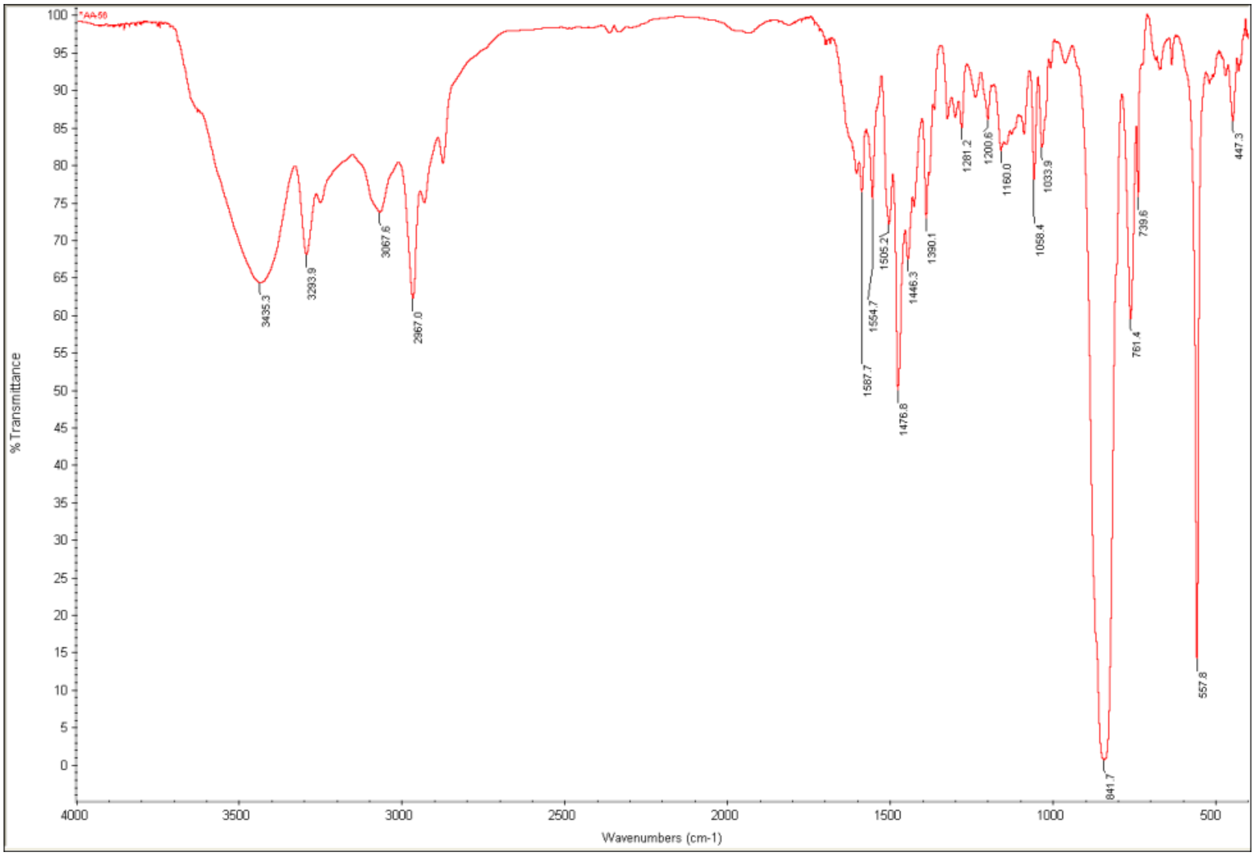

KBr pellet (approx. 1.5 mg in 300 mg KBr), 64 scan, 2 cm^{-1} resolution

Figure S140. FTIR spectrum of **3** (X = BF_4).

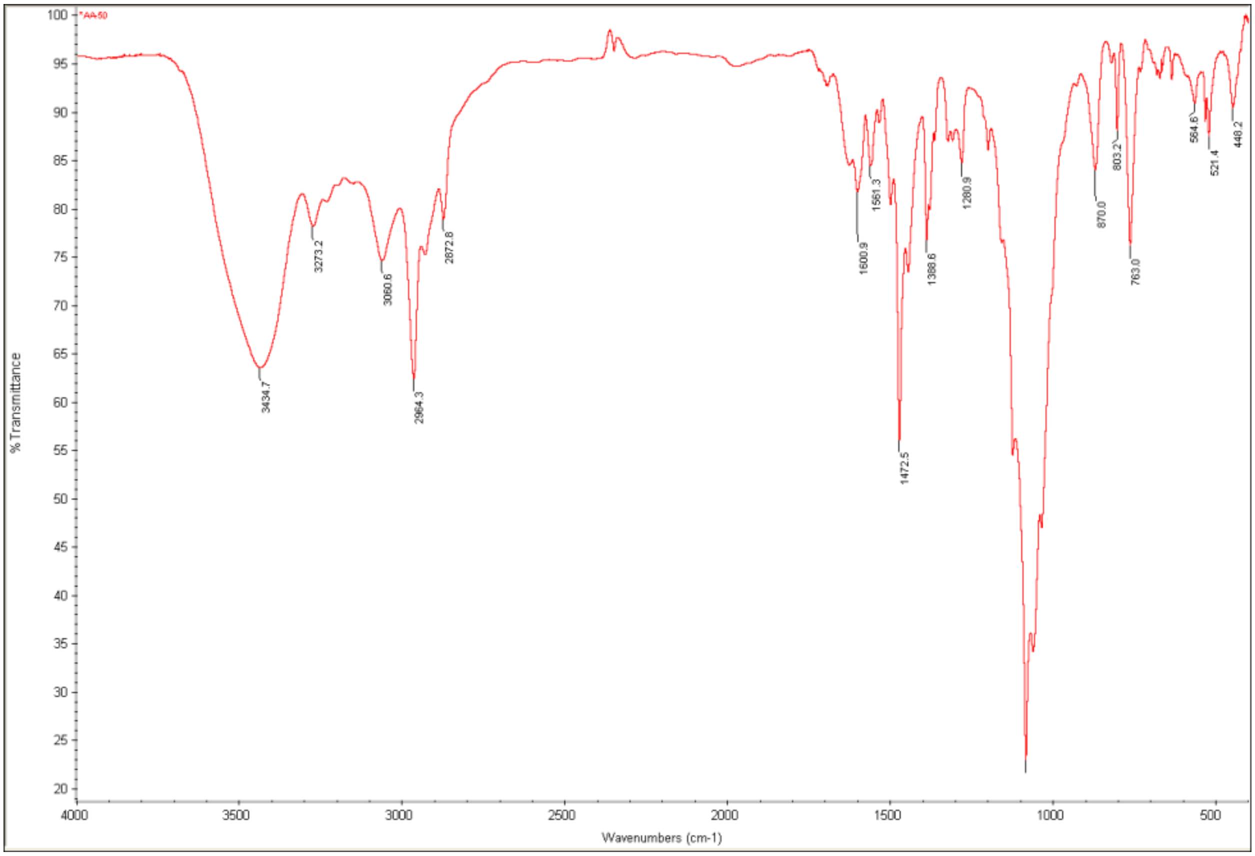

KBr pellet (approx. 1.5 mg in 300 mg KBr), 64 scan, 2 cm^{-1} resolution

ICP-MS Operating Conditions

Instrument NexION® 300D (PerkinElmer Inc.)

Component/Parameter	**Type/Value/Mode**
Nebulizer	Meinhard® glass microconcentric
Spray Chamber	Glass cyclonic
Triple Cone Interface Material	Nickel/Aluminum
Plasma Gas Flow	18.0 L/min
Auxiliary Gas Flow	1.2 L/min
Nebulizer Gas Flow	0.94 L/min
Sample Uptake Rate	250 µL/min
RF Power	1600 W
Integration Time	500 – 1500 ms
Replicate per Sample	3
Mode of Operation	Standard

ICP-MS Results

Sample Id	Method File	Ru 102 (cps)	In 115 (IS) (cps)
1% HNO3	C:\NexIONData\Method\Matthias_Ru.mth	34.4	7004842.3
100 ppb	C:\NexIONData\Method\Matthias_Ru.mth	1767594.3	6724956.2
200 ppb	C:\NexIONData\Method\Matthias_Ru.mth	3998693.5	6142891.8
300 ppb	C:\NexIONData\Method\Matthias_Ru.mth	5700331.1	5888536.2
400 ppb	C:\NexIONData\Method\Matthias_Ru.mth	7651405.7	5756162.0
500 ppb	C:\NexIONData\Method\Matthias_Ru.mth	9437871.7	5669121.2
Blank 1%	C:\NexIONData\Method\Matthias_Ru.mth	1070.8	5954844.7
AA-48	C:\NexIONData\Method\Matthias_Ru.mth	4268278.5	5693382.1
AA-50	C:\NexIONData\Method\Matthias_Ru.mth	5145423.3	5432282.3
AA-52	C:\NexIONData\Method\Matthias_Ru.mth	4257227.9	5598061.5
AA-56	C:\NexIONData\Method\Matthias_Ru.mth	3959390.7	5629185.7
Blank 1%	C:\NexIONData\Method\Matthias_Ru.mth	51317.8	5785570.0
AA-48	C:\NexIONData\Method\Matthias_Ru.mth	4273693.0	5616528.9
AA-50	C:\NexIONData\Method\Matthias_Ru.mth	5167077.2	5451141.8
AA-52	C:\NexIONData\Method\Matthias_Ru.mth	4298873.6	5542255.9
AA-56	C:\NexIONData\Method\Matthias_Ru.mth	4014735.5	5598966.1

	Run 1 (ppb)	Run 2 (ppb)	average	Abs. error ppb	error (%)	%Ru (theor)	% Ru (exp)	4% error
2a (X = BF4)	303.431	308.792	306.112	2.680	0.875	22.61	22.65	0.91
2c (X = BF4)	299.538	303.557	301.547	2.009	0.666	22.61	22.31	0.89
2c (X = PF6)	313.772	319.241	316.507	2.734	0.864	22.61	23.79	0.95
3	308.299	308.492	308.395	0.096	0.031	16.22	18.46	0.73

Figure S141. Calibration Curve (Ru 102).